4. SITE 802[1]

Shipboard Scientific Party[2]

HOLE 802A

Date occupied: 25 December 1989

Date departed: 4 January 1990

Time on hole: 10 days, 13 hr, 45 min

Position: 12°5.778′N, 153°,12.6258′E

Bottom felt (rig floor; m; drill-pipe measurement): 5980.0

Distance between rig floor and sea level (m): 11.40

Water depth (drill-pipe measurement from sea level; m): 5968.6

Total depth (rig floor; m): 6539.80

Penetration (m): 559.80

Number of cores (including cores with no recovery): 62

Total length of cored section (m): 559.80

Total core recovered (m): 165.01

Core recovery (%): 29

Oldest sediment cored:
Depth (mbsf): 499.70
Nature: claystone
Earliest age: Albian-late Aptian
Basement:
Depth (mbsf): 509.20
Nature: basalt

Principal Results: Site 802 is located in the central Mariana Basin at the southeastern end of a magnetic lineation sequence partially identified to the northwest as M22 to M31, which suggests a Late Jurassic basement age. Extrusive basalt underlies late Aptian-Albian (Lower Cretaceous) claystones, suggesting that the basement age should be revised as younger by 60 m.y. at this location, or that original Jurassic basement, and perhaps a significant sedimentary section, has been covered by subsequent Cretaceous lava flows. The overlying sediment section consists mainly of redeposited material, suggesting massive lateral transport over long distances (>300 km) or unmapped large elevations in the more immediate vicinity. Hole 802A consists of the following stratigraphic sequence.

0–15 mbsf: Neogene brown pelagic clay.

15–159 mbsf: Miocene tuff consisting of well-indurated and well-preserved hyaloclastites and volcaniclastic turbidites, presumably derived from the Caroline Island volcanic chain.

159–254 mbsf: Miocene to Eocene tuff, chalk, claystone, volcaniclastic turbidites, and debris flows, apparently all redeposited.

254–330 mbsf: Upper Paleocene nannofossil chalk.

330–348 mbsf: Maestrichtian zeolitic pelagic claystone.

348–460 mbsf: Campanian volcaniclastic turbidites with clay, claystone, silty claystone, porcellanite, and debris flow, mainly redeposited.

460–509 mbsf: Cenomanian to late Aptian-Albian brown claystone, calcareous claystone, radiolarian limestone, and volcaniclastic turbidites with wood fragments in lowest two cores.

509–560 mbsf: Extrusive basalt, uniformly fine-grained, with multiple cooling units and no included sediment. Sheet flow volcanism with some evidence for pillow basalts is suggested. The chilled zone immediately below the sediment contact suggests that the uppermost basalts were recovered.

Standard logging was conducted on the interval from 110 to 320 mbsf after eliminating a bridge above this level and encountering another at its base. A vertical seismic experiment was attempted to test for seismic horizons deeper than the sampled Cretaceous basalts that might indicate underlying Jurassic strata. The experiment was unsuccessful because the tool became stuck in the hole, requiring the logging cable to be severed and terminating operations at this site. A summary of coring statistics for this site appears in Table 1.

BACKGROUND AND OBJECTIVES

After reaching Jurassic sediments and oceanic crust in the single-bit pilot Hole 801B, our plan called for setting a reentry cone at Site 801, drilling a new hole, and casing it all the way into the basement in order to achieve substantial penetration into the oceanic crust. The accidental loss of the reentry camera, however, forced us to delay these operations until a replacement camera could be delivered. Thus, we proceeded to Site 802, proposed site EMB-2A, in the central part of the East Mariana Basin (Fig. 1). We had essentially the same general objectives at Site 802 as at the previous two sites; that is, to sample Jurassic sediments and oceanic crust in order to study the early evolution of the Pacific Ocean.

The East Mariana Basin had already been the location of several attempts to reach Jurassic crust. The earliest was DSDP Leg 20, during which Site 199 was drilled in the northwestern part of the basin near the base of the Ita Mai Tai guyot. Penetration at Site 199 was limited to 565 mbsf and only calcareous turbidites of Campanian age were recovered. The second attempt was at Site 585 (DSDP Leg 89), located approximately 50 nautical miles (nmi) east of Site 199. At Site 585, extremely thick middle Cretaceous volcaniclastic turbidites prevented reaching Jurassic material. These were attributed to a major phase of volcanic edifice-building of Aptian through Cenomanian age, and the likely source for the redeposited material has been recognized as the Ita Mai Tai guyot and other seamounts in the immediate vicinity. Recent multichannel seismic surveys showed that Site 585 is actually located in a basement depression, probably associated with a thinned, crustal section in a fracture zone, and that the sediment at the site is abnormally thick.

The same series of magnetic anomalies as in the Pigafetta Basin has been recognized in the northwestern part of the East Mariana Basin (Handschumacher and Gettrust, 1985; Tamaki et al., 1987; Handschumacher et al., 1988) (Fig. 2), although this basin is separated from the former by the Magellan seamounts, possibly associated with a fracture zone. Near the northern extension of the Mariana trench the youngest, well-identified magnetic anomalies on the Pacific plate are M23–M25. Toward the center of the basin, older anomalies are clearly visible and might extend to M37. Beyond M33, however, their precise identification is less certain than in the Pigafetta Basin.

Table 1. Coring summary for Hole 802A.

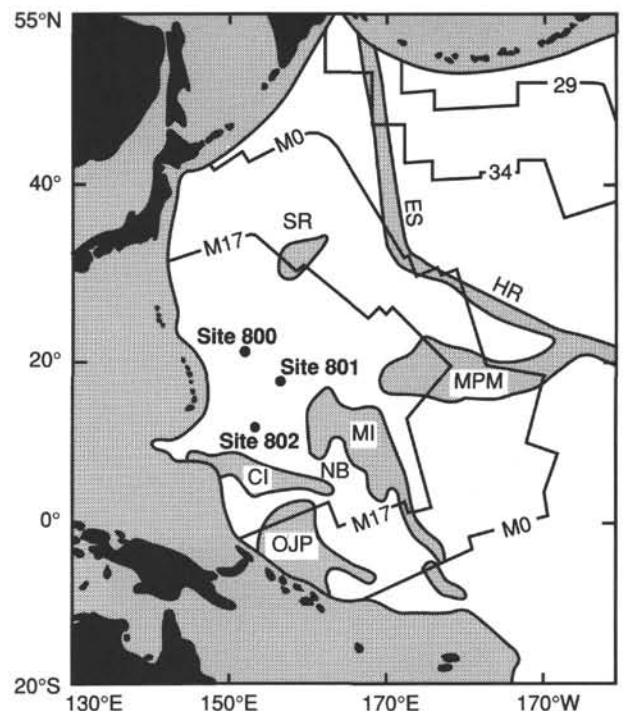| Core no.	Date	Time (UTC)	Depth (mbsf)	Length cored (m)	Length recovered (m)	Recovery (%)
1R	25 Dec. 1989	1345	0.0–5.0	5.0	0.01	0.2
2R	25 Dec. 1989	1730	5.0–14.6	9.6	0.00	0.0
3R	25 Dec. 1989	1935	14.6–24.3	9.7	1.43	14.7
4R	25 Dec. 1989	2250	24.3–33.7	9.4	3.00	31.9
5R	26 Dec. 1989	0135	33.7–42.9	9.2	1.93	21.0
6R	26 Dec. 1989	0350	42.9–52.4	9.5	2.58	27.1
7R	26 Dec. 1989	0745	52.4–61.9	9.5	1.46	15.3
8R	26 Dec. 1989	1110	61.9–71.1	9.2	3.29	35.7
9R	26 Dec. 1989	1410	71.1–80.4	9.3	0.00	0.0
10R	26 Dec. 1989	1620	80.4–89.6	9.2	3.42	37.2
11R	26 Dec. 1989	1830	89.6–98.9	9.3	1.91	20.5
12R	26 Dec. 1989	2020	98.9–108.3	9.4	0.13	1.4
13R	26 Dec. 1989	2230	108.3–114.4	6.1	1.67	27.4
14R	27 Dec. 1989	0100	114.4–122.1	7.7	3.37	43.7
15R	27 Dec. 1989	0445	122.1–131.1	9.0	2.87	31.9
16R	27 Dec. 1989	0655	131.1–140.4	9.3	2.00	21.5
17R	27 Dec. 1989	0845	140.4–149.7	9.3	2.13	22.9
18R	27 Dec. 1989	1055	149.7–159.1	9.4	0.39	4.2
19R	27 Dec. 1989	1330	159.1–168.3	9.2	3.55	38.6
20R	27 Dec. 1989	1530	168.3–177.6	9.3	0.30	3.2
21R	27 Dec. 1989	1740	177.6–187.0	9.4	1.75	18.6
22R	27 Dec. 1989	1940	187.0–196.4	9.4	0.45	4.8
23R	27 Dec. 1989	2230	196.4–206.1	9.7	2.68	27.6
24R	28 Dec. 1989	0010	206.1–215.7	9.6	0.17	1.8
25R	28 Dec. 1989	0450	215.7–225.4	9.7	1.07	11.0
26R	28 Dec. 1989	0640	225.4–235.1	9.7	3.63	37.4
27R	28 Dec. 1989	0805	235.1–244.7	9.6	8.15	84.9
28R	28 Dec. 1989	0935	244.7–254.5	9.8	4.38	44.7
29R	28 Dec. 1989	1105	254.5–264.2	9.7	3.65	37.6
30R	28 Dec. 1989	1400	264.2–273.8	9.6	1.63	17.0
31R	28 Dec. 1989	1630	273.8–283.5	9.7	1.95	20.1
32R	28 Dec. 1989	1900	283.5–292.8	9.3	3.37	36.2
33R	28 Dec. 1989	2125	292.8–302.3	9.5	1.64	17.2
34R	28 Dec. 1989	2355	302.3–311.5	9.2	1.40	15.2
35R	29 Dec. 1989	0220	311.5–320.7	9.2	1.04	11.3
36R	29 Dec. 1989	0445	320.7–329.9	9.2	1.12	12.2
37R	29 Dec. 1989	0650	329.9–339.2	9.3	0.19	2.0
38R	29 Dec. 1989	0900	339.2–348.7	9.5	7.89	83.0
39R	29 Dec. 1989	1120	348.7–358.1	9.4	0.90	9.6
40R	29 Dec. 1989	1325	358.1–365.5	7.4	4.58	61.9
41R	29 Dec. 1989	1540	365.5–372.8	7.3	5.85	80.1
42R	29 Dec. 1989	2000	372.8–382.1	9.3	2.69	28.9
43R	29 Dec. 1989	2210	382.1–391.3	9.2	3.90	42.4
44R	30 Dec. 1989	0015	391.3–400.5	9.2	1.24	13.5
45R	30 Dec. 1989	0215	400.5–410.0	9.5	3.53	37.1
46R	30 Dec. 1989	0405	410.0–419.2	9.2	1.34	14.5
47R	30 Dec. 1989	0600	419.2–428.7	9.5	6.16	64.8
48R	30 Dec. 1989	0750	428.7–438.1	9.4	0.99	10.5
49R	30 Dec. 1989	1000	438.1–447.4	9.3	6.85	73.6
50R	30 Dec. 1989	1200	447.4–453.5	6.1	3.15	51.6
51R	30 Dec. 1989	1420	453.5–459.8	6.3	4.71	74.7
52R	30 Dec. 1989	1800	459.8–469.4	9.6	4.03	42.0
53R	30 Dec. 1989	2045	469.4–478.6	9.2	2.59	28.1
54R	30 Dec. 1989	2335	478.6–487.9	9.3	6.50	69.9
55R	31 Dec. 1989	0220	487.9–497.1	9.2	1.48	16.1
56R	31 Dec. 1989	0445	497.1–506.6	9.5	5.11	53.8
57R	31 Dec. 1989	0820	506.6–516.0	9.4	3.34	35.5
58R	31 Dec. 1989	1440	516.0–525.4	9.4	5.02	53.4
59R	31 Dec. 1989	2130	525.4–534.7	9.3	3.89	41.8
60R	1 Jan. 1990	0140	534.7–544.2	9.5	0.96	10.1
61R	1 Jan. 1990	0620	544.2–550.6	6.4	1.50	23.4
62R	1 Jan. 1990	1910	550.6–559.8	9.2	3.10	33.7
	Coring totals			559.8	165.01	29.5

Figure 1. Map showing location of Pigafetta, Mariana, and Nauru basins, and location of Sites 800, 801, and 802. (Feature abbreviations are as follows: Caroline Islands (CI), Ontong Java Plateau (OJP), Marshall Islands (MI), Nauru Basin (NB), Mid-Pacific Mountains (MPM), Shatsky Rise (SR), Hawaiian Ridge (HR), and Emperor Seamounts (ES). Jagged contours represent magnetic lineations and unshaded areas represent normal Pacific oceanic crust. Shaded areas represent volcanic edifices with thickened crustal sections, as well as the younger areas beyond the Pacific subduction zones.

Two drill sites were proposed in this area. They present very similar characteristics on seismic profiles. Proposed site EMB-1 is located near anomaly M33, whereas proposed site EMB-2A was selected farther to the southeast, within the Jurassic quiet zone. Our choice of proposed site EMB-2A as a preferred target was mainly dictated by its distance from major seamounts. Indeed, we tried to locate this site as far from any large seamount as we could (approximately 160 nmi), although still on what we believed to be Jurassic crust.

Seismic reflection profiles from both of the survey cruises, *Fred H. Moore* 35-12 and MESOPAC II, show the acoustic basement to be alternatively smooth and rough. Site 802 is located in an area characterized by a rough acoustic basement

that lies slightly deeper than its adjacent smooth counterpart (see "Site Geophysics and Seismic Stratigraphy" section, this chapter). The total depth of approximately 8.4 seconds two-way traveltime (s twt) below sea level to this reflector, together with its relatively rough or "hummocky" aspect, led us to believe that it could very well correspond to the top of the extrusive Jurassic oceanic crust, whereas the smooth and slightly shallower acoustic basement of adjacent areas could indicate the presence of sills covering the old crust. As true oceanic crust had just been found at Site 801 at 8.0 s twt, we had reason to believe that this lowermost reflector would indeed again correspond to Jurassic basaltic extrusives.

The age of the crust was tentatively inferred from a simple extrapolation of the nearby magnetic anomalies to be Callovian or Oxfordian (165 to 168 m.y.) (Fig. 3). The total thickness of the section between the seafloor reflector and the acoustic basement is about 500 ms twt. Based on an average sound velocity of 2 km/s for this acoustic interval, we expected the total sediment section to be about 500 m thick. That section on seismic profiles can be roughly divided in two intervals. The uppermost of these, from 0 to 375 ms below the seafloor, appears well layered and shows evidence of ponding. It is tentatively correlated with a series of turbiditic deposits recovered at Site 199 located approximately 170 nmi to the northeast (Heezen, MacGregor, et al., 1973). Below that interval the section is more transparent, and we anticipated that it consisted mostly of pelagic sediments ranging in age from Late Cretaceous at the top to Callovian-Oxfordian at the bottom. The youngest of the two successive equatorial cross-
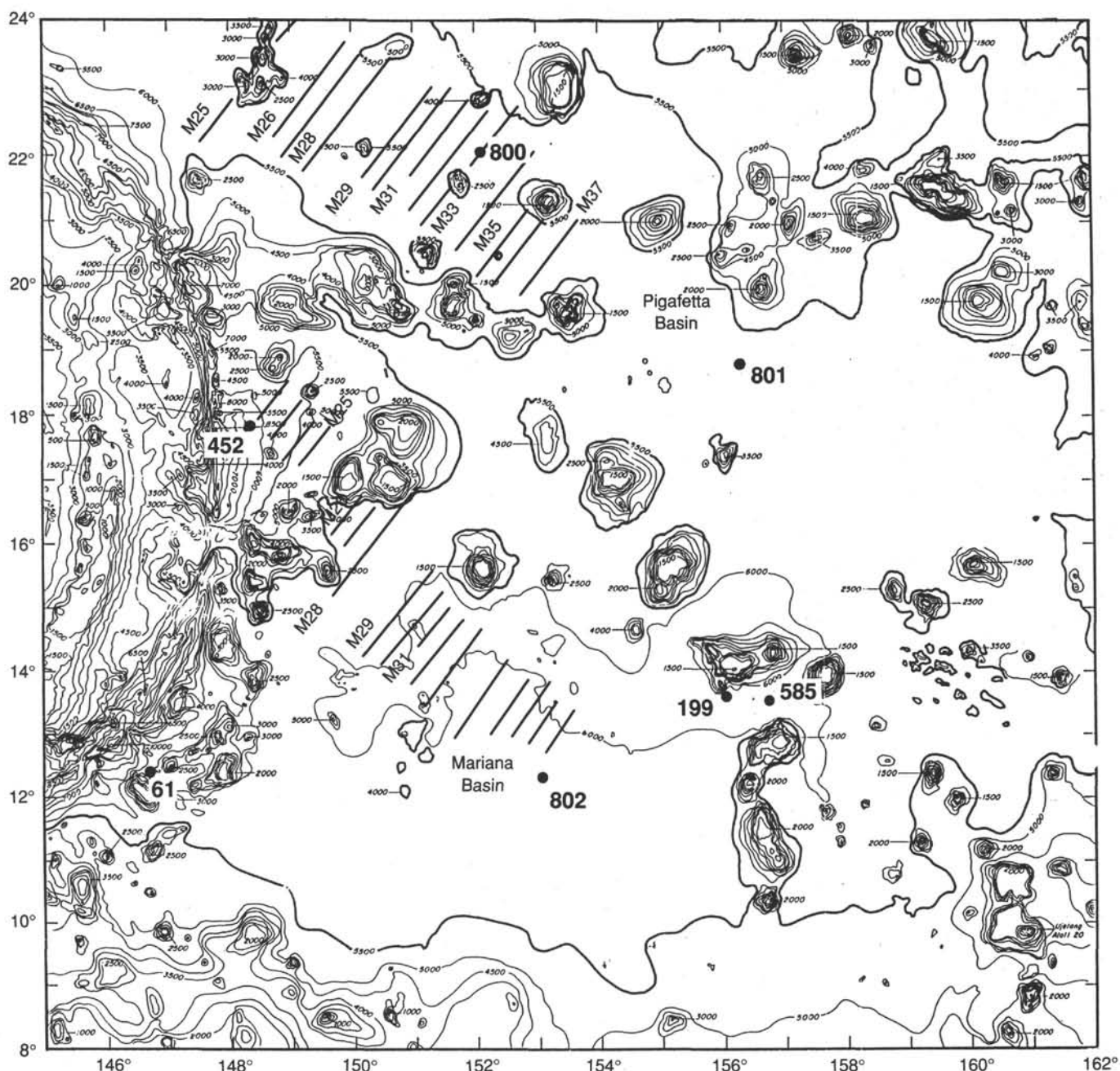
Figure 2. Bathymetry (in meters) of the central western Pacific (from M. Angell and C. Brenner, pers. comm., 1990) showing location of the Pigafetta and Mariana basins, ODP Sites 800, 801, and 802, DSDP Sites 199 and 585, and magnetic lineations, with seafloor topography. Magnetic anomalies modified from Handschumacher and Gettrust (1985), Tamaki et al. (1987), and Handschumacher et al. (1988).

ings predicted for this site was estimated to have occurred during the earliest Tertiary (Lancelot and Larson, 1975; Lancelot, 1978) and, therefore, siliceous pelagic deposits were anticipated to have been incorporated and somewhat diluted within the turbiditic sediments. As a consequence, we expect chert in that interval to be less concentrated than it is to the north. The oldest equatorial crossing, based on experience gained from the two previous sites that documented the geophysical predictions of Larson and Lowrie (1975), was expected to have occurred sometime during the Late Jurassic. We expected chert and possibly some limestone in the lowermost levels of the sediment column just above the basement.

Our strategy for this site was to drill a single-bit hole all the way to basement in order to achieve as much penetration as possible into the oceanic crust, and then to run a full suite of logs, while leaving enough time to sail back to Site 801 in order to fish the lost camera out of the reentry cone if necessary and drill approximately 100 m into the upper layers of the Jurassic crust.

OPERATIONS

Approach to the Site

We approached Site 802 from the north-northeast on course 203°, subparallel to MESOPAC II line 18, at 6 knots, shooting a seismic line with two 80-in.[3] water guns (Fig. 4). Our target was a point at 0030 hr (Universal Time Coordinated, or UTC), 18 November 1987, on FM35-12 line 7, 5 km
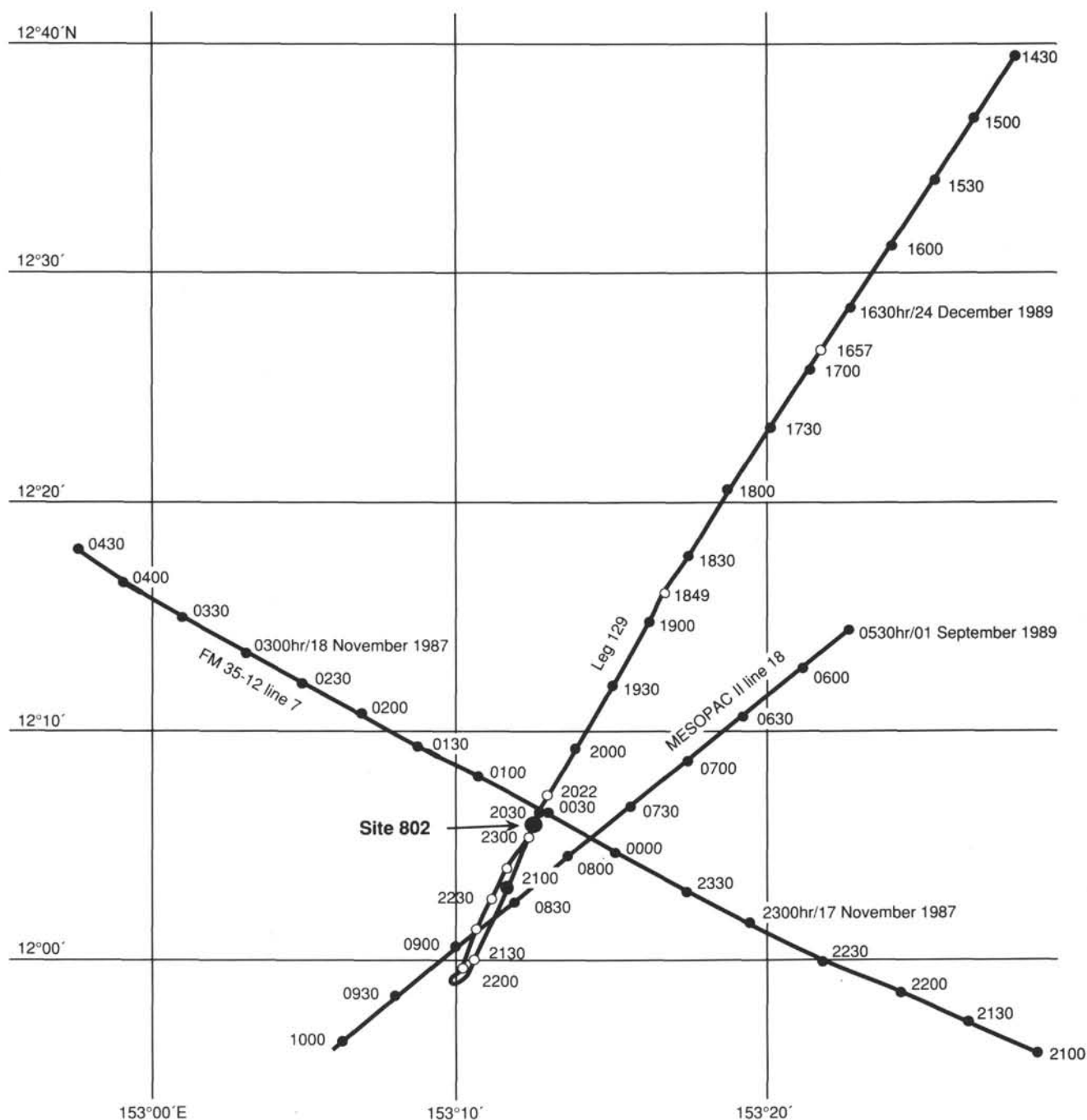
Figure 3. Time calibration plot of the Mesozoic anomalies M0 to M37 and the preceding Jurassic magnetic quiet zone (JQZ). Magnetic anomalies are plotted as cross-strike distance across the Hawaiian lineations for M0 to M25. Anomalies M25 to M37 are normalized to that parameter after Handschumacher et al. (1988). Geologic time scale and radiometric ages are from Harland et al. (1982), as modified by Kent and Gradstein (1985) at the Tithonian/Kimmeridgian boundary. Age ranges from Leg 129 Sites 800, 801, and 802 are also shown. Oldest paleontologic ages in various DSDP holes (numbered) shown as rectangles. Vertical lengths of rectangles show paleontological age ranges from DSDP *Initial Reports* except for Site 100 (Zotto et al., 1987) and Site 105 (Gradstein and Sheridan, 1983). Horizontal lengths show magnetic age ranges from Larson and Hilde (1975) for Sites 303, 304, 166, 100, and 105 and from DSDP *Initial Reports* for Sites 387 and 417D.

west of its intersection with MESOPAC II line 18. At 2035 hr, 24 December 1989, we crossed FM35-12 line 7 at the target location and continued on course for another 10 km, where we reversed course with a Williamson turn and returned toward the target location. At 2303 hr, 24 December 1989, we launched a beacon at 12°5.79′N, 153°12.59′E over a very clear seismic section on the system of the *JOIDES Resolution* (see Fig. 56, ''Site Geophysics and Seismic Stratigraphy'' section, this chapter) about 2 km south of the original target location.

Hole 802A

The bottom-hole assembly (BHA) for Hole 802A consisted of 120 m of 8¼-in. drill collars with a 3-m-long set of Hydrolex jars at 98 m, providing 40,000 lb drilling weight available below the jars. A Rock Bit International C4 coring

bit was chosen as the coring tool. The corrected depth obtained by the precision depth recorder at Hole 802A is 5988 m to the rig floor. The first core taken with the pipe lowered to 5985 m was coated with mud up a length of 5 m, so the mud line was established at 5980 m. We then cored ahead, recovering almost none of the first 21 m of soft pelagic ooze. At 21 mbsf the bit met a hard surface that proved to be very well-indurated, brown clay turbidites. The hard drilling continued, making the next 50 m of penetration a precarious operation. A combination of very light bit weight and slow rotation was used to ease the BHA down into the formation. The lithology quickly graded down into very fresh, coal-black volcaniclastics or reworked hyaloclastites with a high ash content below 40 mbsf. Hard drilling continued until about 100 mbsf, where a soft interval about

Figure 4. Track chart of expeditions FM35-12, MESOPAC II, and Leg 129. Site 802 is located on Leg 129 SCS line (2040 hr UTC, 24 December 1989) at approximately 2 km south of its intersection with FM35-12 line 7 and 4 km east of the intersection of FM35-12 line 7 (0010 hr, 18 November 1987) and MESOPAC II line 6 (0750 hr, 1 September 1989). Portions of each of these lines are displayed in Figures 53, 54, and 56.

20 m thick was cored, but mostly not recovered. Below that level, drilling alternated between hard and soft layers, although the recovery was dominated by the coal-black volcaniclastics or hyaloclastites. Inclination surveys were run at 71 mbsf and at subsequent 100-m intervals that showed 1° or less of hole inclination. At about 150 mbsf the drilling rate of penetration increased dramatically, indicating that we were now coring essentially soft sediment. Recovery was generally very poor in this section. It improved considerably below about 225 mbsf where the formation consists of moderately well-lithified, Miocene turbidites with a high carbonate content. From 300 to 330 mbsf we cored through Paleocene chalks and minor chert with moderate recovery. Recovery generally improved below 340 mbsf in Campanian volcaniclastics. Below 460 mbsf the volcaniclastics/turbidites graded down into alternating brown claystone, calcareous claystone, and radiolarite, with some black, volcaniclastic turbidites at the base of the sedimentary section. The recovery in the interval from 340 to 516 mbsf at the top of basalt was moderate, ranging from about 15% to 60%.

Solid basalt was encountered at 509 mbsf and it was the only lithology recovered from 509 mbsf to the bottom of the hole at 560 mbsf. Drilling records indicate that little, if any, sediment was encountered but not recovered in this interval. The basalt was entirely extrusive in nature and presented no problems for drilling other than a slow rate of penetration. The hole stood up well until just before the last core, when 43 m of fill was encountered in returning to the bottom of the hole after a short wiper trip. That fill, the slow rate of penetration, the uniform nature of the recovered basalts, and the arrival of the replacement television camera by supply boat led us to terminate coring at this point and rig for logging.

The bit was dropped without problem at the bottom of the hole, and the bottom of the pipe was raised to about 60 mbsf. No wiper run was made because of the previously mentioned hole instability. Standard logging was planned for this site using the same three tool strings as at the previous holes. On the first quad combination logging run-in, the tool encountered a bridge at 103 mbsf. We decided this section was too short to log, pulled the logging tool out of the pipe, and lowered the drill pipe to 127 mbsf, below the base of the clay zone that created the bridge. We then ran the quad combination tool string down the pipe a second time and encountered a second bridge at 323 mbsf. We decided to conduct logging in this clear section of hole and collected a quad combination log from 323 to 108 mbsf. We then ran the geochemical and formation microscanner tool strings, but encountered the same bridge and logged essentially the same interval.

Because the age of the oldest sediment above basalt at this site is about 60 m.y. younger than its predicted Jurassic age, the possibility exists that we drilled into a lava flow sequence that covers the original basement surface and perhaps the predicted older sediments. In order to test this possibility, we attempted to run a vertical seismic profile to look for seismic reflectors deeper than the basalt surface that we had sampled, which forms the most obvious, acoustic basement return on the multichannel seismic records across the site. The 400-in.[3] water-gun source was set up and hung off the port-side crane using two large flotation balls. The well seismic tool (WST) was then run into the hole, apparently about 60 m deeper than was reached by the previous tool strings. Although the water gun functioned normally when fired from the logging unit, the WST produced a low signal-to-noise level record despite repeated adjustments. We suspected that the caliper arms had been sheared off the tool while passing out of the bottom of the pipe. When we attempted to raise the tool we discovered that it was also stuck in the hole. Repeated pulls of about 9500 lb (4000 lb overpulls) failed to dislodge the tool. In order to recover as much cable as possible for potential logging runs at the last site, we attempted to sever the cable at the splice 500 m above the WST. The severing tool cut the cable, but on retrieval, we discovered that the cut had been made 3164 m above the WST. We then retrieved the remainder of the logging cable (including the severed section and the WST that were snagged in the BHA) and the drill string, and got underway for our return to Site 801.

LITHOSTRATIGRAPHY AND SEDIMENTOLOGY

Lithostratigraphy

Site 802 was continuously cored from the mud line at 5969.6 meters below sea level (mbsl) to a total depth of 559.8 mbsf. The stratigraphic section recovered from Hole 802A is divided into 10 lithologic units (I through X) based on composition and color (Fig. 5, Table 2). Unit I, very poorly recovered, is inferred to be 14.6 m of brown pelagic clay.

Subunit IIA is 146.0 m thick and consists dominantly of tuff deposited as mass flows, grain flows, and turbidites. Subunit IIB is 76.8 m thick and consists of tuff intercalated with a significant proportion of redeposited calcareous claystone and chalk. Unit III is a 92.5-m interval of nannofossil chalk with minor amounts of interbedded claystone and nodular chert. Unit IV is composed of 19.3 m of zeolitic pelagic claystone and calcareous nannofossil claystone with minor porcellanite, chert, and calcareous siltstone or sandstone. Unit V is 110.8 m thick and consists of volcaniclastic grain flows and turbidites that grade up into pelagic claystones containing both radiolarians and nannofossils. Unit VI is a 9.9-m interval of interbedded claystone and radiolarite. Unit VII is a 27.2-m-thick interval of predominantly calcareous lithologies, chiefly radiolarian limestone, nannofossil chalk, and calcareous claystone, with minor clayey sandstone, radiolarite, porcellanite, and chert. Unit VIII is contained entirely in Core 129-802A-56R and consists of 2.4 m of claystone with thin interbeds of radiolarite. Unit IX is 9.6 m thick and consists of volcaniclastic turbidites and tuffaceous claystone, with minor radiolarite. Unit X is a 50.6-m-thick series of basaltic pillow lava units and one thin flow unit. Because sediment accumulation rates for all units are calculated without including known hiatuses, the values are minimum sedimentation rates only. These calculations are for compacted sediments, as recovered.

Lithologic Units

Unit I. Cores 129-802A-1R through 129-802A-2R (0.0–14.6 mbsf): Pelagic Brown Clay; Quaternary to upper Pliocene

Unit I is composed of homogeneous dark brown pelagic clay. Smear slides show that the main constituents are clay and aggregates of metal-oxyhydroxides, with minor zeolites, micronodules, quartz silt, and radiolarian spines. Although Unit I is considered to extend from the mud line to 14.6 mbsf, recovery was less than 1 m, all from Core 129-802A-1R. The base of this unit is placed above the highest occurrence of tuff (Section 129-802A-3R-1, 0 cm).

Unit II. Core 129-802A-3R to Section 129-802A-27R-2, 81 cm (14.6–237.4 mbsf): Tuff (Volcaniclastic Turbidites); middle Pliocene(?) to lower Miocene

Subunit IIA. Tuff with pelagic clay, middle Pliocene to lower Miocene (Core 129-802A-3R to Section 129-802A-19R-2, 0 cm; 14.6–160.6 mbsf)

Subunit IIA is 146 m thick and consists dominantly of tuff deposited as mass flows, grain flows, and turbidites. Between the tuff beds are pelagic claystone layers representing background sedimentation. Lack of recovery in Core 129-802A-2R precludes speculation about the termination of the influx of volcaniclastic material. The base of Subunit IIA is gradational to Subunit IIB.

Tuff beds are massive and meter-scale in thickness. Overall, Subunit IIA is a sequence that is coarsening and thickening upward, from thin, 5- to 10-cm-thick turbidite beds at the base to mass flows several meters thick at the top. Locally, some beds have planar or cross-laminations, dish or pipe fluid-escape structures, and basal scours or flame structures. In general, beds are normally graded but very poorly sorted, with common lapilli isolated in the tuff matrix or concentrated in indistinct bands. Minor amounts of lapilli tuff (Fig. 6) are intercalated with the tuff; lapilli are subrounded and consist dominantly of volcanic ash (Fig. 7). Rarely are they calcareous, clayey, or palagonitic.

The tuff is very dark, ranging from black to greenish black, and consists of 60%–80% angular, fresh glass shards and
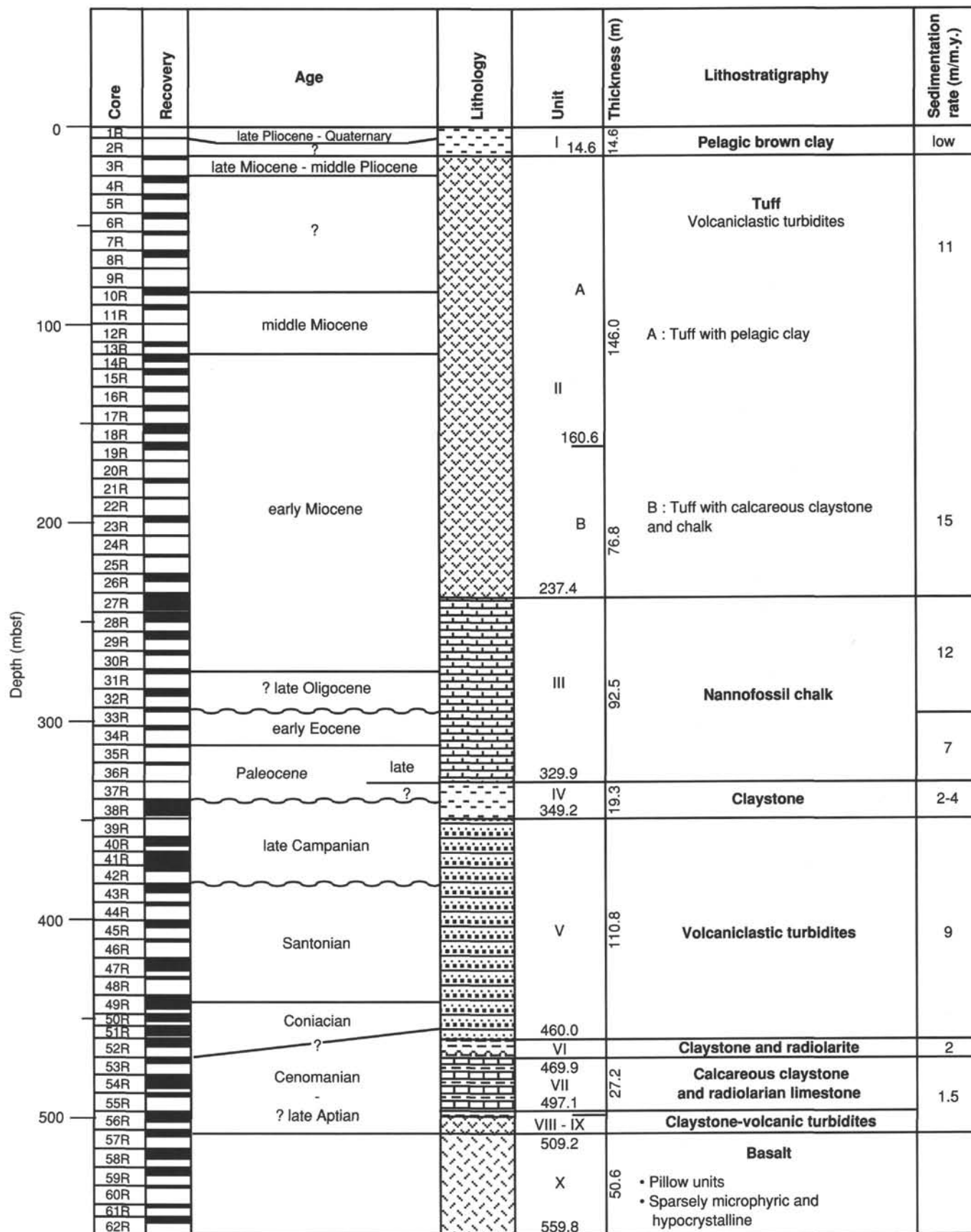
Figure 5. Stratigraphic summary of Hole 802A. (Note: Total depth is 5969 mbsl.)

Table 2. Lithology and ages of cores recovered from Hole 802A.

Core	Depth (mbsf)	Length cored (m)	Length recovered (m)	Major lithology	Age (downcore)
Unit I– Pelagic clay; Cores 129A-802A-1R and -2R (0–14.6 mbsf)					
1R	0.0–5.0	5.0	0.01	Pelagic clay	Quaternary to upper Pliocene
2R	5.0–14.6	9.6	0.00	Pelagic clay (no recovery)	?
Unit II – Tuff (volcaniclastic turbidites); Core 129A-802A-3R to Section 129A-802A-27R-2, 81 cm (14.6–237.41 mbsf)					
Subunit IIA – Tuff with pelagic clay; Core 129-802A-3R through Section 129-802A-9R-2, 0 cm (14.6–160.6 mbsf)					
3R	14.6–24.3	9.7	1.43	Tuff and pelagic clay	middle Pliocene to lower Miocene
4R	24.3–33.7	9.4	3.00	Tuff and lapilli tuff	
5R	33.7–42.9	9.2	1.93	Tuff (volcaniclastic sandstone)	
6R	42.9–52.4	9.5	2.58	Tuff (volcaniclastic sandstone) and lapilli tuff	
7R	52.4–61.9	9.5	1.46	Tuff to lapilli tuff (volcaniclastic sandstone/conglomerate)	?
8R	61.9–71.1	9.2	3.29	Tuff (volcaniclastic sandstone/siltstone)	
9R	71.1–80.4	9.3	0.00	Tuff (?, no recovery)	
10R	80.4–89.6	9.2	3.42	Tuff (volcaniclastic sandstone)	
11R	89.6–98.9	9.3	1.91	Tuff (volcaniclastic sandstone/siltstone)	
12R	98.9–108.3	9.4	0.13	Tuff (volcaniclastic sandstone)	middle Miocene
13R	108.3–114.4	6.1	1.67	Pelagic clay and tuff	
14R	114.4–122.1	7.7	3.37	Tuff (volcaniclastic sandstone turbidites)	
15R	122.1–131.1	9.0	2.87	Tuff (volcaniclastic sandstone turbidites)	
16R	131.1–140.4	9.3	2.00	Tuff (volcaniclastic turbidites)	
17R	140.4–149.7	9.3	2.13	Tuff (volcaniclastic turbidites)	
18R	149.7–159.1	0.4	4.20	Tuff (volcaniclastic sandstone)	
Subunit IIB – Tuff (volcaniclastic turbidites) with calcareous claystone and chalk Sections 129-802A-19R-2, 0 cm, to 129-802A-27R-2, 81 cm (160.6–237.41 mbsf)					
18R	(continued)			Tuff (volcaniclastic sandstone)	
19R	159.1–168.3	9.2	3.55	Tuff (volcaniclastic turbidites, clay); chalk	
20R	168.3–177.6	9.3	0.30	Tuff (volcaniclastic sandstone)	
21R	177.6–187.0	9.4	1.75	Tuff (volcaniclastic sandstone), claystone-siltstone	
22R	187.0–196.4	9.4	0.45	Tuff (volcaniclastic silty sandstone)	
23R	196.4–206.1	9.7	2.68	Tuff (volcaniclastic turbidites) nannofossil clay	lower Miocene
24R	206.1–215.7	9.6	0.17	Chalk; nannofossil clayey siltstone	
25R	215.7–225.4	9.7	1.07	Claystone with nannofossils	
26R	225.4–235.1	9.7	3.63	Clayey chalk; chalk; minor tuff-clay	
27R	235.1–237.4	9.6	8.15	Tuff (volcaniclastic sandstone)	
Unit III – Nannofossil chalk; Section 129-802A-27-2, 81 cm, to Core 129-802A-36R (237.41–329.9 mbsf)					
27R	(continued)			Chalk – debris flow	
28R	44.7–254.5	9.8	4.38	Graded bed – chalk to packstone	
29R	254.5–264.2	9.7	3.65	Claystone; calcareous claystone	
30R	264.2–273.8	9.6	1.63	Nannofossil chalk	
31R	273.8–283.5	9.7	1.95	Nannofossil chalk	?upper Oligocene
32R	283.5–292.8	9.3	3.37	Nannofossil chalk	
33R	292.8–302.3	9.5	1.64	Nannofossil chalk	lower Eocene
34R	302.3–311.5	9.2	1.40	Nannofossil chalk	
35R	311.5–320.7	9.2	1.04	Nannofossil chalk; chert	upper Paleocene
36R	320.7–329.9	9.2	1.12	Nannofossil chalk with foraminifers	

palagonite (Fig. 7). The glass is typically vesicular, sometimes spherulitic, and locally palagonitized. In thin section, the tuff contains up to 10% subhedral feldspar crystals, up to 15% clinopyroxene (augite), and rare olivine crystals, and ranges from crystal vitric tuff to vitric crystal lithic tuff. The tuff also contains a few percent to traces of igneous rock fragments,

tachylite, iron oxides, and opaques. Varying proportions of secondary smectites, zeolites, and calcite may constitute as much as 20% of the tuff. Coarser-grained beds contain planktonic and neritic benthic foraminifers (Fig. 7). The high percentage of glass shards and crystals and the freshness of the glass shards distinguish this tuff from Cretaceous volcani-

Table 2 (continued).

Core	Depth (mbsf)	Length cored (m)	Length recovered (m)	Major lithology	Age (downcore)
Unit IV – Claystone; Core 129-802A-37R to Section 192-802A-39R-1, 45 cm (329.9–349.2 mbsf)					
37R	329.9–339.2	9.3	0.19	Zeolitic pelagic claystone	Paleocene
38R	339.2–348.7	9.5	7.89	Zeolitic pelagic claystone; calcareous silty claystone	upper Campanian
39R	348.7–358.1	9.4	0.90	Porcellanite; claystone	
Unit V – Volcaniclastic turbidites; Sections 129-802A-39R-1, 45 cm, to 129-802A-52R-1, 15 cm (349.2–460.0 mbsf)					
39R	(continued)			Clayey chalk	
40R	358.1–365.5	7.4	4.58	Volcaniclastic turbidites, clay; porcellanite	
41R	365.5–372.8	7.3	5.85	Volcaniclastic claystone, siltstone	
42R	372.8–382.1	9.3	2.69	Volcaniclastic turbidites, claystone	
43R	382.1–391.3	9.2	3.90	Volcaniclastic turbidites, calcareous claystone	Santonian
44R	391.3–400.5	9.2	1.24	Silty claystone, claystone (volcaniclastic?)	
45R	400.5–410.0	9.5	3.53	Turbidites of silty claystone (volcaniclastic?)	
46R	410.0–419.2	9.2	1.34	Turbidites of silty claystone (volcaniclastic?)	
47R	419.2–428.7	9.5	6.16	Turbidites of silty claystone with radiolarians	
48R	428.7–438.1	9.4	0.99	Turbidites of volcaniclastic sandstone to nannofossil clay	
49R	438.1–447.4	9.3	6.85	Silty claystone; siltstone	
50R	447.4–453.5	6.1	3.15	Volcaniclastic silty claystone (debris flow)	Coniacian
51R	453.5–459.8	6.3	4.71	Claystone, debris flow	
52R	459.8–469.4	9.6	4.03	Claystone	
Unit VI – Brown claystone and radiolarite; Sections 129-802A-52R-1, 15 cm, to 129-802A-53R-1, 45 cm (460.0–469.9 mbsf)					
52R	(continued)			Claystone; clayey radiolarite	Coniacian-Cenomanian
53R	469.4–478.6	9.2	2.59	Claystone	
Unit VII – Calcareous claystone and radiolarian limestone; Sections 129-802A-53R-1, 45 cm, to 129-802A-56R-1, 0 cm (469.9–497.1 mbsf)					
53R	(continued)			Nannofossil chalk; clayey radiolarite	Cenomanian
54R	478.6–487.9	9.3	6.50	Limestone; calcareous claystone	
55R	487.9–497.1	9.2	1.48	Radiolarian limestone	Cenomanian to Albian
56R	497.1–506.6	9.5	5.11	Calcareous claystone	Albian to ?upper Aptian
Unit VIII – Claystone and radiolarite; Sections 129-802A-56R-1, 0 cm, to 129-802A-56R-2, 93 cm (497.1–499.6 mbsf)					
56R	(continued)			Claystone; radiolarite	upper Aptian
Unit IX – Volcaniclastic turbidites and claystone; Sections 129-802A-56R-2, 93 cm, to 129-802A-57R-2, 112 cm (499.6–509.2 mbsf)					
57R	506.6–516.0	9.4	3.34	Tuffaceous claystone; volcaniclastic turbidites	?
Unit X – Basalt; Section 129-802A-57R-2, 112 cm, to Core 129-802A-62R (509.2–559.8 mbsf)					
57R	(continued)			Basalt	
58R	516.0–525.4	9.4	5.02	Basalt	
59R	525.4–534.7	9.3	3.89	Basalt	
60R	534.7–544.2	9.5	0.96	Basalt	
61R	544.2–550.6	6.4	1.50	Basalt	
62R	550.6–559.8	9.2	3.10	Basalt	

clastic sediments at Sites 800 and 801, and from those lower at Site 802.

Lithologic trends in the tuff of Subunit IIA include a decrease in bed thickness downsection, and a less-pronounced decrease in grain size. Lapilli tuff is ubiquitous as a minor lithology. Microfossils were observed only in the tuff of

Cores 129-802A-10R to -19R. Miocene foraminifers and nannofossils are abundant in Core 129-802A-10R.

Fractures and voids in Cores 129-802A-7R and -8R, and Coares 129-802A-14R through -18R, are filled with a combination of white zeolites and anhydrite. X-ray-diffraction (XRD) analysis of one fracture filling indicates these zeolites
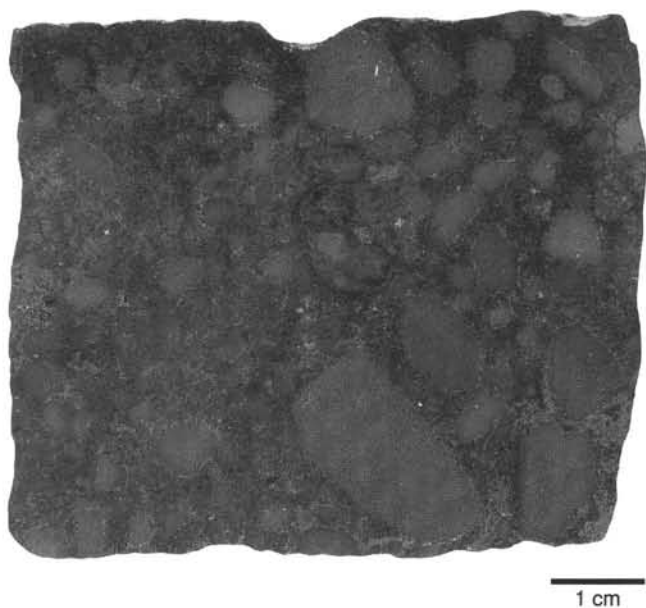
Figure 6. Photograph of lapillistone from tuff Subunit IIA, interval 129-802A-4R-1, 134–141 cm. (Note the subrounded clasts and poor sorting.)

include laumontite, analcime, and some members of the solid solution series between analcime and wairakite, which are calcium-rich varieties. Petrographic inspection shows the intergrowth and successive growth of zeolites and anhydrite (Fig. 8). XRD analysis also indicates the presence of phillipsite in tuff of Sample 129-802A-15R-1, 149 cm.

The tuff, redeposited as grain flows or turbidites, is sharply interbedded in Cores 129-802A-3R, -13R, and -19R with dark brown to greenish gray pelagic claystone. The claystone is massive to very finely laminated where it is not disturbed by drilling, and in Core 129-802A-3R contains up to 35% iron oxides and opaques, up to 15% zeolites, up to 10% volcanic glass, and, in one smear slide, 65% micrite. An agglutinated foraminifer and a trace of nannofossils were noted in single slides. Smear slides from Core 129-802A-13R contain up to 20% nannofossils, 10% volcanic glass, 5% zeolites, 5% iron oxides and opaques, and a few percent radiolarian spines. The claystone in Core 129-802A-19R contains 30% nannofossils, 20% volcanic glass, and only traces of metal oxides. Therefore, a general downhole decrease in the metal component and an increase in nannofossil content are observed. The nannofossil claystone in Core 129-802A-19R also indicates a transition to the nannofossil chalk that characterizes Subunit IIB and Unit III. XRD analyses indicate that the claystone contains various zeolites, clinoptilolite or phillipsite, and accessory minerals, possibly barite and celestite.

The calculated minimum sedimentation rate for Subunit IIA is 11 m/m.y.

Subunit IIB. Tuff with calcareous claystone and chalk; lower Miocene (Sections 129-802A-19R-2, 0 cm, to 129-802A-27R-2, 81 cm; 160.6–237.41 mbsf)

Subunit IIB is 76.8 m thick and consists of tuff intercalated with a significant proportion of redeposited calcareous claystone and chalk. The upper and lower boundaries of this subunit are gradational. Tuff is not present in every core, but its presence defines Unit II. The base of Subunit IIB is placed at the lowest occurrence of volcaniclastic sandstone, and the top is placed at the highest occurrence of chalk.
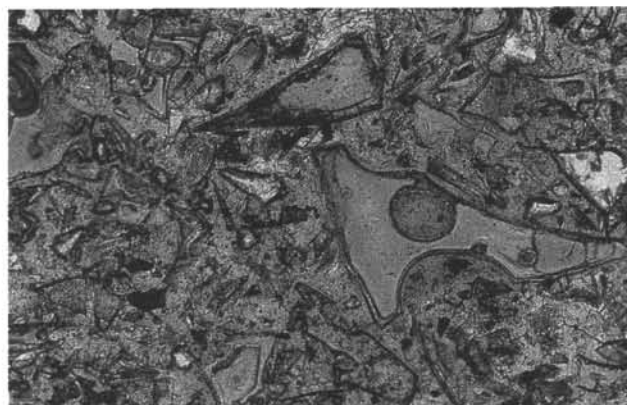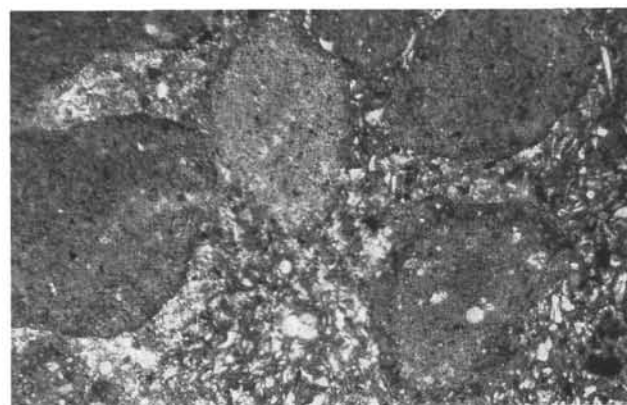
Figure 7. Photomicrographs of thin sections from tuff Subunit IIA. **A.** Sample 129-802A-5R-1, 21–22 cm, plane light, showing cuspate glass shards. **B.** Sample 129-802A-11R-1, 64–66 cm, plane light, showing Miocene foraminifers and volcanic glass. **C.** Sample 129-802A-11R-1, 64–66 cm, plane light, showing rounded lapilli composed of ash in vitric tuff matrix.

A

100 μm

B

100 μm
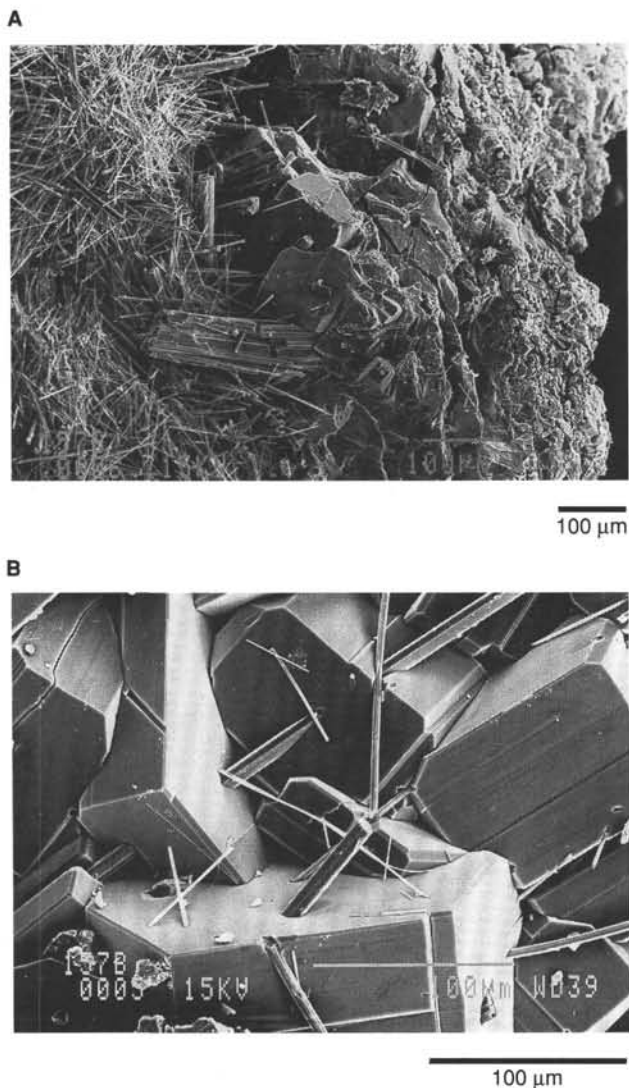
Figure 8. Scanning electron photomicrographs of fracture-filling in tuff, Subunit IIA, interval 129-802A-15R-2, 105–114 cm. **A.** Note the sequence inward from the edge of the fracture, right to left, of microcrystalline host rock, blocky sodium-calcium zeolite, and acicular anhydrite crystals. **B.** The inward growth of zeolite, then anhydrite, was not completely sequential. Note the intergrowth of zeolite and anhydrite needles.

The tuff is grayish green to gray, mostly massive, and finely laminated in places. It is poorly to moderately sorted, fine- to coarse-grained with lapilli and rip-up clasts up to 3 cm in diameter. Massive beds with sharp contacts are mass flows and grain flows (Fig. 9); beds that grade to glass-rich claystone or chalk are turbidites (Fig. 10). Thin sections of the volcaniclastic deposits indicate that Core 129-802A-19R contains crystal vitric tuff consisting of approximately 70% volcanic glass and 5% clinopyroxene, with 20% igneous rock fragments, and a few percent of smectites, secondary calcite, and trace foraminifers. The base of Subunit IIB, in Core 129-802A-27R, is a tuffaceous sandstone that contains about 55% volcanic glass, 10% igneous rock fragments, a trace of clinopyroxene, and about 30% benthic and planktonic foraminifers, bryozoans, red and green algae, nannofossils, and microspar calcite (Fig. 11). There are wood fragments in the core catcher of Core 129-802A-25R.
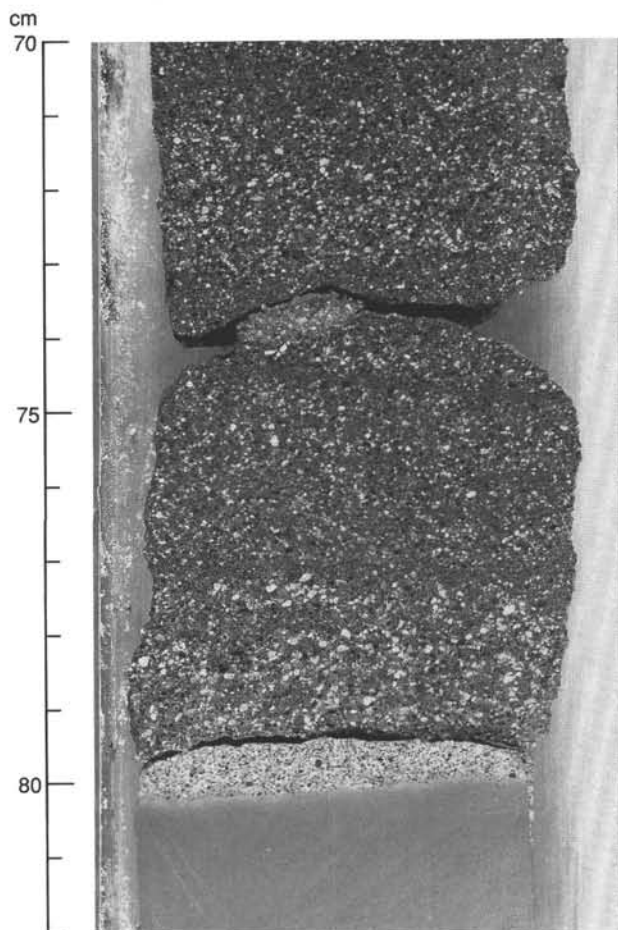
Figure 9. Photograph of contact at base of Subunit IIB, interval 129-802A-27R-2, 70–82 cm. Note 1 cm of alteration to white zeolites at contact, grading, and indistinct laminations in tuff. Below contact is nannofossil chalk of Unit III.
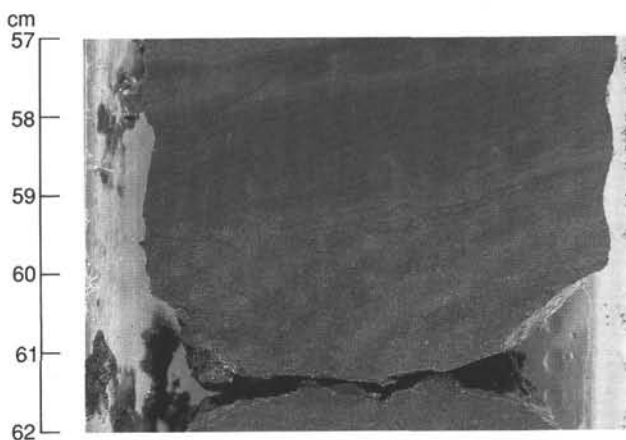
Figure 10. Photograph of tuffaceous turbidites from Subunit IIB, interval 129-802A-19R-2, 57–62 cm, showing flame structures and deformed (convoluted) laminations.

Tuffaceous claystone in Subunit IIB is dark gray to dark greenish gray, consisting of roughly 40% clay, 30% volcanic glass, 15% igneous rock fragments, and 5% nannofossils and calcite. It grades to claystone composed of about 80% clay, 10% volcanic glass, and 10% opaques, crystals, and igneous rock fragments, or to olive gray clayey chalk composed of 35% clay, 30% nannofossils, 20% secondary calcite, 10% volcanic glass, and 5% igneous rock fragments.

The chalk grades locally to clayey chalk with up to 25% clay and 5% volcanic glass. It is olive gray to pale brown, and contains up to 50% nannofossils, 20% secondary calcite, and 15% clay, with a few percent volcanic glass, radiolarians, foraminifers, fish remains, and zeolites. The chalk is found in Core 129-802A-19R and from Core 129-802A-24R to -27R in Subunit IIB, and is thus more prevalent near the basal contact with the underlying chalk (Unit III). The chalk is massive, moderately bioturbated, and contains up to 10% angular to subrounded rip-up clasts up to 1 cm long of moderate yellowish brown calcareous claystone, indicating that it consists predominantly of redeposited pelagic sediments.

A
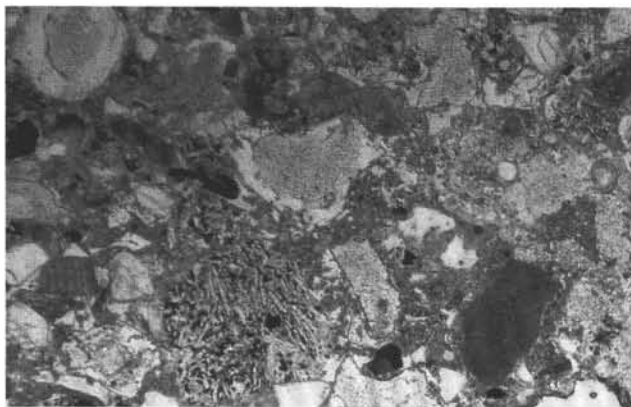
0.5 mm

B

0.5 mm

Figure 11. Photomicrographs of thin section from base of Subunit IIB. **A.** Sample 129-802A-27R-2, 73–78 cm, plane light, showing igneous rock fragment and shallow-water carbonate debris, including red algae, echinoderm fragments, and coated grain. **B.** Photomicrograph in plane light showing bryozoans, foraminifers, and other shallow-water carbonate debris, tachylite, and igneous rock fragments.

The calculated minimum sedimentation rate for this unit is 15 m/m.y.

Unit III. Section 129-802A-27R-2, 81 cm, to Core 129-802A-36R (237.4–329.9 mbsf): Nannofossil Chalk; lower Miocene to upper Paleocene

Unit III is a 92.5-m-interval of nannofossil chalk with foraminifers and minor amounts of interbedded foraminiferal chalk, claystone, porcellanite, and nodular chert. As tuff and chalk are intercalated throughout much of Subunit IIB, the top of Unit III is placed at the base of the lowest tuffaceous turbidite. The base of this unit is set between the lowest chalk and the top of the nearly continuous claystone of Unit IV. Unit III is thickly bedded, with beds ranging from 10 cm to 5.5 m, most of which are between 50 and 80 cm thick. Many strata are graded, with thinly laminated or cross-laminated bases defined by foraminiferal fragments. Bioturbation is common throughout, with burrows especially numerous near the top of beds. The chalk contains many small flakes or clasts of claystone or mudstone. Bedding characteristics and mixed assemblages of Late Cretaceous through Oligocene nannofossils suggest that these chalks are redeposited and reworked nannofossil oozes, not *in-situ* pelagic deposits.

The nannofossil chalk trends from light brown to light grayish brown in Cores 129-802A-27R to -33R, to light gray to pinkish white in Cores 129-802A-34R to -36R. The change in color at Core 129-802A-33R corresponds with a downhole increase in silica and a change in associated minor lithologies from zeolitic claystone (upper half) to nodular chert (lower half). An Oligocene through Eocene hiatus was recognized between Sections 129-802A-32R-CC and 129-802A-33R-CC on the basis of nannofossils and foraminifers (see "Biostratigraphy" section, this chapter). Foraminifers are common in the chalk, usually comprising 5%–20%, and locally up to 35% of the sediments, in which case it is designated foraminiferal chalk (Fig. 12A, -B). Thinly laminated (millimeter- to centimeter-scale) chalk turbidites toward the base of the unit are composed of foraminifer-rich layers overlying micrite-rich layers with exceedingly small (1 mm high) flame structures (Fig. 13). Hard silicified chalks with subconchoidal fractures that are present in Cores 129-802A-35R and -36R contain 10%–25% replacement microquartz.

Thinner beds, 5 to 50 cm thick, of dark brown zeolitic claystone are interbedded with the nannofossil chalk in the upper half of this unit (237.4–284.3 mbsf). The claystone is extensively bioturbated, and claystone fills burrows in the tops of underlying, lighter-colored chalk beds (Fig. 14). Smear slides show that the claystone contains 50%–80% clay, 10%–30% zeolites, up to 10% volcanic glass and oxides, and a few percent radiolarians or nannofossils. The complete bioturbation of chalk and zeolitic claystone in Core 129-802A-29R produced some nearly homogeneous beds of light yellowish brown nannofossil claystone.

Chert comprises less than 3% of the total recovery of Unit III, and occurs as scattered nodules only in the lower portion of the unit, from 293 to 321.7 mbsf. The chert is dark brown to dark red to olive gray, with a vitreous luster and conchoidal fracture. Chert nodules have sharp, irregular contacts with the nannofossil chalk. They contain abundant calcareous inclusions and usually reflect the locally massive or laminated structure of the host chalk. Only a few pieces of porcellanite were recovered in Core 129-802A-32R, immediately above the hiatus in the upper part of the unit.

Cores 129-802A-27R and -28R are distinguished by the thickest single bed recovered in the unit: a 5.5-m graded bed that fines upward from a grain-supported algal foraminiferal packstone to a matrix-supported nannofossil chalk (base of
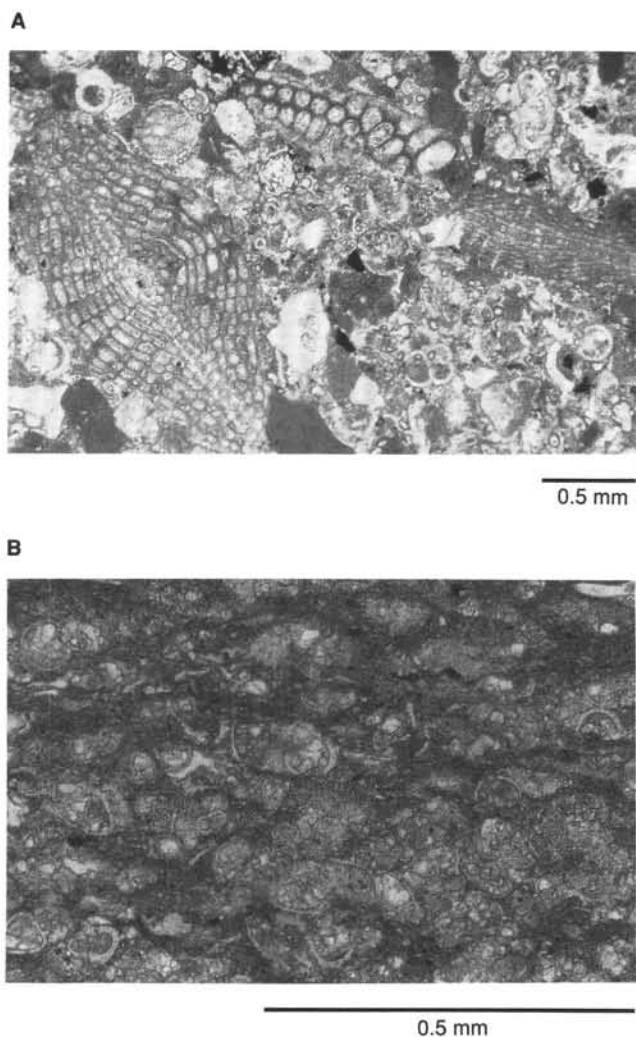
A

0.5 mm

B

0.5 mm

Figure 12. **A.** Photomicrograph of thin section from Unit III, Sample 129-802A-28R-3, 117–122 cm, plane light, showing algal foraminiferal packstone with foraminifers, bryozoans, and other shallow-water carbonate debris. **B.** Photomicrograph of thin section from the base of Unit III, Sample 129-802A-36R-1, 61–63 cm, plane light, showing a lamination of densely packed, broken foraminifers in chalk turbidite.

Figure 13. Photograph of thinly laminated chalk turbidites from the base of Unit III, interval 129-802A-36R-1, 23–31 cm. Light laminations are foraminifer-rich; darker laminations are dominantly micrite.

Core 129-802A-28R to Section 129-802A-27R-5, 100 cm). The very coarse-grained lower half is composed chiefly of neritic benthic foraminifers and red algae, along with planktonic foraminifers (see ''Biostratigraphy'' section, this chapter), bryozoans, echinoid fragments, and volcanic rock fragments in a nannofossil and micrite matrix (Fig. 12A). The upper part of the bed is a deformed, horizontally sheared nannofossil chalk with abundant fine-grained rip-up clasts and incorporated coarse-grained carbonate material similar to that found at the base of the bed (Fig. 15). This very thick gravity-flow deposit directly underlies the mixed tuffaceous/bioclastic turbidites at the base of Subunit IIB.

The calculated minimum sedimentation rate is about 12 m/m.y. above the Oligocene through Eocene hiatus, and about 7 m/m.y. below.

Unit IV. Core 129-802A-37R through Section 129-802A-39R-1, 45 cm (329.9–349.2 mbsf) Claystone; Paleocene to upper Campanian

Unit IV consists of 19.3-m beds of zeolitic pelagic claystone and calcareous nannofossil silty claystone with minor porcellanite, chert, and calcareous siltstone or sandstone. The top of this unit is placed below the lowermost chalk bed; the lower boundary is set at the top of the highest occurrence of Cretaceous volcaniclastics. The upper part of this unit (329.9–345.8 mbsf) contains interbedded zeolitic pelagic claystone and calcareous siltstone or sandstone. The pelagic claystone is very similar to that of Unit I, containing 15%–40% zeolites and 3%–10% radiolarian spines and tests, with the remainder made up of aggregates of clay and iron-manganese oxyhydroxides; it is mottled light brown to gray. This entire section is thinly laminated and burrowed. Layers of thinly laminated, gray and black calcareous siltstone or sandstone, 2 to 5 cm thick, or millimeter-scale interlaminated sandstone and claystone, make up the graded bases of pelagic claystone beds. Flame structures, basal cross-lamination, and convolute layering indicate that the coarser-grained material was redeposited. Silt and sand grains are composed of foraminifers, volcanic material, and some radiolarians. One piece of pale yellowish brown chert (silicified claystone) was recovered in Core 129-802A-37R.

The lower section of Unit IV (345.8–349.2 mbsf) is composed of calcareous nannofossil silty claystone and porcellanite. The brown to olive gray silty claystone is massive to thinly laminated with some small flame structures, distinctly lacking in burrows, and composed of 10%–25% nannofossils and 5%–10% micrite. The porcellanite is reddish brown, thinly laminated, and contains scattered dark grains of metal oxides.

The calculated minimum sedimentation rate of 2 to 4 m/m.y. for this unit probably reflects a Paleocene through upper Campanian hiatus.

Unit V. Sections 129-802A-39R-1, 45 cm, to 129-802A-52R-1, 15 cm (349.2–460.0 mbsf): Volcaniclastic Turbidites; upper Campanian to Coniacian-Cenomanian

Unit V is 110.8 m thick and consists of volcaniclastic grain flows and turbidites that grade up into pelagic claystones
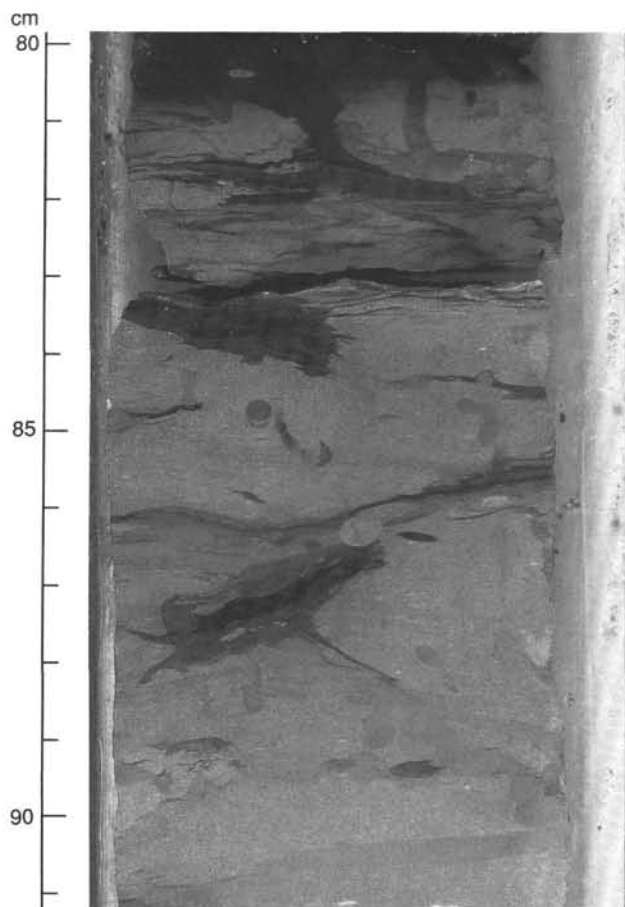
Figure 14. Photograph of burrows at the top of chalk turbidite filled with pelagic clay from Unit III, interval 129-802A-32R-1, 80–91 cm.
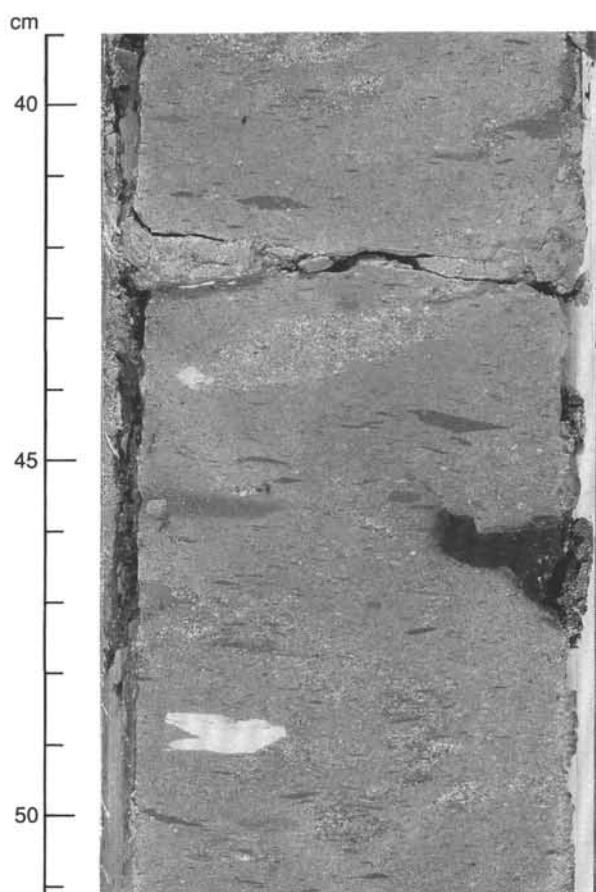

Figure 15. Photograph of chalk debris flow deposit from top of Unit III, interval 129-802A-27R-5, 39–51 cm, showing matrix-supported fragments of claystone and coarser-grained carbonate material.

containing both radiolarians and nannofossils. The top of the unit is placed at the level of the highest tuffaceous sandstone bed in Core 129-802A-39R, which also corresponds to a downhole color change from green to brown and gray. The base of the unit is placed at the lowermost claystone that still contains significant amounts of volcanic glass. It corresponds to a downhole color change from green (Unit V) to brown (Unit VI). Both unit boundaries are gradational.

The volcaniclastic sandstones, siltstones, and claystones in Unit V are generally dark blue-gray to greenish gray. The lowest beds in the unit are debris flow deposits composed of pebbly claystone up to several meters thick. These give way upsection to coarser-grained (silty and sandy) but thinner-bedded turbidites (Fig. 16). The turbidites vary from 10 cm to 1 m thick; there are no overall stratigraphic trends of thinning or fining upward in this unit. The turbidites are characterized by sedimentary structures such as graded beds with basal scour, flame structures or load casts, planar- and cross-laminations, convolute layers (Fig. 17), and rip-up clasts. Some beds are bioturbated. The pelagic claystones between turbidite beds are finely laminated to massive.

The volcaniclastic sandstones include some tuff, but are mostly tuffaceous sandstones with abundant, rounded igneous rock fragments of unknown derivation. A thin section of tuffaceous sandstone in Sample 129-802A-39R-1, 52–55 cm (Fig. 18A), contains roughly 60% volcanic glass and palagonite, 15% igneous rock fragments, 10% iron oxides and opaques, 5% clinopyroxene, 5% feldspar, and a few percent each of second-

ary calcite, smectites, radiolarians, and red algae. Tuffaceous claystones in the unit contain up to 35% volcanic glass and 15% igneous rock fragments, a few percent radiolarians and/or nannofossils, and as much as 25% secondary calcite. These tuffaceous claystones grade to pelagic claystones containing up to 20% radiolarians or nannofossils (Fig. 18B). A clayey radiolarite in Sample 129-802A-51R-3, 14 cm, marks a transition to the underlying claystone and radiolarite unit. A rip-up clast of radiolarite in the debris flow in Sample 129-802A-49R-3, 25 cm, is probably derived from the underlying unit. At the top of the unit, in Sample 129-802A-39R-1, 64–89 cm, is the only clayey chalk in Unit V, consisting of 60% nannofossils, 25% clay, 5% volcanic glass, and a few zeolites. This chalk is overlain by 10 cm of tuffaceous claystone with 15% radiolarians, in turn overlain by the uppermost tuffaceous sandstone in the unit. The chalk marks a transition to the overlying claystone and nannofossil chalk units.

Diagenetic minerals in Unit V include various zeolites which are present in both the sandstones and claystones. The claystone also contains rather remarkable blades of celestite(?), up to 6 mm long, in interval 129-802A-49R-4, 59–72 cm, and green spherules composed of celadonite or glauconite in Sections 129-802A-41R-2 and 129-802A-41R-3. The volcanic glass in the sandstones is 30% to 50% palagonitized; volcanic glass in the claystones is almost entirely palagonitized.

The calculated minimum sedimentation rate is 9 m/m.y., with a probable brief hiatus in the lower Campanian.
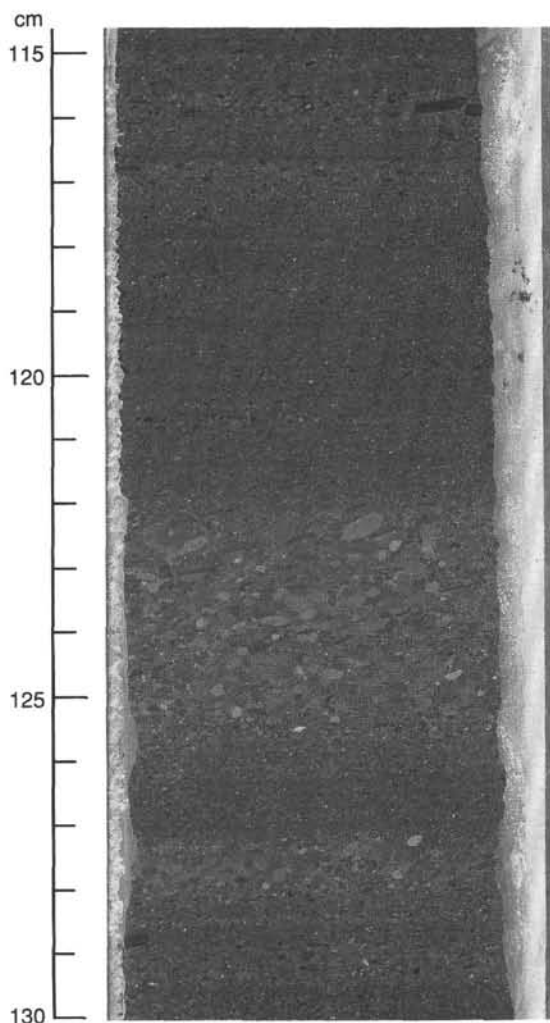
Figure 16. Photograph of volcaniclastic turbidites from Unit V, interval 129-802A-40R-2, 115–130 cm, showing normal- and reverse-graded layering.

Unit VI. Sections 129-802A-52R-1, 15 cm, to 129-802A-53R-1, 45 cm (460.0–469.9 mbsf): Claystone and Radiolarite; Coniacian to upper Aptian

Unit VI is a 9.9-m-interval of interbedded brown claystone and radiolarite. The top of the unit is placed between the lowermost bluish gray volcaniclastic deposits and the uppermost reddish brown claystone; the base of the unit is set at the top of the underlying nannofossil chalk. Both lower and upper boundaries are gradational.

The reddish brown to dark brown claystone occurs in thick, mostly massive beds (40 to 125 cm thick; 65 cm is average), and is thinly interlayered with radiolarite. The claystone has a composition similar to pelagic clay, containing approximately 70% clay, 30% iron-manganese oxides, minor zeolites, and minor radiolarians concentrated in some layers, which provide a locally slightly sandy texture. Thin (<1 mm), discontinuous black layers, producing a distinct horizontal fabric in the interval 129-802A-52R-1, 80–140 cm, are composed of up to 50% iron-manganese oxides. Centimeter-scale, light green reduction halos surround a few dark green, pyritic concretions, 1–2 mm in diameter.

Radiolarite occurs as laminations to thin beds that are 0.3–4.0 cm thick, light grayish green to light brown, and interlayered

with claystone. The radiolarite contains trace to abundant (50%) clay, with the radiolarians providing a friable, sandy texture (Fig. 19). Contacts with the claystone are mostly sharp, but some are gradational (Fig. 20). The inferred, relatively high permeability of the radiolarite layers may control the location of greenish bands of reduction that occasionally blossom discordantly outward into the neighboring claystone.

The calculated minimum accumulation rate for Unit VI is 2 m/m.y.

Unit VII. Sections 129-802A-53R-1, 45 cm, to 129-802A-56R-1, 0 cm (469.9–497.1 mbsf): Calcareous Claystone and Radiolarian Limestone; Cenomanian to upper Aptian

Unit VII is a 27.2-m-thick interval of predominantly calcareous lithologies, chiefly radiolarian limestone, nannofossil chalk, and calcareous claystone, with minor clayey sandstone, radiolarite, porcellanite, and chert. This unit contains fine-grained calcareous turbidites and radiolarian silty sand layers. Bedding is quite variable, ranging from 2 to 135 cm thick, averaging 35 cm thick. Beds range from laminated to massive; many are gently graded with burrowed tops. Turbiditic deposition is chiefly indicated only by a color change to darker clay-rich tops and by sharp bedding contacts (Fig. 21). The boundaries of this unit are placed at the highest and lowest occurrences of carbonate rocks.

The limestone is dark brown to light gray to bluish gray, and contains 10%–35% clay, 10%–30% nannofossils, and 5%–25% calcitized radiolarians. Some of the limestone is silicified, especially where it is adjacent to brown chert and pinkish gray porcellanite in Cores 129-802A-54R and -55R, respectively.

The nannofossil chalk varies widely in composition, with 40%–70% nannofossils, 5%–25% clay, 7%–15% volcanic glass, and up to 5% foraminifers. The chalk is light brown to pinkish brown, mostly massive to thinly laminated, in graded beds with sharp, sometimes scoured bases. The calcareous claystone occurs in numerous shades of grayish blue and green; it is thinly laminated and displays few burrows. The claystone contains 20% nannofossils, 15% micite and calcite, and a few percent foraminifers and radiolarians.

Brown to light reddish brown radiolarite, and bluish gray to greenish gray clayey siltstone and sandstone, make up thin, 2-cm-thick layers between limestone or claystone beds. The coarser texture of the clayey siltstone and sandstone is derived from the presence of foraminifers, radiolarians, volcanic glass, and zeolites. All lithologies are thinly laminated, but the siltstone and sandstone often have sharp, scoured bases, and the radiolarite layers commonly have gradational clay-rich upper and lower boundaries.

A minimum accumulation rate is calculated for Units VII, VIII, and IX together because the resolution of the biostratigraphy is inadequate for discrete calculations for individual units. The average accumulation rate for this lowest part of the stratigraphic section is low, approximately 1.5 m/m.y.

Unit VIII. Sections 129-802A-56R-1, 0 cm, to 129-802A-56R-2, 93 cm (497.1–499.6 mbsf): Claystone and Radiolarite; Cenomanian to upper Aptian

Unit VIII is contained entirely in Core 129-802A-56R and is composed of 2.4 m of claystone with thin interbeds of radiolarite. The unit is bounded by carbonates above and volcaniclastic turbidites below.

The claystone is light brown to dusky yellowish brown, pervasively thinly laminated, with common burrows. It is hematitic, containing 10%–25% iron oxides, up to 10% zeolites, as well as abundant dark metalliferous nodules (sometimes with pyrite), 1–2 mm in diameter. The occurrence of these nodules shows some association with bioturbation.
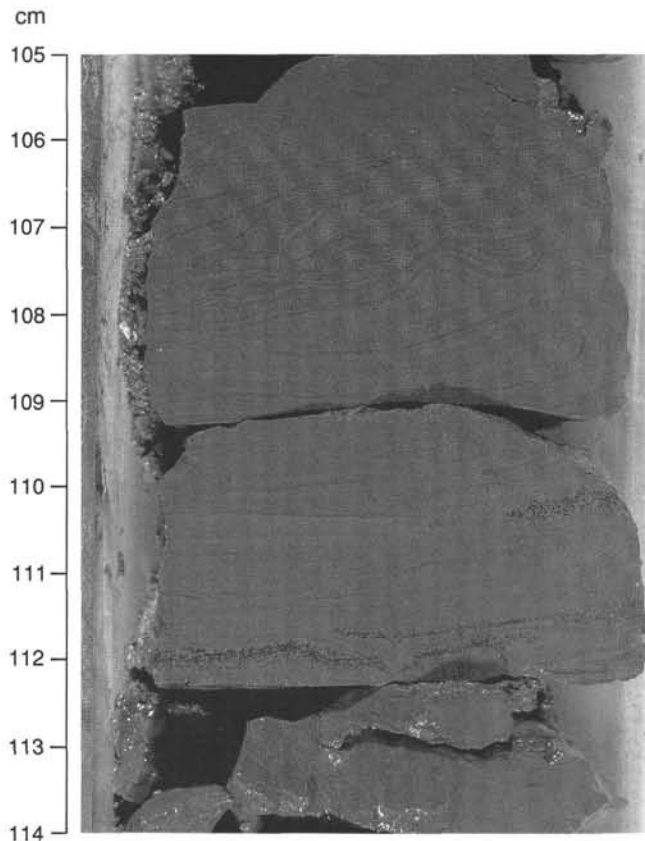
cm

Figure 17. Photograph of deformed (convolute) layers in fine-grained volcaniclastic turbidites from Unit V, interval 129-802A-15R-2, 105–114.

Radiolarite beds, 1 to 4 cm thick, are scattered through the claystone (Fig. 22), making up about 10% of the recovered interval. The radiolarite is light to moderate brown and friable, with a medium-grained sandy texture. Layers are sometimes graded, with sharp tops and bottoms, but not with scoured bases. Interval 129-802A-56R-2, 80–83 cm, is reduced and bleached to olive green.

Unit IX. Sections 129-802A-56R-2, 93 cm, to 129-802A-57R-2, 112 cm (499.6–509.2 mbsf): Volcaniclastic Turbidites and Claystone; Cenomanian to upper Aptian

Unit IX is 9.6 m thick and consists of volcaniclastic turbidites and tuffaceous claystone, with minor radiolarite. The top of the unit is placed at the highest occurrence of green, volcaniclastic material; the base of the unit is placed at a sharp depositional contact on pillow basalt. Both unit boundaries are sharp, but the presence of radiolarite in Sections 129-802A-56R-3 and 129-802A-56R-4 links Unit IX environmentally with Unit VIII (claystone and radiolarite).

The volcaniclastic turbidites consist of 2- to 25-cm-thick beds of tuffaceous sandstone grading to radiolarian claystone. The turbidites have sharp, scoured bases and are pervasively bioturbated. The tuffaceous claystone is finely laminated to massive, and commonly burrowed (Fig. 23). The turbidites are greenish gray to dusky green and composed of igneous rock fragments, volcanic glass, smectites, opaques, a trace of nannofossils, and up to 20% radiolarians. The tuffaceous claystone is brownish black to black, and contains approximately 50% volcanic glass, abundant smectites, and minor amounts of igneous rock fragments and metal oxides or opaques.

A

B
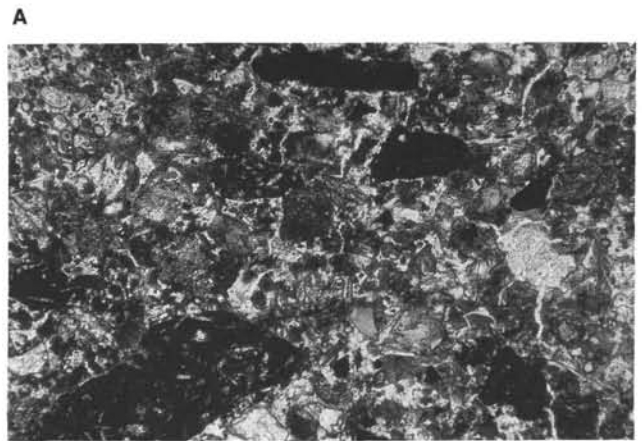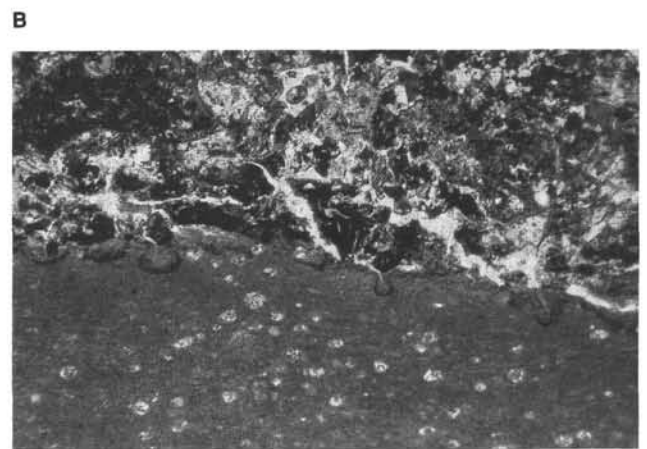
Figure 18. **A.** Photomicrograph of volcaniclastic sandstone thin section from Unit V, Sample 129-802A-39R-1, 52–55 cm, plane light, showing poorly sorted volcanic rock fragments and palagonite. **B.** Photomicrograph of same thin section showing contact of volcaniclastic sandstone above radiolarian claystone, with zeolitic alteration at contact.

Radiolarite intercalated with the tuffaceous claystone is light to moderate brown, and locally reduced to olive green. The beds are planar, laminated, with sharp (but not scoured) contacts, and subtly graded. The laminations, together with the low clay content, suggest deposition by currents and possible winnowing of fines.

Diagenetic features in Unit IX include prolific crystallization of dark green clay minerals in burrows within the turbidites, silicification of the radiolarian-rich tops of the turbidite beds, and convoluted and faulted calcite veins in the tuffaceous claystone.

Unit X. Section 129-802A-57R-2, 112 cm, to Core 129-802A-62R (509.2–559.8 mbsf): Basalt; upper Aptian(?)

Unit X is a 50.6-m-thick series of thin (<1–2 m thick) basaltic pillow lava units and one thin (4 m thick) basaltic flow unit. Seventeen units are described in the "Igneous Petrology" section (this chapter). Alteration is slight and dominated by smectites, carbonate, and pyrite, characteristic of low-
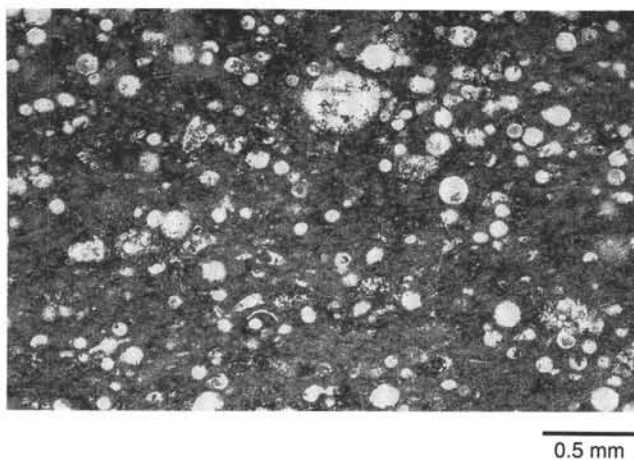
Figure 19. Photomicrograph of siliceous clayey radiolarite from Unit VI, Sample 129-802-53R-1, 4–6 cm, showing matrix-supported texture.
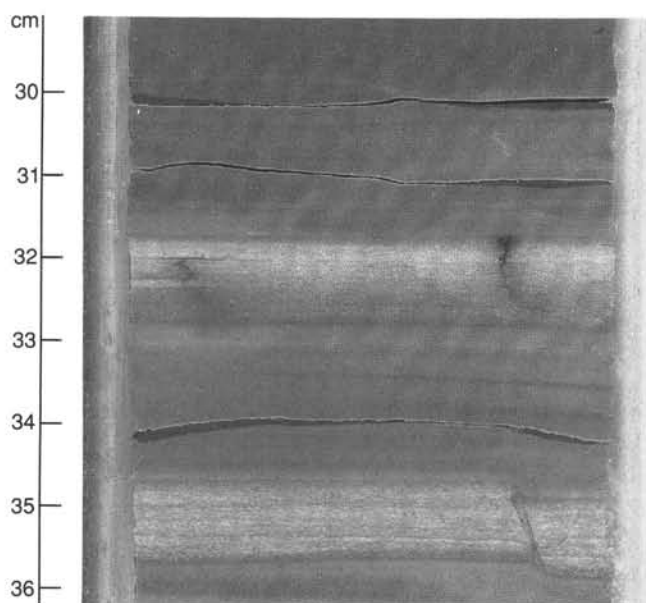

Figure 20. Photograph of alternating radiolarite and claystone layers in Unit VI, interval 129-802A-52R-2, 30–36 cm, showing sharp contacts and laminations in radiolarite.
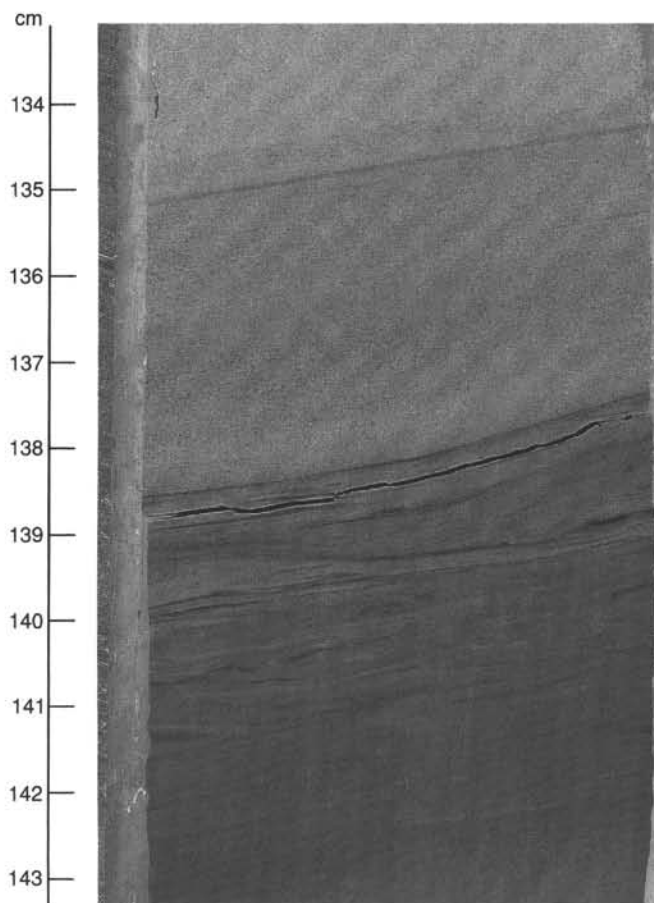

Figure 21. Photograph of calcareous claystone and radiolarian limestone turbidites of Unit VII, interval 129-802A-54R-1, 134–143 cm.

grade, submarine "weathering" under mildly alkaline, reducing conditions.

Sedimentology

Sedimentological observations and their implications are presented below in chronological order, or from the base of Hole 802A to the top, and followed by a brief sedimentation history of this site. The Cretaceous basaltic flows at the base of the hole may overlie older sedimentary deposits, so the history presented here could represent only the later history of the eastern Mariana Basin.

The main implications of sedimentary features observed at Site 802 include the following:

1. The stratigraphic section at Site 802 is dominated by redeposited material.

2. Since middle Cretaceous time the background sedimentation of the Mariana Basin (Fig. 1) has been pelagic, frequently interrupted by redeposited volcaniclastic material derived from sporadic volcanic activity in the general vicinity, and by intermittent calcareous or siliceous turbidites made up of redeposited pelagic biogeneous material.

3. Comparison of thicknesses of correlative lithologies from other DSDP holes drilled in this area indicate that chalk deposits in the eastern part of the Mariana Basin may have been transported from the northeast during the Late Cretaceous through the Eocene, and volcaniclastics from the south to southeast during the Miocene.

4. Volcaniclastic sediments from both the Cretaceous and Miocene contain shallow-water carbonate debris and wood fragments, indicating that the source seamounts were at least temporarily above sea level.

5. Site 802 was located in very deep water, well below the carbonate compensation depth (CCD), from the middle Cretaceous to the present. The only preserved calcareous- or radiolarian-rich sediments were redeposited from higher elevations as turbidites, and preserved by rapid burial.

6. From the middle Cretaceous to the present, while Site 802 drifted northward from approximately 15°S to 12°N latitude (see "Paleomagnetism" section, this chapter), the background (nonturbiditic) sedimentation changed from pure clay to clay with radiolarians, to clay with few radiolarians and nannofossils (nearest the equator), to clay with radiolarians, and finally to clay rich in metal oxides and opaques.
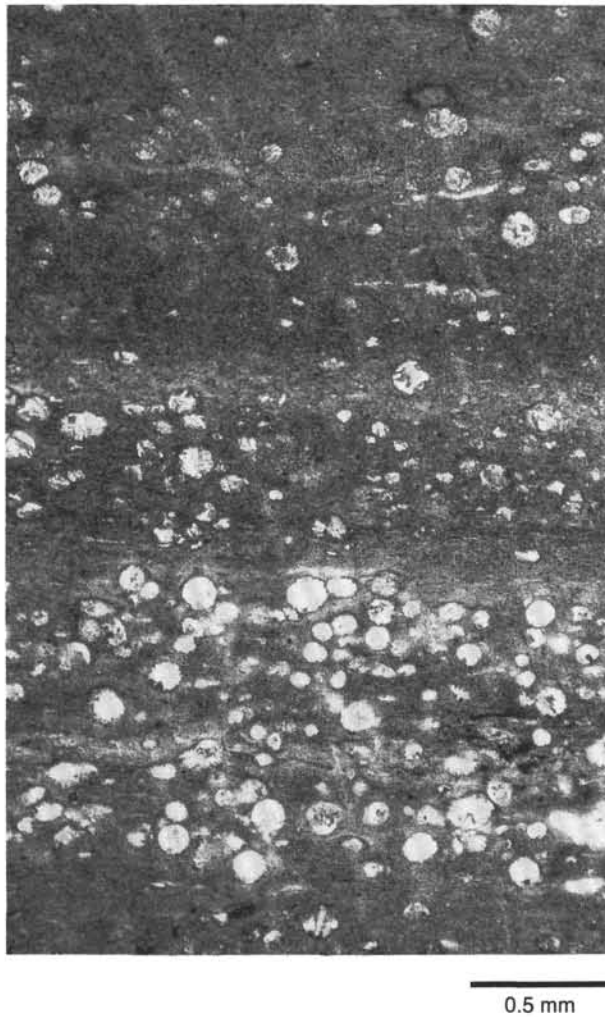
0.5 mm

Figure 22. Photomicrograph of laminated claystone and radiolarite from Unit VIII, Sample 129-802-56-1, 55–56 cm.

7. The most abundant redeposited chalks correspond to the time of equator crossing, and these chalks contain chert nodules, signifying the presence of siliceous as well as calcareous plankton.

8. Bottom waters were mildly oxidizing after the middle Cretaceous.

Implications of Sedimentary Features Observed in Each Lithostratigraphic Unit

Upper Aptian(?) to Cenomanian Volcaniclastic Turbidites and Claystone (Unit IX)

The base of Unit IX is marked by a depositional contact of tuffaceous turbidites 3–8 cm thick on pillow basalt. Grain size and bed thickness suggest that these deposits are probably distal to their source. Their age relation to the underlying basalt flows is unknown. Volcanic activity that produced seamounts and volcaniclastic turbidites of similar age was noted at Site 585 (Moberly, Schlanger, et al., 1986), located to the northeast of Site 802 (Figs. 23 and 24). Volcaniclastic turbidites at Site 801 are pre-Albian to mid-Cenomanian (see "Site 801" chapter, this volume), and thus overlap in age with Unit IX of Site 802 (Figs. 2 and 25).

The tuffaceous turbidites grade upward into a tuffaceous claystone that dominates the unit. The claystone is ex-
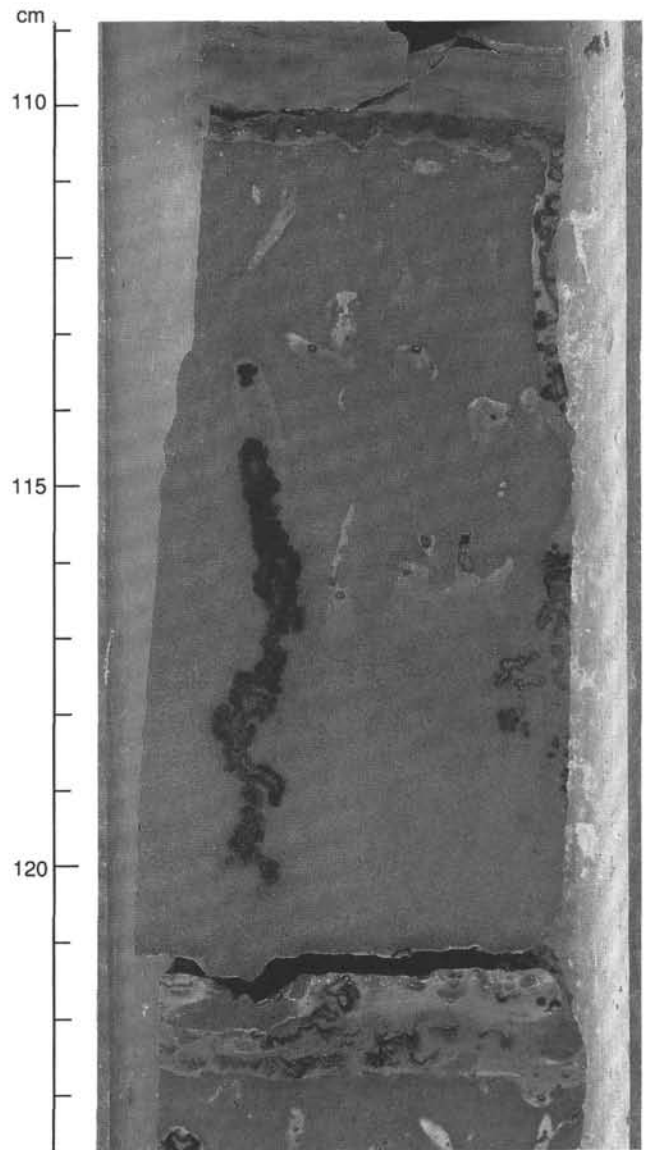

Figure 23. Photograph of volcaniclastic turbidite from Unit IX, interval 129-802A-56R-2, 109–123 cm. Note graded beds and smectite(?)-filled burrows. Bed tops grade to silicified radiolarian claystone.

tremely dark brown to black in color, suggesting low oxygen conditions. The claystone contains a few obvious burrows, and its massive character may be due to homogenization by bioturbation; the underlying turbidites contain burrows as well. Chemical analyses (Table 3) of the dark claystones indicate extremely low organic carbon content, whereas yellow sulfur blooms suggest that the dark, reduced color may be derived from finely disseminated iron sulfides. The presence of pollen and wood fragments in the claystone suggests that some of the seamounts in the vicinity had formed islands.

During the middle Albian, Site 802 may have been at approximately 15°S latitude, which would be an area of low surface productivity. Few microfossils were observed in the tops of the tuffaceous turbidites, although this site was well below the CCD at this time (with a depth calculated according to the thermal subsidence curve of Parsons and Sclater (1977) and Marty and Cazenave (1989), assuming a basement
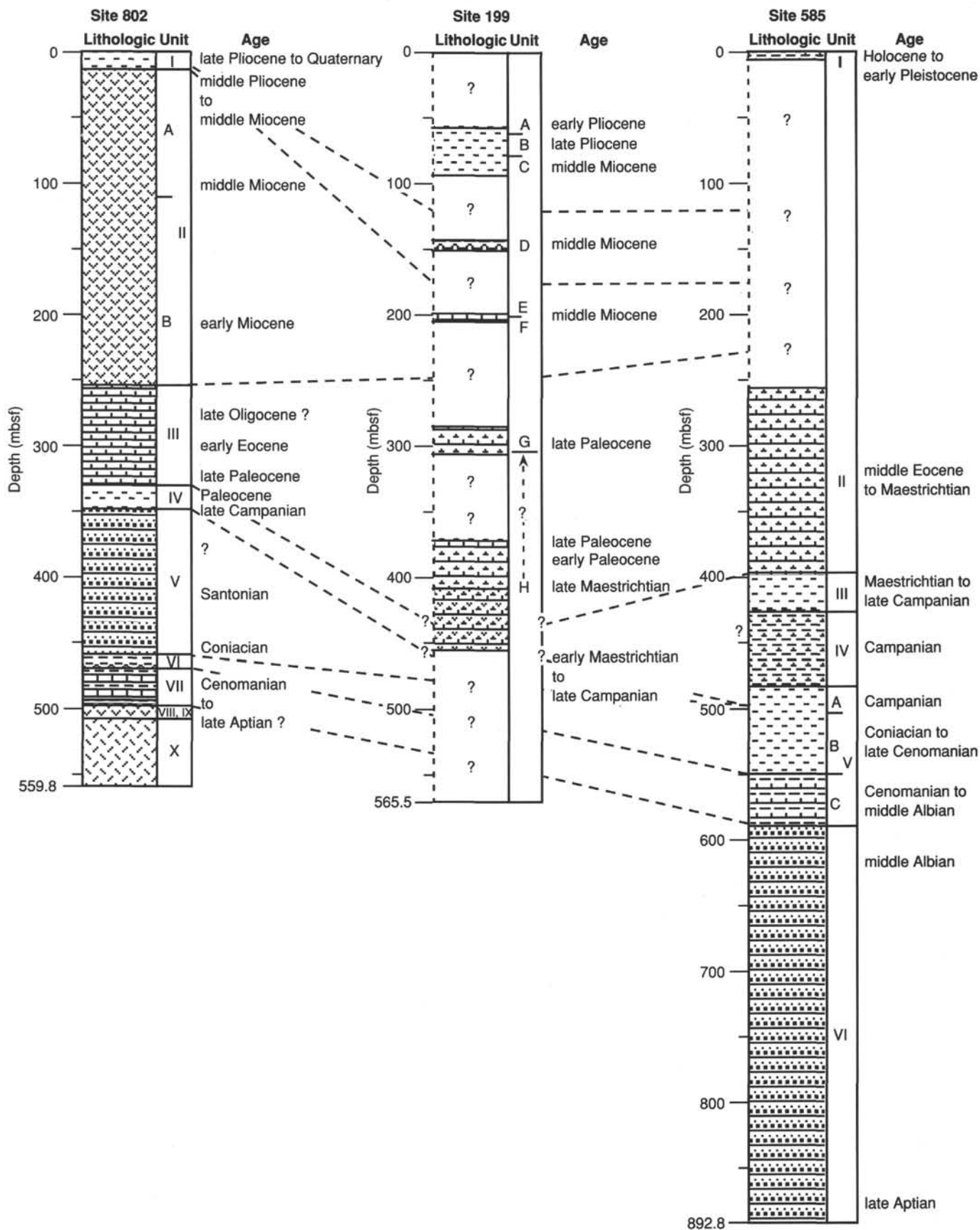
Figure 24. Lithologic correlation diagram for Site 802, and for DSDP Sites 199 and 585. Lithologic symbols are explained in Figure 5.

Table 3. Calcium carbonate and organic carbon of samples from Hole 802A.

Core, section, interval (cm)	Depth (mbsf)	CaCO$_3$ (wt%)	Organic carbon (wt%)	Lithology
129-802A-				
3R-1, 21–23	14.81	0.2		Tuff (sand)
3R-1, 110–113	15.70	0.3		Pelagic brown clay
4R-1, 140–150	25.70	10.0		Tuff (silty sand)
4R-2, 6–8	25.86	33.1		Volcaniclastic breccia
4R-2, 86–88	26.66	0.2		Volcaniclastic sandy
5R-1, 126–128	34.96	0.3		Tuff (sand)
6R-2, 0–10	44.40	0.7		Tuff (silty sand)
6R-2, 60–62	45.00	0.6		Volcaniclastic sandstone
7R-1, 101–103	53.41	0.8		Volcaniclastic sandstone
8R-2, 41–43	63.81	0.8		Tuffaceous silty sandstone
10R-1, 69–71	81.09	1.5		Tuff (sand)
10R-2, 140–150	83.30	1.8		Tuff (sand), foraminifers
11R-2, 10–12	91.20	2.5		Tuff (sand)
12R-1, 7–9	98.97	1.0		Volcaniclastic sandstone
13R-1, 47–49	108.77	0.3		Pelagic brown clay
13R-1, 53–58	108.83	0.5		Pelagic brown clay
14R-2, 73–75	116.63	0.5		Volcaniclastic sandstone
15R-2, 37–39	123.97	1.0		Volcaniclastic sandstone
16R-1, 108–110	132.18	0.9	0.01	Volcaniclastic sandstone
17R-1, 36–38	140.76	1.1		Tuff (sand)
18R-1, 3–5	149.73	1.0		Tuff (sand)
19R-1, 112–114	160.22	1.1		Siltstone
19R-2, 79–81	161.39	2.1		Volcaniclastic sandstone
19R-2, 107–117	161.67	3.0		Calcareous silty clay
20R-1, 10–12	168.40	1.1		Volcaniclastic sandstone
21R-1, 103–110	178.63	2.7		Claystone
21R-2, 9–11	178.79	2.2		Volcaniclastic silty
21R-2, 50–52	179.20	1.2		Volcaniclastic silty sandstone
22R-1, 10–12	187.10	1.2		Volcaniclastic sandstone
23R-1, 10–12	196.50	14.1		Calcareous nannofossil clay
23R-1, 66–68	197.06	1.1		Volcaniclastic sandstone
24R-1, 3–5	206.13	29.7		Calcareous mudstone
25R-1, 12–14	215.82	5.2		Claystone with nannofossils
25R-CC, 5–8	216.67	4.2	1.16	Tuffaceous claystone
26R-1, 0–10	225.40	21.8		Calcareous nannofossil claystone
26R-1, 42–44	225.82	25.5		Calcareous claystone
27R-1, 103–105	236.13	40.2		Volcaniclastic sandstone
27R-3, 112–114	239.22	60.9		Nannofossil chalk
27R-5, 26–28	241.36	43.3		Nannofossil chalk
28R-1, 36–38	245.06	53.6		Nannofossil chalk
28R-3, 54–56	248.24	78.3		Tuffaceous packstone with nannofossil foraminifers
29R-1, 15–17	254.65	78.8		Calcareous claystone
29R-2, 68–70	256.68	46.1		Calcareous claystone
29R-3, 29–34	257.79	0.4		Pelagic clay
30R-1, 71–73	264.91	75.5		Nannofossil chalk
31R-1, 20–22	274.00	52.2		Nannofossil chalk
32R-1, 13–15	283.63	83.5		Nannofossil chalk
32R-2, 96–98	285.96	40.4		Nannofossil chalk
32R-2, 140–150	286.40	53.5		Nannofossil chalk
33R-1, 53–55	293.33	81.8		Nannofossil chalk
34R-1, 60–62	302.90	90.3		Nannofossil chalk
35R-1, 6–8	311.56	42.6		Nannofossil chalk
35R-CC, 5–7	312.42	0.2		Chert
36R-1, 31–33	321.01	91.0		Nannofossil chalk
36R-1, 80–88	321.50	85.4		Nannofossil chalk
38R-2, 63–65	341.33	0.2		Pelagic clay
38R-4, 91–93	344.61	39.7		Pelagic clay
39R-1, 58–60	349.28	3.0		Tuff (fine-grained)
40R-2, 103–105	360.63	4.8		Volcaniclastic sandstone
40R-2, 140–150	361.00	0.5		Volcaniclastic claystone
40R-3, 11–13	361.21	4.5		Volcaniclastic claystone
41R-1, 10–12	365.60	0.2		Volcaniclastic claystone
41R-4, 121–123	371.21	9.3		Volcaniclastic sandy/silty claystone
42R-1, 96–98	373.76	7.0		Volcaniclastic sandy siltstone
42R-2, 111–113	375.29	6.4		Volcaniclastic claystone
43R-1, 114–116	383.24	9.1		Volcaniclastic claystone

Table 3 (continued).

Core, section, interval (cm)	Depth (mbsf)	CaCO$_3$ (wt%)	Organic carbon (wt%)	Lithology
43R-1, 140–150	383.50	13.0		Volcaniclastic sandstone
43R-2, 15–17	383.75	8.8		Volcaniclastic sandstone
44R-1, 50–52	391.80	2.2		Silty claystone
45R-2, 41–43	402.41	2.1		Silty claystone
46R-1, 60–62	410.60	7.6		Silty claystone
47R-1, 45–47	419.65	3.7		Silty claystone
47R-2, 140–150	422.10	2.2		Volcaniclastic silty claystone
47R-3, 74–76	422.94	3.6		Silty claystone
47R-4, 30–32	424.00	1.7		Volcaniclastic sandstone
48R-1, 66–68	429.36	2.0		Silty claystone
49R-1, 17–19	438.27	0.3		Silty claystone
49R-3, 128–130	442.38	6.1		Silty claystone
50R-1, 92–94	448.32	0.4		Volcaniclastic silty claystone
50R-2, 66–68	449.56	1.3		Claystone breccia
50R-2, 140–150	450.30	1.7		Volcaniclastic silty claystone
51R-1, 66–68	454.16	5.2		Claystone breccia
51R-3, 98–100	457.48	0.4		Claystone
52R-2, 114–116	462.44	0.2		Claystone
52R-3, 34–36	463.14	0.2		Radiolarite
53R-1, 75–77	470.15	22.7		Clayey nannofossil chalk
53R-1, 120–130	470.60	23.2		Volcaniclastic claystone with nannofossils
53R-2, 23–25	470.93	37.3	0.19	Nannofossil chalk
54R-1, 15–17	478.75	59.9		Clayey limestone
54R-3, 15–17	481.75	31.8		Clayey siltstone
54R-3, 50–52	482.10	28.7	0.11	Claystone
55R-1, 114–116	489.04	35.9		Siliceous limestone
56R-1, 101–103	498.11	0.2	0.09	Claystone
56R-2, 140–150	500.00	0.6	0.02	Tuffaceous silty claystone
56R-3, 33–35	500.43	0.9	0.06	Volcaniclastic sandstone
56R-4, 7–8	501.67	0.2	0.02	Claystone with radiolarians
56R-4, 34–35	501.94	0.4	0.12	Claystone with radiolarians
57R-1, 37–39	506.97	0.5	0.06	Claystone
57R-1, 72–74	507.32	1.4	0.22	Claystone
57R-1, 127–129	507.87	1.0	0.26	Claystone
57R-2, 87–89	508.97	0.4	0.02	Tuffaceous turbidite
57R-2, 104–106	509.14	0.6	0.04	Tuffaceous turbidite

age of 165 Ma). Thin layers of laminated radiolarite with sharp tops and bases occur in a few intervals in the claystone; these are interpreted as redeposited sediments. Thus the dominant background sedimentation at Site 802 at this time was of tuffaceous pelagic clay, at very low rates of deposition.

Upper Aptian(?) to Cenomanian Claystone and Radiolarite

The brown, thinly laminated claystone that comprises most of Unit VIII is probably representative of background pelagic sedimentation below the CCD. It accumulated at a very slow rate. The claystone is iron oxide-rich and zeolitic. It includes scattered micronodules and few radiolarians; thus, it closely resembles the Cenozoic pelagic clay recovered at all sites on Leg 129 (Fig. 2 and 25). The small metalliferous nodules are most commonly associated with burrowed intervals and may be related to periods of unusually slow deposition and associated early diagenesis.

Thin beds of radiolarite, intercalated within the dominant claystone, are for the most part graded, with sharp tops and bottoms, but do not display scoured bases or load casts. These layers are most likely the results of redeposition. They are either downslope turbidites or condensed deposits transported and winnowed by bottom currents.
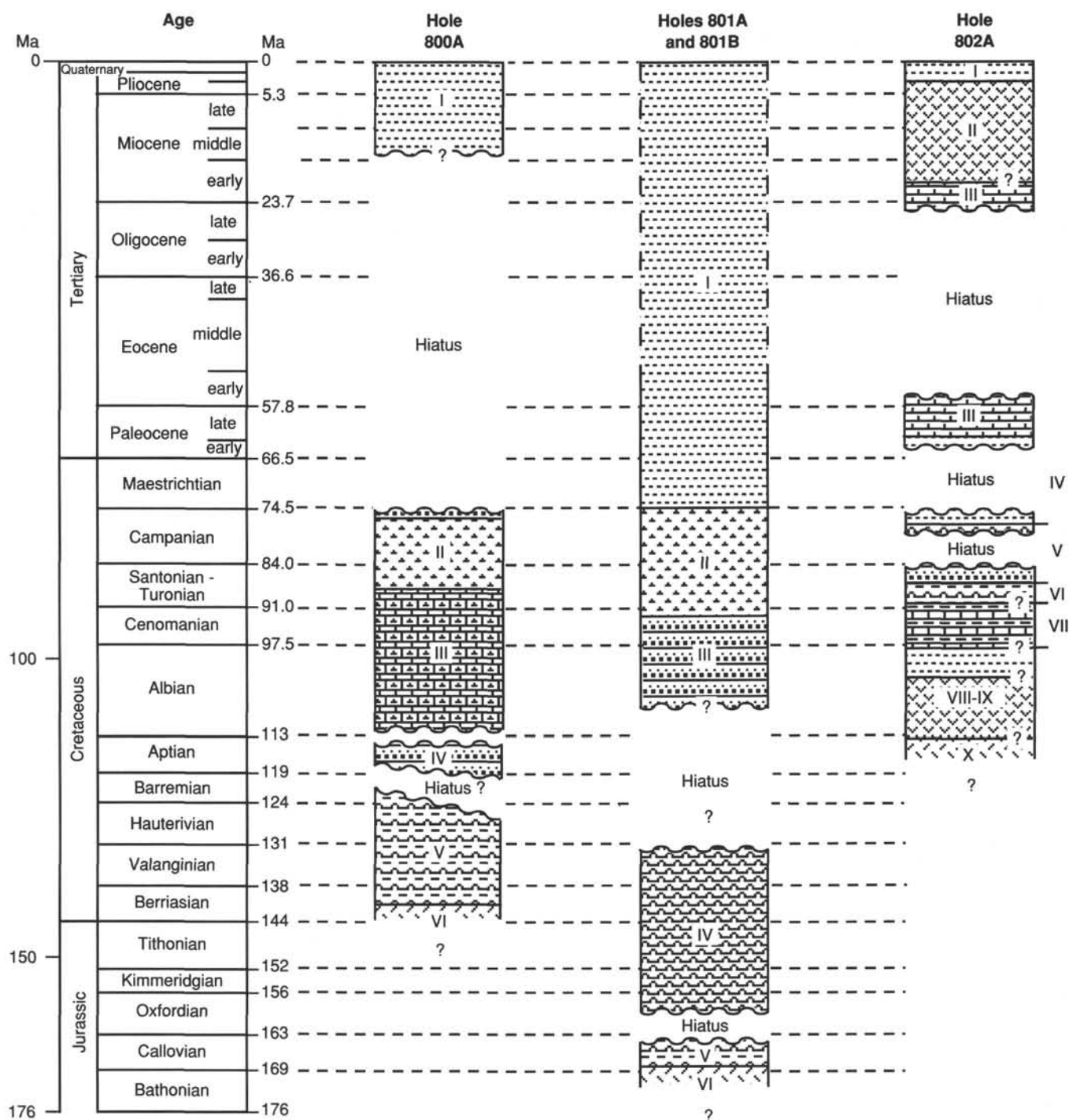
Figure 25. Age correlation diagram for Sites 800, 801, and 802. Lithologic symbols are explained in Figure 5.

Upper Aptian(?) to Cenomanian Calcareous Claystone and Radiolarian Limestone

Unit VII consists mainly of fine-grained radiolarian limestone, nannofossil chalk, and calcareous claystone turbidites. Turbiditic deposition is indicated by laminated to massive, gently graded beds with scoured bases that darken and become more clay-rich upward. The tops of the beds are commonly bioturbated. Although most of Unit VII was probably redeposited from above the CCD, much of the radiolarian

limestone is poorly sorted and probably represents minimally reworked (unsorted) pelagic sedimentation.

Intercalated with the limestone, chalk, and claystone are thin beds of massive to planar- and cross-laminated radiolarite and clayey bio-volcaniclastic siltstone or sandstone. The radiolarite layers have sharp boundaries, but some beds are graded. These coarse-grained deposits may have several different modes of origin, including (1) turbiditic deposition, (2) transportation and reworking by bottom currents, (3) winnowing, and (4) pelagic deposition (radiolarian blooms).

Most of the radiolarians in the carbonate rocks are replaced and filled by calcite, probably during or subsequent to the formation of beds and nodules of chert and porcellanite, and the silicification of limestone in Cores 129-802A-54R and -55R (see the following discussion of Unit III, this section).

The Cenomanian to Coniacian claystone and radiolarite (Unit VI) is very similar to Unit VIII in terms of composition, bedding, and sedimentary structures. Compositionally, the claystone is comparable to pelagic clay and apparently represents normal background sedimentation below the CCD. Overall, the sedimentary rocks of Unit VI accumulated at the moderately slow rate of about 2 m/m.y. Black, iron-manganese oxide-rich discontinuous laminations in Section 129-802A-52R-1 may record extremely slow rates of deposition or perhaps more oxygenated bottom water. These primary depositional conditions are contrasted by later diagenesis in which small pyritic concretions were surrounded by light green, reduction halos. The originally oxide-rich bands of the claystone are sharply truncated at the circumferences of the halos; the metals have evidently been remobilized within the reducing diagenetic microenvironment.

Thin deposits of structureless to laminated radiolarite are probably reworked. Most bedding contacts with the claystone are sharp. The beds are not clearly graded, but deposits of well-sorted radiolarians allow little grain-size differentiation. These sediments may have been deposited by turbidity or grain-flow mechanisms. Zones of diagenetic reduction are mostly restricted to the granular radiolarite beds inferred to have relatively high permeability.

Cenomanian(?) to upper Campanian Volcaniclastic Turbidites

The base of Unit V is a debris flow of volcaniclastic material that overlies a larger debris flow of pebbly claystone with a minor component of volcanic glass. These debris flows are as much as several meters thick but cannot be truly "proximal" facies because the nearest possible sediment sources are seamounts at least 100 km to the northeast (Fig. 2). Unit V has no correlative volcaniclastic deposit at Site 585 (Moberly, Schlanger, et al., 1986; Fig. 24), indicating that the source of these sediments was to the south or west. Upsection in Unit V the redeposited volcaniclastic sediments become coarser-grained and thinner-bedded. The lack of any consistent fining- or thinning-upward stratigraphic trends implies that they are the product of intermittent depositional events, and are thus "distal" to their source rather than the product of an evolving sedimentary apron to a seamount. The thick beds must therefore represent fairly intense seismo-volcanic events. The presence of shallow-water carbonate debris, including red algae, is evidence that the source was near or above sea level.

The volcaniclastic deposits of Unit V are coeval with long-lived edifice-building Cretaceous volcanic activity (late Albian to Maestrichtian) that followed the major Hauterivian-Aptian phase at Site 462 in the Nauru Basin (Larson, Schlanger, et al., 1981). The deposits overlap only slightly with the last phase of volcanic activity recorded at Site 801 (see "Site 801" chapter, this volume), which is pre-Albian to mid-Cenomanian (Fig. 26). The data from Sites 801, 802, 585, and 462 indicate that volcanism in this part of the Pacific Ocean was diachronous in the Mesozoic (Figs. 24 and 26).

The background sedimentation in Unit V is pelagic clay, richer in radiolarians near the base of the unit, when the site was located at approximately 10°S latitude, and richer in nannofossils near the top of the unit, when the site had moved to within a few degrees of the equator (see "Paleomagnetism" section, this chapter). During this time, the site was always

well below the CCD, but because of high rates of turbidite accumulation, nannofossils were buried and preserved together with the radiolarians. The dark bluish and greenish gray colors of these deposits indicate relatively low oxygen depositional and/or diagenetic conditions.

Upper Campanian to Paleocene Claystone

The laminated and burrowed zeolitic claystone of Unit IV records normal, slow pelagic sedimentation below the CCD (as in Units VIII and VI), occasionally punctuated by redepositional events that left thin beds of calcareous siltstone and sandstone. The upper part of this unit is virtually identical to the claystone and radiolarite of Units VIII and VI, except for the better development of graded beds, cross-lamination, and flame structures that clearly identify the coarse-grained deposits as turbidites.

Paleocene to lower Miocene Nannofossil Chalk (Unit III)

Unit III is defined by the predominance of foraminiferal-nannofossil-chalk turbidites, indicated by graded beds with laminated and cross-laminated bases, rip-up clasts, and increased bioturbation toward the tops of beds. Mixed Mesozoic and Cenozoic fossil assemblages (see "Biostratigraphy" section, this chapter) also indicate redeposition and reworking of nannofossil oozes. The unit can be subdivided into an upper and a lower part on the basis of minor lithologies, color, and biostratigraphy at an Eocene through Oligocene hiatus (Fig. 25), during which time Site 802 crossed the equator (see "Paleomagnetism" section, this chapter). Unit III sediments accumulated at the relatively fast rate of 7 m/m.y., closer to the accumulation rates of the volcaniclastic turbidites than to the those rates of the principally pelagic intervals. The much greater thickness of correlative Upper Cretaceous through Paleogene chalk and chert at Sites 199 and 585 (Heezen, MacGregor, et al., 1973; Moberly, Schlanger, et al., 1986) indicate that their principal source was to the northwest (Fig. 24).

The upper Paleocene to lower Eocene part of this unit contains light gray to pale pink, thinly laminated chalk turbidites with scattered chert nodules. Radiolarians in the chalk are replaced and filled by calcite, whereas foraminiferal casts are quartz-filled. A thin bed of pelagic claystone may be the only indicator of the background sedimentation during this period, which was dominated by carbonate redeposition.

In lower Unit III (below the hiatus), the biogenic components had sufficient time or the proper environment to undergo the following observed diagenetic sequence: (1) beginning of radiolarian dissolution, (2) infilling of foraminifers with quartz, (3) beginning of chert nodule formation during ongoing radiolarian and sponge spicule dissolution, (4) completion of radiolarian dissolution, leaving hollow molds, and (5) calcite precipitation in molds. This diagenetic sequence finally resulted in the peculiar association of radiolarian molds filled with calcite and foraminiferal molds filled with quartz.

The upper half of this unit contains upper Oligocene to lower Miocene, dark brown zeolitic claystone interbedded with light grayish brown carbonate turbidites. The zeolitic claystone is representative of normal pelagic sedimentation at that time. Redeposition from above the CCD was less common than in the lower part of this unit, and a much larger proportion of pelagic claystone was able to accumulate between carbonate redeposition events. In the upper part of Unit III (above the hiatus), siliceous microfossils are well-preserved and abundant in the chalk and coarser beds. Porcellanite is very rare.

Our observations support the thesis of Keene (1975), who suggested that in areas of normal geothermal gradient, the
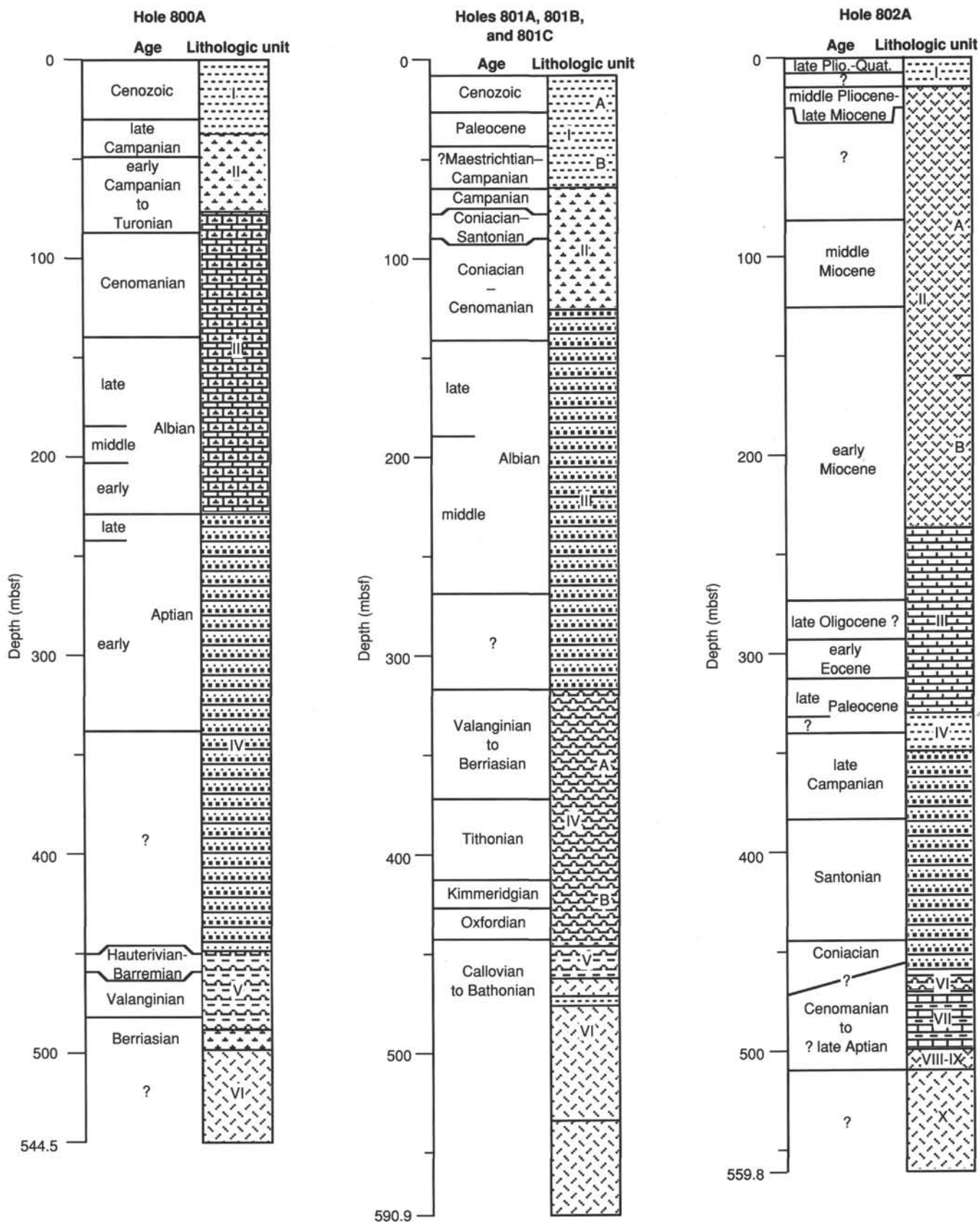
Figure 26. Stratigraphic depth correlation diagram for Sites 800, 801, and 802. Lithologic symbols are explained in Figure 5.

formation of deep-sea chert and porcellanite may require 40–50 m.y. to occur. In Unit III above the hiatus, radiolarians are undissolved and only rare porcellanite has formed in the carbonates, which are less than 30 m.y. old. Below the hiatus, in the lower part of Unit III, which is greater than 52 m.y. old, radiolarians have completely dissolved, and significant quantities of chert and porcellanite have formed. These two distinct diagenetic states occur in physically adjacent, originally similar rocks, deposited on either side of a 20-m.y. hiatus.

Lower Miocene Tuff with Calcareous Claystone and Chalk

Lower Miocene tuffs overlie and are intercalated with redeposited chalks and clayey nannofossil chalks. Subunit IIB is characterized by a decrease in calcium carbonate content upsection (Fig. 27); the transition to Subunit IIA corresponds to the upward transition from tuff interbedded with chalk to tuff interbedded with pelagic clay.

The tuffs were deposited mainly as mass flows and grain flows with meter-scale thicknesses toward the base of the unit. These beds thin and fine upward to turbidite beds 10–30 cm thick. Near the base of the unit, shallow-water carbonate debris and wood fragments indicate that the sources of some of the turbidites were above sea level. The nearest volcanos dated as Miocene are the islands of Truk and Pohnpei along the Caroline Ridge, 350 km south of Site 802 (Fig. 1). Thus, although some of the beds are quite thick, the sediments have traveled a considerable distance. The upward-thinning stratigraphic trend is probably the result of a large initial build-up of volcaniclastic material in the Caroline Islands associated with the construction of the Miocene islands, followed by gradual sloughing of slope accumulations of tuffaceous debris.

The interbedded chalks and calcareous claystones are redeposited pelagic material, as indicated by matrix-supported debris-flow textures and mixtures of Miocene to Cretaceous microfossils. The source of the pelagic calcareous material is not established, but could be various seamounts in the vicinity of the Mariana Basin or the Caroline Ridge. Site 802 was probably moving northward across 5°N latitude during the early Miocene (see "Paleomagnetism" section, this chapter), at depths exceeding 5000 m. At these depths, background sediment accumulation would be expected to be dominantly pelagic clay, although south of 5°N the surface waters would be expected to be highly productive. The dark blue, gray, reduced colors of the deposits may be the result of post-burial diagenetic reduction of the normal pelagic components by interaction with the volcanic material. Bioturbation is ubiquitous in the unit, especially at the tops of turbidite beds and in clay intervals.

Lower Miocene to middle Pliocene(?) Tuff with Pelagic Clay

The tuffs of Subunit IIA are turbidite and mass flow deposits interbedded with brown to green pelagic claystones. The unit displays an overall thickening- and coarsening-upward of bedding and grain size, from thin (5–10 cm) turbidites to meter-scale, massive beds at the top. The very thick beds at the top of the unit are remarkable, like those at the base of Subunit IIB, because they are at least 350 km from their inferred source in the Caroline Islands (Fig. 1). The coarsening- and thickening-upward trend may reflect an increase in volcanic or tectonic activity toward the end of the Miocene and early Pliocene for at least one source seamount on the Caroline hotspot chain. Benthic, neritic foraminifers included in the unit indicate that the summits of the edifices were near sea level.

The pelagic claystone with abundant zeolites, iron oxyhydroxides, and opaques is more metalliferous than the older
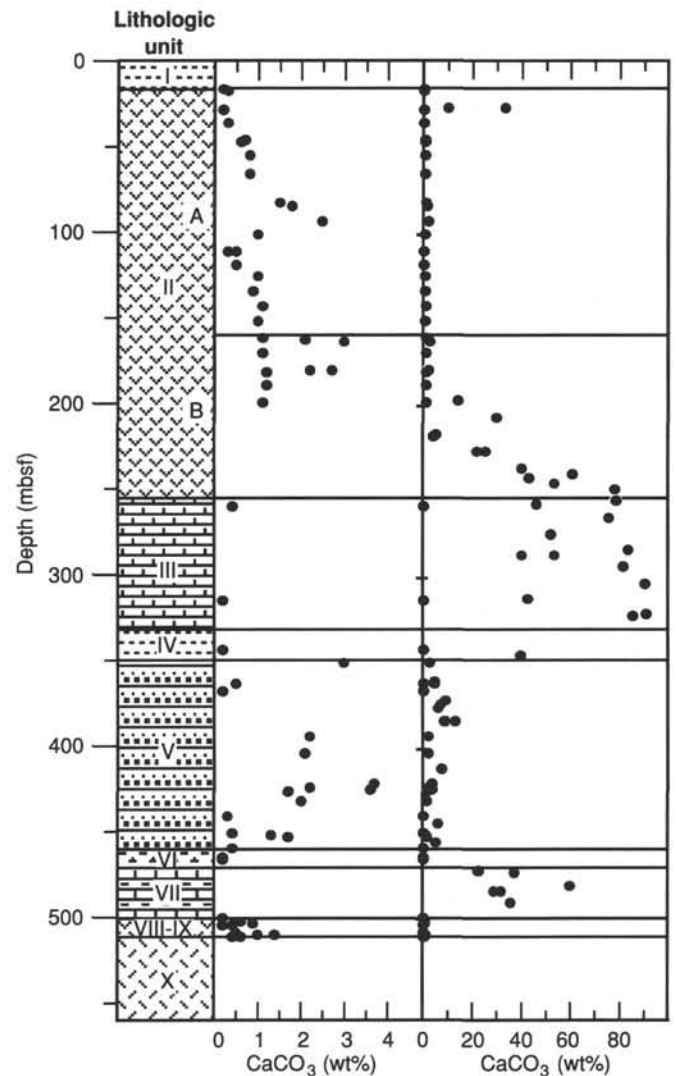

Figure 27. Calcium carbonate content for lithostratigraphic section in Hole 802A.

pelagic deposits at Site 802. The higher metal content is typical of sediments that very slowly accumulated below the CCD (Karpoff, 1989). The uphole decrease in nannofossils and increase in metal content are consistent with passage of the site away from the highly fertile environment of the equatorial divergence zone to about 10°N (see "Paleomagnetism" section, this chapter), and with water depths approaching 6000 m. The slow sedimentation rates for the claystone in this subunit are masked by the thick tuff deposits in the general accumulation rate calculated for this subunit.

Upper Pliocene to Quaternary Pelagic Clay

The zeolitic, iron-manganese oxyhydroxide-rich clay of Unit I is representative of slow pelagic deposition and authigenesis below the CCD, undiluted by volcaniclasts and carbonate. This clay is the unlithified equivalent of much of the claystone of Units VIII, VI, and IV, and is comparable to that found in the upper parts of the sedimentary sections at Sites 800 and 801.

Summary of Sedimentation History at Site 802

Pillow basalts, remote from any seamounts or mid-ocean ridge, were extruded at the seafloor no later than the Cenomanian. The oldest sediments above this basalt are tuffaceous

clays that accumulated slowly, interrupted by rare, distal, volcaniclastic turbidites. From the Albian-Cenomanian to the Coniacian, pelagic clay accumulated slowly, punctuated by occasional events of radiolarian redeposition. Within this interval, during the late Albian to Cenomanian, the background sedimentation was overwhelmed by a more rapid accumulation of radiolarian-rich calcareous turbidites from sources above the CCD. The Coniacian to the late Campanian was dominated by volcaniclastic turbidites, with radiolarian clay deposited in between turbidite events. Sediments from the Maestrichtian through the earliest Paleocene are missing. Slow deposition of pelagic clay from the Paleocene was overwhelmed by pelagic chalk turbidites during the late Paleocene through the early Miocene. Most of the Eocene through Oligocene section is missing. The Miocene was characterized by the accumulation of abundant tuff, at first alternating with chalk turbidites, and later with slowly deposited pelagic clays. Slow pelagic clay sedimentation continued on into the late Pliocene to the present.

BIOSTRATIGRAPHY

The sediment sequence recovered at Site 802 consists of 57 cores dated Pliocene-Quaternary to late Aptian-Albian in age. Core-catcher samples and, when necessary, additional samples from within the cores were investigated for nannofossils, foraminifers, radiolarians, and palynomorphs.

The biostratigraphy is based mainly on nannofossils and planktonic foraminifers. In Cenozoic sediments radiolarians occur sporadically and are rare; in Mesozoic sediments they are few to abundant. Palynomorphs are absent through most of the sequence, except for one sample from the lower Miocene and some samples dated as late Aptian to Albian at the bottom of the hole.

The nannofossils provided useful datums for the middle to early Miocene, late Paleocene, and middle to Late Cretaceous. The foraminifers were useful for age determination in the Miocene, Eocene, and Cretaceous. Radiolarian biozones were recognized as Albian to Cenomanian, and palynomorphs were used to date the last two cores above the basalt as upper Aptian to Albian. A summary of the biostratigraphy of Site 802A is provided in Figure 28.

A hiatus is suspected at the base of Core 129-802A-32R, from which core-catcher samples are tentatively dated as upper Oligocene. Another hiatus is suspected at the base of Core 129-802A-37R, between Paleocene and upper Campanian samples. The position of the Cretaceous/Tertiary boundary could not be determined at Site 802. An additional hiatus may be present between the upper Campanian and Santonian sediments at the base of Core 129-802A-42R.

The microfossil assemblages in the Tertiary sediments were frequently reworked, making precise zonation and dating difficult.

Sporomorphs, wood fragments, and cuticles indicate sources from emergent seamounts during the late Aptian-Albian. Dominance of spores in this interval indicates a humid climate. Further emergence of seamounts is suggested by abundant terrestrial palynomorphs in early Miocene sediments. Abundant larger foraminifers typical of shallow-water reefal habitats support this interpretation.

Calcareous Nannofossils

One-hundred twenty-four samples were examined for nannofossils from Hole 802A. Thirty-five were barren, whereas the remaining 89 contained rare to very abundant nannoflora. Preservation of the nannofossils from this site was generally poor to moderate. Figure 29 shows the distribution of nanno-

fossils compared to the abundance of radiolarians and to the paleolatitudes recorded from Site 802.

Three distinct intervals were discernible and dated using nannofossils: (1) middle to early Miocene (possibly latest Oligocene), (2) late Paleocene, and (3) Late to middle Cretaceous. Most of the Tertiary samples contain a considerable amount of reworked nannofossils from significantly older sediments. Figure 28 summarizes nannofossil zonal assignments compared to those of other fossil groups at Site 802. In the description below we use zonal schemes of Martini (1971) and Okada and Bukry (1980) for the Cenozoic section. For the Cretaceous we used the zonal scheme of Sissingh (1977).

Cenozoic Sediments

Core 129-802A-1R is barren of nannofossils and Core 129-802A-2R had no recovery. The core-catcher sample from Core 129-802A-3R, however, contains rare specimens of *Discoaster pentaradiatus, D. variabilis,* and *Coccolithus* sp. These discoasters range roughly from the middle Pliocene to upper Miocene.

Subsequent cores are barren down to Core 129-802A-10R, in which rare specimens of *Reticulofenestra pseudoumbilica* (middle Pliocene to middle Miocene) and *Sphenolithus moriformis* (late Miocene to early Eocene) were encountered within the core catcher.

An increase in nannofossil abundance was observed near the top of Section 129-802A-11R-1, along with the first paleontologic evidence of reworked sediments recovered from this site. The assemblage is characterized by *Cyclicargolithus floridanus, Discoaster deflandrei, Sphenolithus moriformis, S. conicus, S. heteromorphus,* and *Cyclicargolithus abisectus.* The two latter species are not known to co-exist, so we deduce that at least the older fossils are reworked. The first occurrence of *S. heteromorphus* defines the base of the lower Miocene CN3 Zone, and we assign samples recovered down to Core 129-802A-23R to that zone.

Despite the significant problem of reworking, two reliable nannofossil markers were encountered in their proper sequence within the ensuing cores. Rare specimens of *Sphenolithus belemnos* were observed only in Sample 129-802A-24R-CC. The total range of this species defines the upper and lower limits of the lower Miocene NN3 Zone. The last occurrence of *Triquetrorhabdulus carinatus* coincides with the first occurrence of *S. belemnos* on the range chart of Perch-Nielsen (1985a, p. 442). We observed the last occurrence of the former only two cores below in Sample 129-802A-26R-CC, and encountered that species fairly consistently down to Sample 129-802A-32R-CC. Although the *T. carinatus* Zone (CN1) is actually defined on other markers, the nominal species is reported to generally range throughout that zone (Perch-Nielsen, 1985a). Perch-Nielsen (1985a) also reports that *T. carinatus* is sometimes found in the uppermost Oligocene NP25 Zone, so it is possible that the aforementioned interval extends into the Oligocene.

A significant change in the nannofossil assemblage was observed in Samples 129-802A-33R-CC to 129-802A-36R-CC. The Miocene assemblage with reworked Oligocene and Eocene nannofossils described above is replaced by a predominantly late Paleocene assemblage occurring with abundant reworked Late Cretaceous nannofossils. The youngest fossil identified thus far is *Discoaster multiradiatus,* which ranges through the uppermost Paleocene and up into the lowermost Eocene. We therefore assign this sequence of cores to the NP9/CP8 Zone to possibly the NP10/CP9A Zone. Cores 129-802A-33R and -34R are assigned to the lowermost
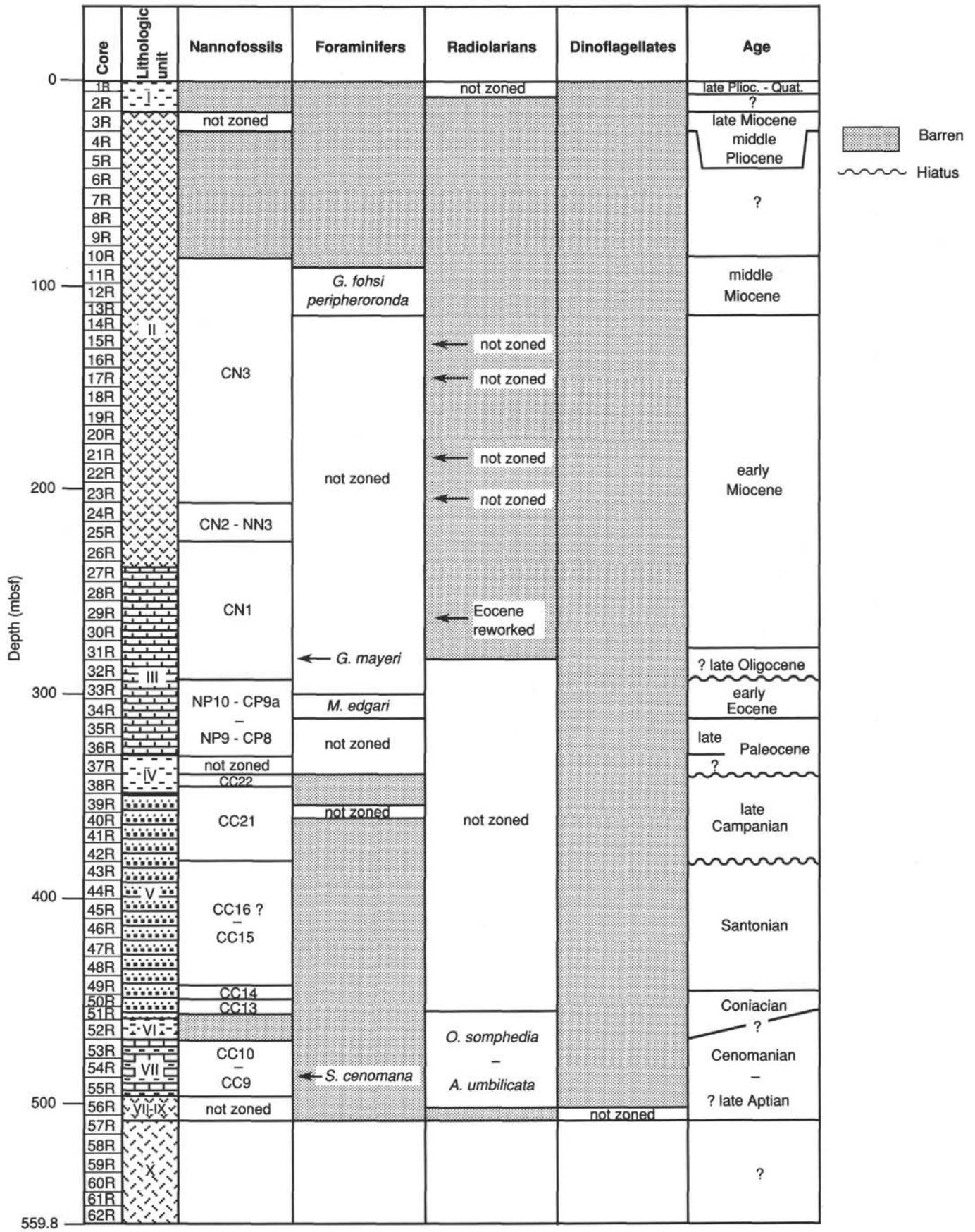
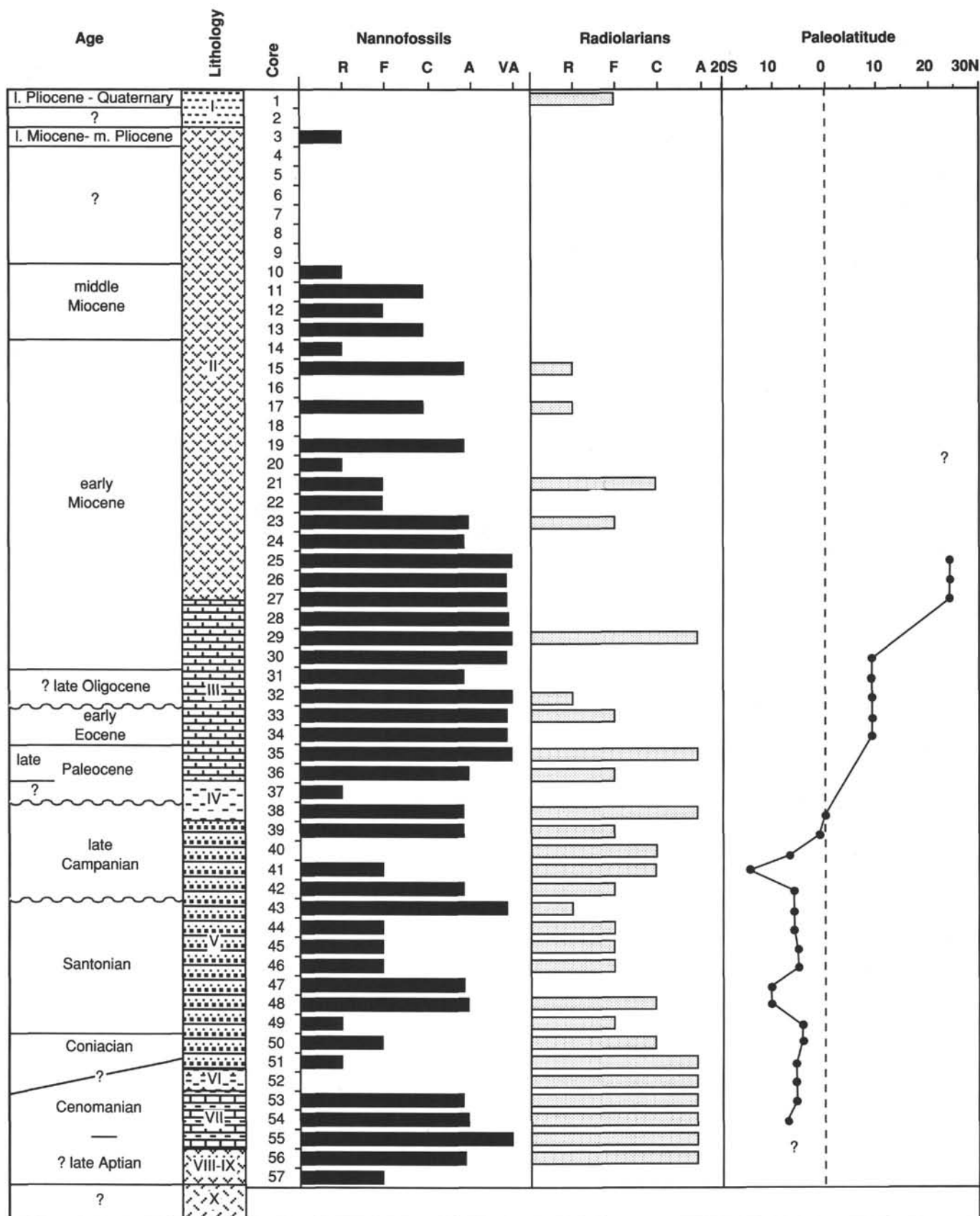Figure 28. Summary of the biostratigraphy for Hole 802A.

Figure 29. Abundance of calcareous nannofossils and radiolarians in Hole 802A plotted against age, lithostratigraphy, and paleolatitude. Relative abundance is denoted as rare (R), few (F), common (C), abundant (A), and very abundant (VA). (See ''Explanatory Notes'' chapter, this volume, for further discussion of abundance parameters.)

Eocene *Morozovella edgari* Zone by the Leg 129 foraminiferal paleontologists. Other Paleocene nannofossils noted include *Chiasmolithus* sp., *Fasciculithus* sp., *Cruciplacolithus tenuis*, *Toweius eminens*, and *Heliolithus kleinpelii*. Core 129-802A-37R consists only of a core-catcher sample that contained only very rare Paleocene nannofossils in calcareous claystone adjacent to chert.

Cretaceous Sediments

The first Cretaceous sediments encountered were from Sample 129-802A-38R-1, 1 cm, and included rare specimens of *Watznaueria*, *Micula*, and *Cretarhabdus*. Total abundance fluctuates from very abundant to barren throughout the remainder of Hole 802A. Reworking of sediments was not obvious, as is the case in the Tertiary sediments described previously.

Whereas several reliable nannofossil markers occurred in their expected stratigraphic sequence, other diagnostic species were conspicuously absent or very rare. These include *Lithastrinus floralis*, *L. septenarius*, *Calculites obscurus*, *Reinhardtites anthophorus*, *Aspidolithus parcus*, *A. parcus constrictus*, *Lucianorhabdus cayeuxii*, and *L. maleformis*.

Nannofossils provided several reliable and useful age determinations constituting the basic biostratigraphic framework for the Cretaceous interval of Hole 802A. Figure 30 illustrates the ranges of important species used in age determination from the Cretaceous sequence.

Sections 129-802A-38R-1, 1 cm, through 129-802A-38R-2, 29 cm, were assigned to the upper Campanian CC22 Zone, based on the first occurrence of *Quadrum trifidum* and the extinction of *Lithastrinus grillii* within this interval. The last occurrence of *Ceratolithoides verbeekii* also coincides with the lower boundary of this zone.

Samples 129-802A-38R-3, 105–106 cm, through 129-802A-42R-CC were assigned to the CC21 Zone of early late Campanian age. A hiatus may be present between Samples 129-802A-42-CC and 129-802A-43-1, 112–113 cm. *Ceratolithoides aculeus*, *C. verbeekii*, *Calculites obscurus*, *Quadrum gothicum*, and *Q. sissinghii* have their last downhole occurrence in the former sample, while *Marthasterites furcatus* was first observed in the latter sample. The Cretaceous range chart of Perch-Nielsen (1985b) shows considerable overlap of these species. The remaining Campanian Zones CC21b down through CC17, and the Santonian Zone CC16, are not represented in this sequence.

Subsequent samples down through Sample 129-802A-49R-3, 107–109 cm, were assigned to the Santonian Zone CC15 (and part of Zone CC16), based on the first occurrence of *Lithastrinus grillii*. A very short Zone CC14 spans only the interval from Samples 129-802A-49R-CC through 129-802A-50R-2, 45–46 cm, where the first occurrence of *Micula decussata* was observed. The Santonian/Coniacian boundary falls within the Zone CC14.

Only the next four samples examined, from 129-802A-50R-2, 83–85 cm, to 129-802A-51R-1, 89-90 cm, can be assigned to Zone CC13 with any certainty, as they contain the lowermost occurrence of *Marthasterites furcatus*. Sections 129-802A-51R-CC through 129-802A-52R-CC are barren or contain very rare nannofossils, which does not allow further zonal or boundary assignment to be made.

Nannofossils are abundant in Samples 129-802A-53R-1, 66–67 cm, down to 129-802A-55R-CC. Markers observed in this interval include *Eiffellithus turriseiffelii* and *Cruciellipsis chiastia*. The first occurrence of the former marks the lower boundary of Zone CC9 (beginning of the late Albian) while the last occurrence of *C. chiastia* marks the upper boundary of Zone CC10 (late Cenomanian). In Section 129-802A-55R-1, 16 cm, poorly preserved specimens resembling *Lithraphidites acutus*, a

species restricted to the Cenomanian Zone CC10, were observed. We assign this interval to Zones CC9 and CC10.

All samples from Sections 129-802A-56R-1, 69 cm, through 129-802A-57R-2, 100 cm, are barren or contain rare, poorly preserved nannofossils. The occurrence of *Lithastrinus floralis* and *Parhabdolithus angustus* indicates an age younger than late Aptian.

Foraminifers

A total of 51 core-catcher samples and two additional samples from within the cores were examined for foraminifers in Hole 802A. Twenty-four of the samples yielded foraminifer assemblages that were common to abundant and of moderate to good preservation. Although the assemblages provided a biostratigraphic framework for the Neogene, Paleogene, and Cretaceous, the precision normally offered by evolutionary lineages of planktonic foraminifers cannot be realized in material from Hole 802A because of a high degree of reworking. Despite this problem, two planktonic foraminiferal biozones are recognized in the lower Miocene and the lower Eocene.

Foraminifers are absent from Samples 129-802A-1R-CC to 129-802A-10R-CC. Sample 129-802A-11R-1, 116-120 cm, yielded an abundant, well-preserved assemblage of planktonic foraminifers assignable to the *Globorotalia fohsi peripheroronda* Zone (early middle Miocene; Bolli and Saunders, 1985). The relatively diverse assemblage found in this zone contains *G. fohsi peripheroronda*, *Orbulina universa*, *O. suturalis*, *Globorotalia scitula*, *G. obesa*, *G. continuosa*, *G. mayeri*, *Globigerina venezuelana*, *G. praebulloides*, *Globigerinoides obliquus*, *G. ruber*, *G. trilobus*, and *Globoquadrina dehiscens*. Rare specimens of *Globigerinoides altiaperturus*, *G. bisphericus*, and *Catapsydrax dissimilis* in this interval appear to be reworked from the lower Miocene sediments.

The oldest find of *Orbulina universa* in Sample 129-802A-13R-CC was used to place the boundary with the underlying lower Miocene. Subsequent assemblages of planktonic foraminifers recovered down to Sample 129-802-23R-CC are very similar to those mentioned previously; however, the presence of *Globigerinoides bispericus* indicates that this interval is not older than the *Praeorbulina glomerosa* and/or *Globigerinatella insueta* Zone (upper part of the lower Miocene; Bolli and Saunders, 1985).

Samples 129-802A-24R-CC through 129-802A-31R-CC lack representatives of the *G. bisphericus-Praeorbulina-Orbulina* evolutionary lineage, and are therefore considered to be early early Miocene in age. The absence of other age-diagnostic foraminifers precludes more detailed subdivision of these cores. Reworking of the assemblages in samples from Cores 129-802A-25R to -28R makes biostratigraphic zonation difficult. Most species typical of the early Miocene, such as *Catapsydrax dissimilis*, *Globorotalia mayeri*, *G. continuosa*, *G. dehiscens*, and *G. obesa* are found in comparatively low abundance in contrast to the abundant Cretaceous and Paleogene species. Sample 129-802A-27R-CC in particular contains typical Eocene species such as *Turborotalia cerroazulensis*, *Morozovella aragonensis*, *Acarinina* div. spec., *Hantkenina* sp., and *Globigerina* div. spec., in addition to representatives of the Cretaceous genera *Globigerinelloides*, *Rugoglobigerina*, *Hedbergella*, and *Globotruncana* that indicate reworking.

Diverse foraminifer assemblages recovered from Sample 129-802A-28R-CC include shallow-water larger foraminifers belonging to the *Nummulitidae* and *Lepidocyclinidae*, which are typical of reef paleoenvironments. Neritic to bathyal benthic genera were also found including *Pararotalia*, *Rotalia*, *Amphistegina*, *Asterigerina*, *Stichocibicides*, *Vaginuli-*
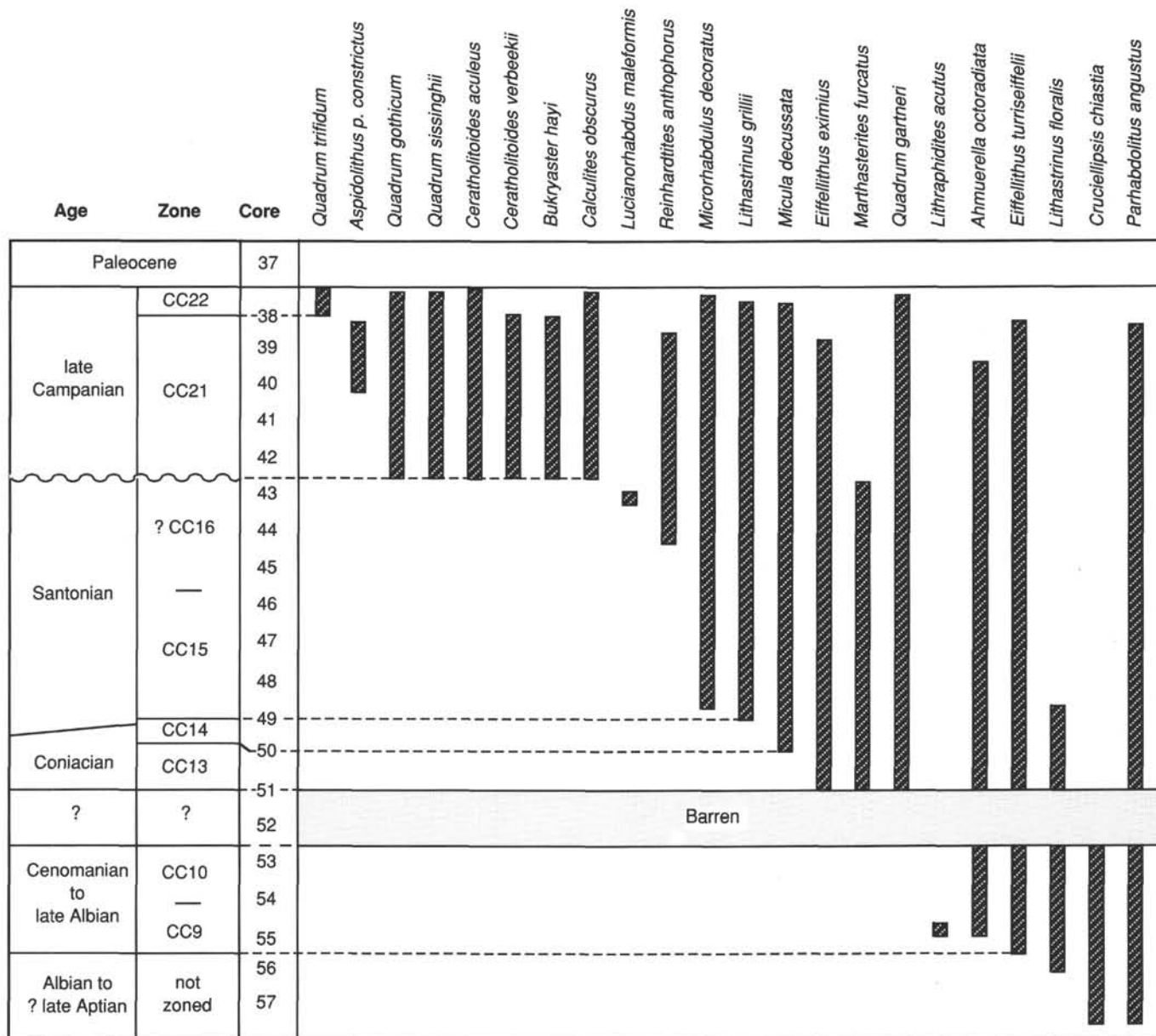
Figure 30. Distribution of important calcareous nannofossils in Cretaceous sediments of Hole 802A.

nopsis, *Stilostomella*, *Chrysalogonium*, and *Bolivina*, in addition to several reworked planktonic species.

Core-catcher samples from Cores 129-802A-29R to -31R contained few planktonic foraminifers of only moderate preservation. However, the presence of *Globorotalia mayeri* in Sample 129-802-31R-CC indicates a late Oligocene or younger age according to the range chart of Bolli and Saunders (1985).

Sample 129-802A-32R-CC is barren. Samples 129-802A-33R-CC and 129-802A-34R-CC contain diverse planktonic foraminifer assemblages including *Morozovella edgari*, *M. subbotinae*, *M. formosa gracilis*, *M. acuta*, *Planorotalites chapmani*, *Acarinina primitiva*, *A. nitida*, *A. soldadoensis*, and *Globigerina triloculinoides*. These assemblages are attributed to the *M. edgari* Zone, dated as earliest early Eocene (Toumarkine and Luterbacher, 1985). Also present are *Globotruncanella citae*, *Hedbergella holmdelensis*, *Heterohelix striata*, *H. navarroensis*, *Globigerinoides ultramicra*, *Moro-*

zovella pseudobulloides, and *Acarinina mckannai*, which are regarded as reworked Campanian to Paleocene species. In subsequent core-catcher samples from Cores 129-802A-35R to -37R, Tertiary planktonic foraminifers were still observed but were of very poor preservation and did not allow precise age determination.

Sample 129-802A-38R-CC and an additional Sample 129-802A-38R-3, 101–105 cm, were barren of foraminifers.

The first evidence of Cretaceous age sediments is in Sample 129-802A-39R-CC, where we observed a diverse and moderately preserved assemblage dominated by very small specimens of *Brizalina* sp., *Heterohelix globulosa*, *Globigerinelloides praehillensis*, *Globigerinoides ultramicra*, *Hedbergella holmdellensis*, *Rugoglobigerina* sp., and *Archaeoglobigerina* sp. The planktonic species indicate a Campanian age according to the range chart of Caron (1985), but do not permit a more exact zonation.

Very small specimens of *Schackoina cenomana* in Sample 129-802A-54R-CC indicate a Cenomanian age. Small undetermined species of *Hedbergella* sp. and *Globigerinelloides* sp. were also found in this interval. The remaining core-catcher samples from Hole 802A are barren of foraminifers.

Radiolarians

Fifty-three core-catcher samples and 97 additional samples within the cores were examined for radiolarians in Hole 802A.

Sample 129-802A-1R-CC contains few but well-preserved radiolarians, together with a few diatoms. Species observed include *Spongaster tetras* and *Euchitonia* sp., indicating a late Pliocene to Quaternary age. Cenozoic sediments from Cores 129-802A-3R to -37R are almost barren of radiolarians. Of 73 samples examined from this interval, 10 contain poorly preserved radiolarians in low abundances ("rare" to "few"). Sample 129-802A-29R-CC, however, yielded an abundant, well-preserved assemblage of reworked Eocene radiolarians, including *Podocyrtis mitra, P. chalara, P. trachodes, Dictyopora mongolofieri, D. amphora, Phormocyrtis trachodes,* and *Lithochytris vespertilio.*

Cores 129-802A-38R to -50R contain rare to few (rarely common) but poorly preserved radiolarians of Cretaceous age. The scarcity of radiolarian-rich horizons and the poor preservation do not permit zonal assignment of this interval. The interval from Samples 129-802A-51R-3, 11–13 cm, to 129-802A-56R-2, 57–61 cm, yielded abundant, poorly to moderately preserved radiolarians. Samples 129-802A-51R-3, 11–13 cm, to 129-802A-55R-1, 59–62 cm, contained *Thanarla veneta* and/or *Pseudodictyomitra pseudomacrocephala.* The possible co-occurrence of these species indicates that the upper *Acaeniotyle umbilicata* to lower *Obesacapsula somphedia* Zone (upper Albian to Cenomanian) may be present. The interval between Samples 129-802A-55R-CC and 129-802A-56R-2, 57–61 cm, does not contain the above-mentioned diagnostic species but is otherwise similar to the radiolarian faunal association seen in the overlying sediments, indicating that the interval is still within the same zones. The dark gray claystone of Cores 129-802A-56R and -57R is barren of radiolarians.

Palynomorphs

Fifty-six core-catcher samples and 15 additional samples from within the cores were investigated for palynomorphs. Samples 129-802A-1R-CC through 129-802A-24R-CC and Samples 129-802A-26R-CC through 129-802A-55R-CC are barren of palynomorphs. Sample 129-802A-25R-CC contains abundant wood fragments, cuticles, and a few spores and pollen grains. The palynologic evidence indicates that some of the seamounts were above sea level during the early Miocene.

Samples 129-802A-56R-CC and 129-802A-57R-2, 57–61 cm, yielded a rich palynoflora including common dinoflagellate cysts. The dinoflagellate assemblage is characterized by the *Oligosphaeridium* group (*O. pulcherrimum* and *O. complex*), *Cassiculosphaeridia* sp., *Canninginopsis collivieri,* and *Dingodinium cerviculum. Dingodinium cerviculum* ranges from the Valanginian to the late Aptian/early Albian and *Canninginopsis collivieri* ranges from the Aptian to the Turonian, indicating an Aptian to Albian age for these samples. Sporomorphs in this interval are dominated by spores; pollen grains are rare. The spore assemblage is dominated by *Cyathidites* spp., and rare specimens of *Cicatricosisporites* spp. Bisaccate pollen are rare, although the monosaccate pollen *Callialasporites dampieri* and *C. trilobatus* are relatively common. The abundance of sporomorphs, wood fragments, and cuticles indicates emergent seamounts during the late Aptian to Albian, and the dominance of spores implies a humid climate.

Sedimentation Rates

Figure 31 shows the sedimentation rates for Site 802, as determined on the basis of nannofossil, radiolarian, foraminiferal, and dinoflagellate biostratigraphy. Three hiatuses were depicted at the base of the late(?) Oligocene, at the base of the Paleocene, and at the base of the late Campanian, respectively.

PALEOMAGNETISM

Methods

Measurements of natural remanent magnetization (NRM) were made on all cores in the interval from Cores 129-802A-30R to -56R and on a few selected cores higher in the hole. As most cores of this hole represented semicontinuous recovery, nearly all were measured as continuous cores rather than discrete fragments. Alternating field (AF) demagnetization was generally performed using steps of 5, 10, and 15 mT. More detailed demagnetization was done in certain intervals, for example in the Upper Cretaceous cores where, in order to investigate small intervals of apparent reversed polarity, a larger number of more closely spaced steps were used. The measurement interval chosen for this site was 3 cm, and the near-continuous recovery for most of the hole allowed the use of this interval in most of the magnetic measurements. Magnetic behavior was analyzed by the systematic evaluation of equal area and orthogonal-axis vector plots, intensity-decay patterns (J/J_0), and raw volume-susceptibility (K_a) data for the different lithologic groups. Inclinations and relative declinations were calculated for selected core levels using least squares regression along linear segments of the magnetization decay trajectories.

Sediment Magnetic Behavior

AF demagnetization response and susceptibility values are characteristically different for the various lithologic units encountered at Site 802, and the properties will be discussed on the basis of the major lithologic groups (as defined in "Lithostratigraphy and Sedimentology" section, this chapter).

The Miocene tuff unit (Cores 129-802A-3R through -26R) was investigated by an examination of Cores 129-802A-3R, -6R, -10R, -19R, -25R, and -27R. Intensity of NRM magnetization for the more tuffaceous upper part of the unit averages approximately 22 mA/m; median destructive fields (MDF) range widely from as low as 3 mT to greater than 200 mT. Analysis of the magnetization decay on orthogonal axes plots indicated a general ineffectiveness of AF demagnetization to separate the magnetic components in these samples. Susceptibilities were notably uniform in this upper portion of the tuff unit, ranging from core averages of 103 to 207 SI units.

The lower portion of the tuff unit contains chalks and calcareous claystones, which yielded higher NRM intensities (approximately 103 mA/m). Consistently higher values for susceptibility were also observed. Unlike the upper part of this unit, response to AF demagnetization showed a tendency to decay in the general direction of origin, although not yet directly toward it.

The nannofossil chalks, Cores 129-802A-27R through -36R, have low NRM intensities, and generally quite low values of MDF (about 5 mT). These cores also show greatly reduced susceptibility, especially in the base of the unit. Core-averaged susceptibility ranges from 223 SI units at the uppermost portion of the unit (chalk debris flow) to 14 SI units in the lowermost core of this lithology.
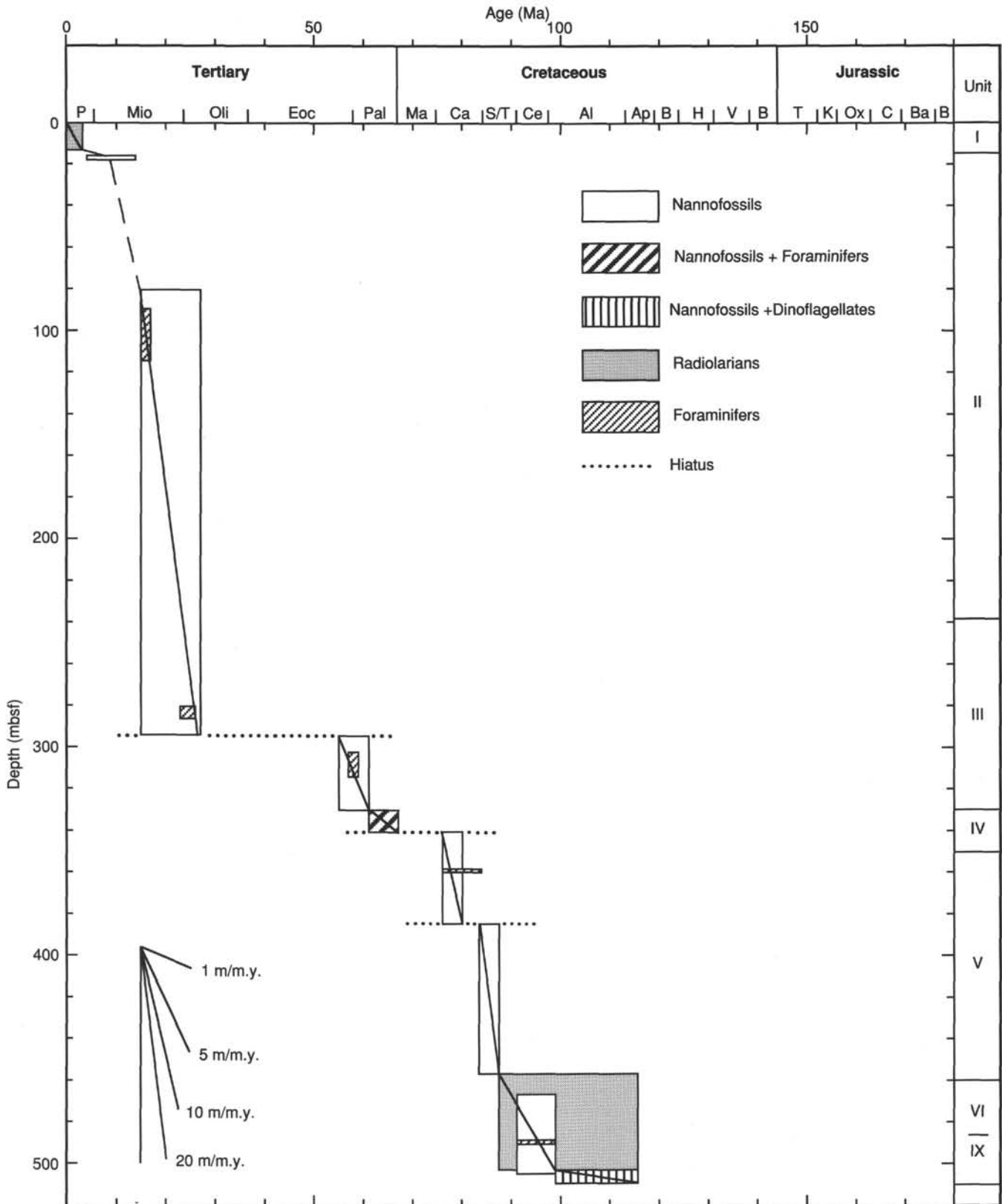
Figure 31. Sedimentation rates for Hole 802A.

The claystone unit consisted of only a single core, 129-802A-38R. Susceptibility values ranged widely from approximately 90 to nearly 700 SI units. Such high susceptibilities had not been encountered in sedimentary units previously on this leg. NRM intensities are also high, averaging approximately 205 mA/m. In addition, MDF values were consistently high, around 15 mT. Overall, the response to AF demagnetization was good. Decay of magnetization as indicated on orthogonal-axis plots showed movement in the direction of, although not yet directly toward, the origin, indicating that a significant portion of the overprinting magnetization was removed by demagnetization to 15 mT. However, the fact that appreciable magnetization intensity remains and that spectra still overlap indicate the presence of higher coercivities in this lithology.

The volcaniclastic turbidites (Cores 129-802A-39R through -51R) show variability in susceptibility ranging from approximately 200 to 500 SI units. The variability, in this case, can be accounted for by changes in grain size. NRM, MDF values, and general magnetic behavior are quite similar to those of the overlying claystone unit.

The lowest sediment cores, 129-802A-52R through -56R, showed basically the same characteristics as the volcaniclastic turbidites and claystones located above, except that the variability in susceptibility is much reduced in magnitude, by a factor of approximately 10.

Magnetostratigraphy

Reversals of magnetic polarity were observed in many of the cores from this site. A large number of reversed polarity intervals are observed in the lower Miocene through Santonian sequence (Cores 129-802A-30R through -46R). Exclusively normal polarity is observed in all cores below Core 129-802A-46R. The polarity interpretations are diagrammed in Figure 32, along with the biostratigraphic age determinations from the "Biostratigraphy" section (this chapter).

For the sequence encompassing the early Miocene through Paleocene (Cores 129-802A-30R through -37R), there are no serious discrepancies between the biostratigraphic and the magnetostratigraphic age determinations. The early Miocene and late Oligocene ages of Cores 129-802A-30R through -32R are compatible with the magnetostratigraphy, but the abundance of reversals of polarity in this time interval precludes assignment of the observed reversals to recognized polarity chrons. The lower Eocene Cores 129-802A-33R and -34R are suggested by the magnetostratigraphy to be of middle to early Eocene age because of the predominance of reversed polarity in the recovered portions of these cores and the large interval of reversed polarity in the geomagnetic polarity time scale for that time. The biostratigraphic late Paleocene age of Cores 129-802A-35R through -37R is in good agreement with the magnetostratigraphic evidence of dominantly reversed polarity.

Disagreement between magneto- and biostratigraphy begins with upper Campanian Cores 129-802A-38R through -42R. The biostratigraphic age would predict that these cores should have exclusively normal polarity magnetizations. While they are predominantly normally magnetized, there are four to five relatively short intervals which are either of clearly reversed magnetization or display demagnetization behavior suggestive of reversed magnetization. In Core 129-802A-38R two intervals show behavior suggesting, but not clearly indicating, reversed magnetization. The observed high coercivities, in conjunction with the red-brown color, indicate that demagnetization is incomplete. Therefore, the reality of these apparent reversed intervals, and hence their significance, must await more extensive demagnetization. However, Core 129-802A-39R, a mixture of chert/porcellanite and volcaniclastics, contains true reversed polarity, although the length of the interval cannot be determined because of the fragmentary recovery. Core 129-802A-40R also has two intervals of definite reversed polarity; these are represented only by small blocks, as the material above and below the reversed portions has been crushed into very small pieces or ground into a mush, so again the length of the reversed polarity intervals cannot be determined. In the case of Core 129-802A-40R it is possible that core disturbance, coupled with the width of the sense region of the magnetometer, has caused the apparent reversed characteristics. Overall, however, the reason for the discrepancy of numerous small indications of reversed polarity in the late Campanian, within an interval that should be entirely normal, is presently unclear, but the problem is compounded by further conflicts between the magneto- and biostratigraphy in the Santonian-age cores immediately below this interval.

Cores 129-802A-43R through -46R are biostratigraphically determined to be of Santonian age, but again, their magnetization displays reversed polarity intervals. The Santonian is well known as a time of exclusively normal polarity, as it is the youngest part of the 34 m.y. of extended normal polarity during the Cretaceous long normal polarity interval (Helsley and Steiner, 1969; Irving and Pullaiah, 1976; Kent and Gradstein, 1986). However, two or three intervals of definite reversed polarity are observed in Cores 129-802A-43R and -44R (Fig. 32). In addition, we observed a relatively small interval of probable reversed polarity in Core 129-802A-45R, as well as another interval in Core 129-802A-46R with clear and less clear reversed polarity characteristics in the demagnetization response (Fig. 32). The intervals in the latter two cores are suggestive of reversed polarity, but the evidence is not entirely certain; the former two or three are clearly intervals of reversed polarity.

The definite reversed polarity in Cores 129-802A-43R and -44R precludes them from being Santonian in age unless some peculiarity resulting from redeposition or remagnetization is somehow responsible for the reversed polarity. It might be, for example, that the reversed remanent magnetization remaining after demagnetization is not the primary magnetization, but a drilling remanence or the result of some other secondary magnetization. There is no evidence for this at present, but such possibilities cannot be entirely ruled out. More extensive demagnetization studies in shore-based investigations will address these ambiguities.

Below Core 129-802A-46R no further reversals of polarity are observed and it would appear that Cores 129-802A-47R through -56R are within the Cretaceous long normal polarity interval.

Paleolatitude

An important objective of Leg 129 was the determination of paleolatitudes from the measured paleomagnetic inclinations. The improved recovery at Site 802 permitted calculation of paleolatitude data from a large portion of the recovery, although these results are nevertheless preliminary because the AF demagnetization was insufficient to completely reveal the characteristic magnetization.

As at previous sites, selected core levels were chosen for least squares regression analysis on the basis of a uniformity of declination and inclination over a given portion of a core segment. While all samples showed progressive decay of magnetic vectors in the general direction of the origin on orthogonal-axis plots, decay directly to the origin was rare.
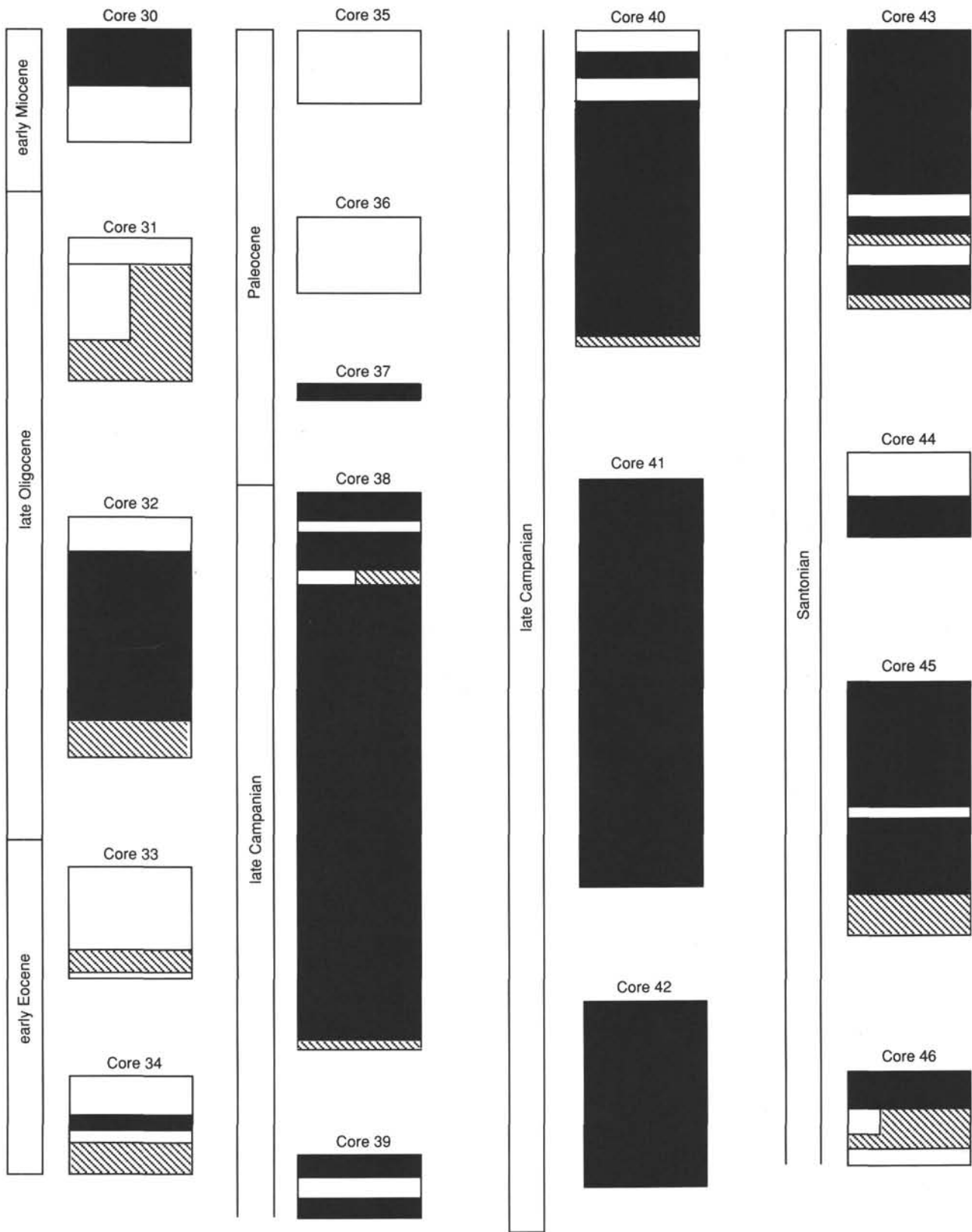
Figure 32. Polarity interpretation of lower Tertiary through Upper Cretaceous cores from Hole 802A in which intervals of reversed polarity were observed. Individual segments represent the core recovery, hachured areas indicate the absence of data, black areas are normal polarity, and white areas are reversed polarity. Half-column width indicates uncertainty in the polarity interpretation. Ages of each column are to the left of the respective columns.

Table 4. Inclination and paleolatitude values from selected segments of the sedimentary cores.

Core(s)	N	INC	K	Paleolatitude (°)	α_{95}	SD
129-802A-						
25R–27R	8	40.1	8.3	22.9N	18.0	10.4
30R–34R	7	15.5	43.1	7.9N	5.1	3.0
38R	15	−2.4	198.4	1.2S	1.6	0.9
39R	6	−4.7	83.8	2.3S	5.8	3.3
40R	13	15.8	30.9	8.0N	5.6	3.2
41R	11	29.5	31.1	15.8N	5.9	3.4
42R–44R	14	14.0	35.8	7.1N	4.2	2.4
45R–46R	10	−12.8	40.8	6.5S	5.2	3.0
47R–48R	9	−23.7	47.4	12.4S	5.6	3.2
49R–50R	9	−11.5	102.4	5.9S	2.8	1.6
51R–53R	11	−13.8	42.3	7.0S	4.3	2.5
54R	12	−16.6	170.7	8.5S	1.8	1.0

Note: N is the number of regions used to calculate each point; INC is the mean inclination; K is the precision parameter; α_{95} is the half-radius of the 95% circle of confidence; and SD is the standard deviation.

This indicates the presence of secondary magnetization that was not removed by the low-level demagnetization. The secondary magnetization appears to be similar to the present-day magnetic inclination at the site, and thus will bias Southern Hemisphere normal polarity samples toward shallower inclinations, and reversed polarity ones toward steeper ones. Statistical analysis was performed on the inclinations generated by regression analysis, using the method of Kono (1980), and the results are listed in Table 4.

Figure 33A illustrates the inferred latitudinal component of Pacific plate motion as recorded at Site 802. Although preliminary, the results suggest that this part of the Pacific plate crossed the paleoequator in the period of time spanning the earliest Paleocene to late Campanian. Again the data used in the calculation of the paleolatitudes were predominantly of normal polarity. If the data are preferentially shallow because of incomplete demagnetization, as previously suggested, a Campanian age for the equator crossing is the least plausible, and a crossing in the Paleocene (or possibly Eocene) is more likely.

Data from Cores 129-802-40R through -44R show an anomalous equator crossing, unexpected both in terms of the results from Sites 800 and 801, and from previous paleomagnetic and magnetic anomaly studies (see "Site 800" and "Site 801" chapters, this volume). Samples within these cores display significant intensity increases during demagnetization and a subsequent decay pattern on orthogonal-axis plots that could be associated with reversed polarity, although they lack the characteristic large-scale shift in declination. If these are reversed and have a secondary magnetization that is sufficiently resistant to the low-level AF demagnetization employed, the demagnetization may well have been be inadequate to reveal the declination shift and the reversed nature of the magnetization. If the samples are of reversed polarity and are not representative of Northern Hemisphere paleolatitudes, then the paleolatitude plot for Site 802 should look like that shown in Figure 33B. More extensive demagnetization studies onshore will ascertain the true polarity and paleolatitude in this interval.

Basalt Magnetism

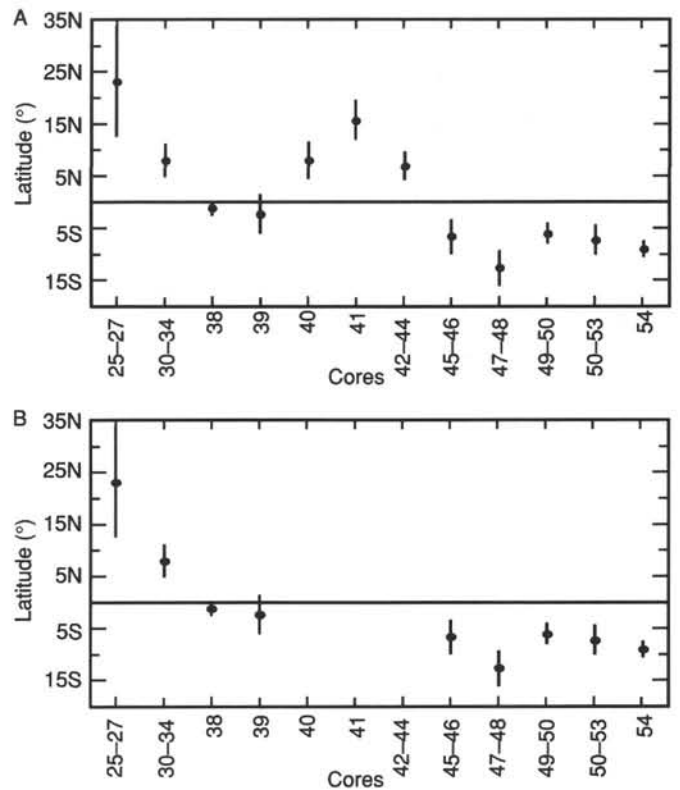Core segments from three of the six basalt cores were analyzed using the cryogenic magnetometer. Most of the

Figure 33. **A.** Paleolatitude values plotted against their corresponding Cores 129-802A-25R through -54R. Error bars represent one standard deviation on either side of the mean value. **B.** The same data as in as (A), but with Cores 129-802A-40R through -44R removed because of the possibility of reversed polarity and significantly incomplete demagnetization.

remainder of the recovered basalts could not be measured with the cryogenic magnetometer because the intensities were too strong to be able to keep accurate count of the scale over-ranging. AF demagnetization was carried out on the three segments that could be measured with the cryogenic magnetometer; AF increments from 2 to 20 mT were used. Volume magnetic susceptibility was measured for all basalt cores.

NRM intensity varies between 1.1 and 3.2 mA/m, but most samples have values below 2.0 mA/m (Fig. 34A). NRM intensities that exceed this value seem to be related to microphyric textures, although the number of data available does not allow positive correlation.

In response to AF demagnetization, all samples displayed large rises in intensity, most probably associated with the overprinting of a normal Northern Hemisphere polarity magnetization (Brunhes Chron) onto a normal Southern Hemisphere characteristic remanence. The majority of samples are not sufficiently demagnetized by the AF treatment to reveal the median destructive fields. Inclinations were calculated by linear regression of segments of the decay path; these are plotted in Figure 34B. The negative inclinations indicate normal polarity in the Southern Hemisphere. The dispersion displayed by the data probably results from incomplete demagnetization. Higher AF demagnetization in shore-based studies will be necessary to define the true inclinations of these basalts. Despite the dispersion, the few data, and the
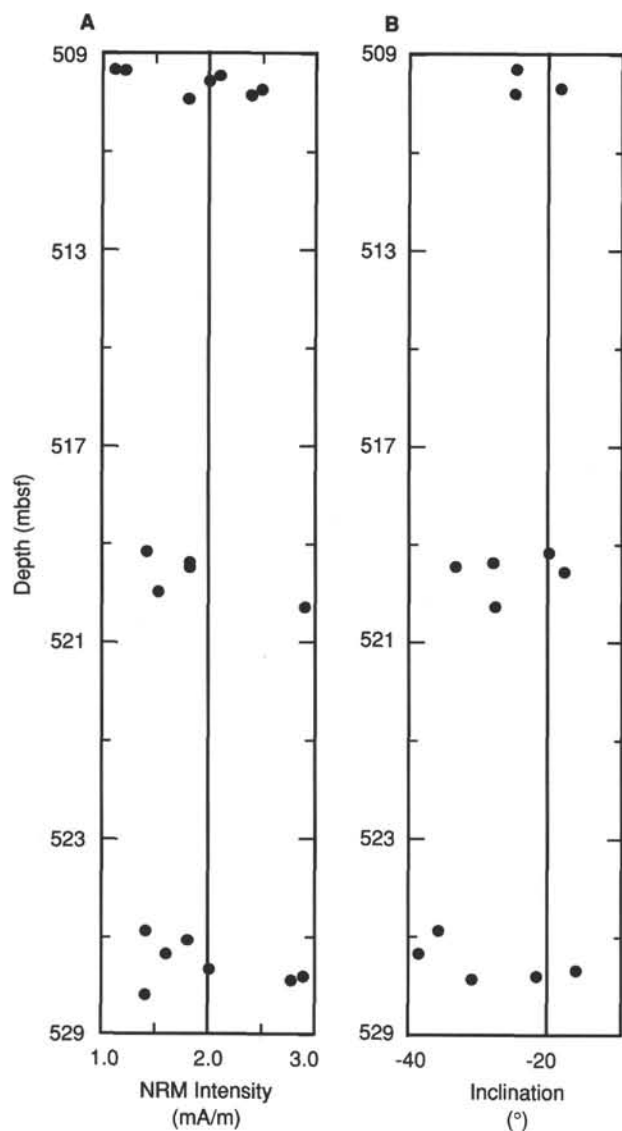
Figure 34. Basalt NRM intensity (**A**) and inclinations (**B**) plotted against depth (mbsf) for sections within Cores 129-802A-57R through -59R.

probable lack of averaging of secular variation, the inclinations imply a paleolatitude consistent with the 12° to 15° paleolatitudes for Aptian/Albian sediments of Sites 800 and 801.

Susceptibility values are shown Figure 35. Correlations with the observed petrographic units (as defined in the "Igneous Petrology" section, this chapter) are not obvious except for the unit located between 545 and 552 mbsf (Fig. 35). Susceptibility values are notably higher here than in the basalts above, averaging about 2.0 SI units, approximately twice that of the rest of the basalt. These high values seem to correspond to a sparsely microphyric flow unit in Cores 129-802A-61R and -62R. Other high values of susceptibility in the cores recovered above seem to be associated with well-defined pillow lavas.

INORGANIC GEOCHEMISTRY

Interstitial water samples were squeezed from sediment cores at sixteen levels in Hole 802A. The samples are distributed between 26 and 500 mbsf in the tuff of lithologic Unit II, the nannofossil chalk of Unit III, the volcaniclastics turbidites
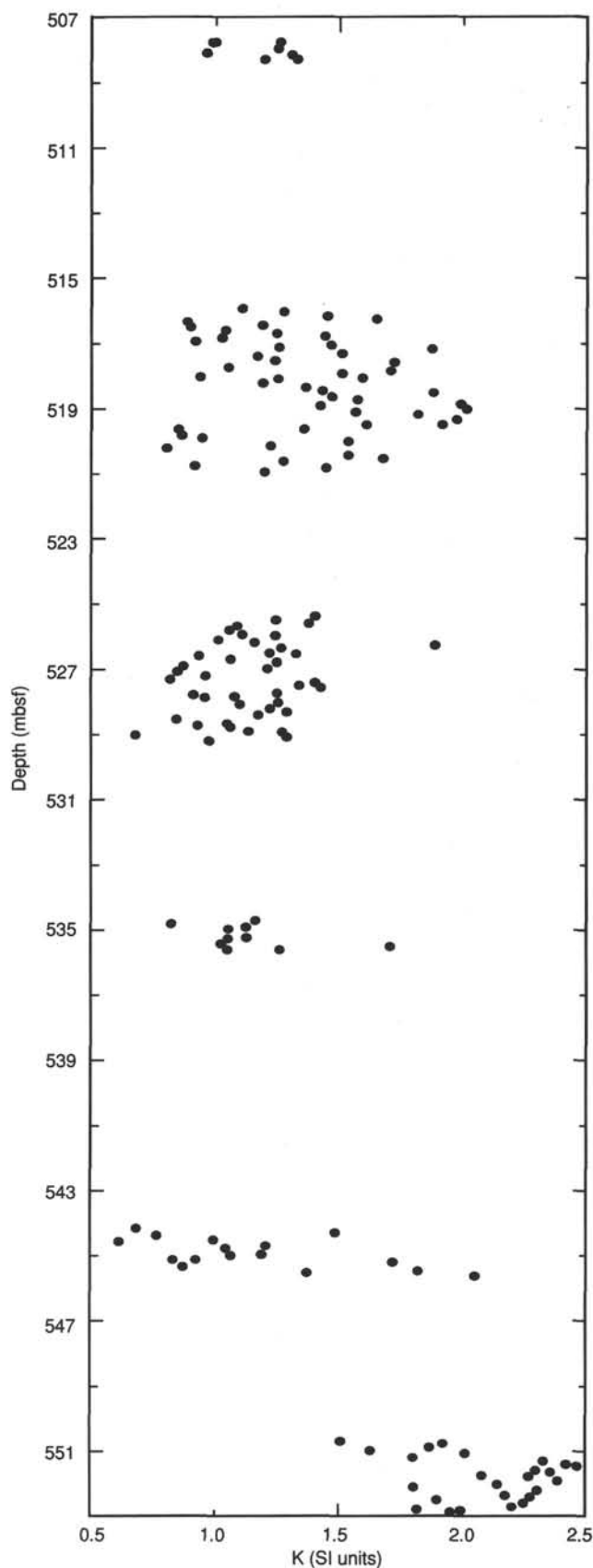

Figure 35. Volume magnetic susceptibility plotted against depth (mbsf) for all basalts from Site 802 (Cores 129-802A-57R through -62R). Every third value of susceptibility from the shipboard measurements is plotted in the diagram.

Table 5. Chemical composition of interstitial water extracted from sediments in Hole 802A.

Core, section, interval (cm)	Depth (mbsf)[a]	Alkalinity (meq/L)	Cl (mmol/L)	SO₄ (mmol/L)	pH	Salinity (‰)	Ca (mmol/L)	Mg (mmol/L)	K (mmol/L)	Na* (mmol/L)	Mn (μmol/L)	Si (μmol/L)	Sr (μmol/L)	Lithology
129-802A														
4R-1, 140–150	26	1.4	554.1	26.8	7.8	34.8	16.2	39.9	12.2	484	7	162	95	Tuff (silty sand)
6R-2, 0–10	44	0.8	547.2	36.5	8.3	36.1	42.3	15.7	11.0	494	13	78	167	Tuff (silty sand)
10R-2, 140–150	83	0.6	631.1	0.4	9.0	39.0	125.2	0.2	2.7	378	19	194	381	Tuff (silty sand)
13R-1, 53–58	109	0.5	627.2	3.7	7.8	39.0	130.2	4.0	2.1	364	22	197	380	Pelagic brown clay
19R-2, 107–117	162	0.6	610.4	9.9	8.5	37.7	108.3	3.8	2.1	404	17	157	447	Calcareous silty clay
21R-1, 103–110	179	0.6	613.3	11.9	8.5	38.5	114.3	3.4	1.7	400	11	124	459	Claystone
26R-1, 0–10	225	0.4	612.3	12.2	8.1	38.3	118.4	2.7	1.8	392	20	151	480	Calcareous claystone
29R-3, 29–34	258	0.6	583.7	12.0	7.2	37.5	115.5	4.4	1.9	363	41	913	473	Pelagic clay
32R-2, 140–150	286	0.2	575.8	12.5	6.5	37.5	96.1	12.9	4.6	376	46	637	395	Nannofossil chalk
40R-2, 140–150	361	0.6	587.6	15.0	8.0	36.5	80.5	10.2	2.6	432	35	499	238	Volcaniclastic turbidite
43R-1, 140–150	384	0.6	578.8	15.1	7.9	36.0	77.3	11.7	2.5	427	49	556	295	Volcaniclastic sandstone
47R-1, 140–150	422	0.6	530.4	13.2	7.9	33.8	66.8	11.5	2.2	398	53	203	255	Volcaniclastic sandstone
50R-2, 140–150	450	0.8	553.1	13.6	7.9	34.7	74.0	10.5	2.2	409	54	179	274	Volcaniclastic sandstone
56R-2, 140–150	500	0.8	585.7	15.7	8.2	36.5	81.5	2.8	1.2	447	22	216	167	Tuffaceous claystone

Note: Na* calculated by charge balance.
[a] Depth rounded to nearest meter.

of Unit V, and the claystone of Units VIII–IX. Squeezing yielded between 0.9 ml/cm and 5.5 ml/cm in whole-round samples. Highest yields (3.3–5.5 ml/cm) were obtained between 109 and 226 mbsf. At 321 and 471 mbsf the amount of water recovered was so low that analysis will be required onshore. Chemical analyses are summarized in Table 5 and presented in Figures 36 and 37. Except at 26 mbsf, pollution by drilling fluids can be ruled out, as potassium, calcium, and magnesium have concentrations very different from those of seawater or drilling mud (see Table 4, "Inorganic Geochemistry" section, "Site 800" chapter).

Results

From 22 to 83 mbsf, concentration profiles show very intense enrichments in calcium and chloride and depletions in magnesium, potassium, sodium, strontium, sulfate, and alkalinity. Within only 60 m, salinity increases from 34.8‰ to 39‰, calcium increases to 770% of seawater content, strontium to 400%, and chloride to 114%. In the same interval, magnesium is reduced to 0.5% of seawater content, potassium to about 22%, and sodium to about 78%. Below 83 mbsf compositions are roughly similar until 225 mbsf. At 258 mbsf, within a level of pelagic clay in the chalk of Unit III, concentrations remain similar except for silica, which increases to 913 μmol/L. Below this level, from 258 to 500 mbsf, the general trend is a progressive decrease of salinity (about 39‰ to 34‰) as a result of decreases in calcium and chloride contents. In this interval, sodium and magnesium increase slightly.

Manganese gradually increases from seawater concentration at 26 mbsf to 54 μmol/L at 450 mbsf and drops down to 22 μmol/L at 500 mbsf.

Discussion

The most important feature of concentration profiles in Hole 802A is the very large increase in calcium and chloride concentrations between 26 and 83 mbsf. This very high gradient is not related to any kind of porosity or water content change in the first hundred meters of the hole (see "Physical Properties" section, this chapter). Therefore, it implies that the tuffs of Unit II are presently undergoing very intense reactions; otherwise, diffusion would have reduced the gradients. These reactions are likely to be limited to Unit II because the calcium and chloride contents begin to decrease below 258 mbsf (top of the chalk of Unit III). In Unit II, the calcium release can be due either to alteration of the volcanic glass and the plagioclase, which are abundant in this unit, or to dissolution of carbonates, which represent 0.5% to 1% of the

rock at the top of Unit II (see "Lithostratigraphy and Sedimentology" section, this chapter). Dissolution of carbonate should be accompanied by an increase in alkalinity and is therefore unlikely. The alteration of volcanic material is probably responsible for the strontium release which correlates with the calcium release.

In Unit II the calcium change is balanced by the uptake of sodium, magnesium, and potassium and also by a chloride increase. Chloride concentration in pore water can be enhanced by dissolution of evaporites, gas hydrate formation, clay membrane filtration, or uptake of water by early diagenetic reactions. As evaporites are not present in the sediment and organic matter content is very low, the first two processes can be ruled out. Membrane filtration is also unlikely because the clay content is typically below 20% and the compaction of this unit is not very important. Formation of authigenic phases such as smectite and zeolite is therefore the most probable process and it is consistent with the reactions that deplete the pore water in magnesium, sodium, and potassium. This is supported by the presence of fractures filled by mixtures of zeolites such as analcime, analcime-wairakite, and/or laumontite at 63, 81, 115, and 168 mbsf (XRD determination). At the limit between Unit II and III, the silica content changes abruptly from 151 μmol/L at 225 mbsf to 913 μmol/L at 258 mbsf. This very rapid change suggests that silica is intensively taken up in diagenetic reactions in Unit II.

Below 258 mbsf the calcium and chloride contents decrease and the depletions in magnesium and sodium are less extreme. Concentrations in the underlying units are probably influenced by those of Unit II because of diffusion. It is therefore difficult to determine if reactions occur in these units or not. Unit V and VIII through X are likely to undergo reactions, as suggested by a decrease in silica content below Unit III.

Conclusion

Pore-water chemistry in Hole 802A is dominated by intense alteration and diagenetic reactions in the tuff of Unit II. These reactions are responsible for a extremely high gradients in calcium and chloride contents in the first 100 m of the hole. Similar gradients in calcium and chloride have been reported in ODP Hole 793 due to reactions within volcanic material (Leg 126, Shipboard Scientific Party, 1990). However, in that case the high gradients were enhanced by a slow diffusion barrier at the top of the formation. There is no such barrier in Hole 802A, suggesting that the rate of alteration of volcanic material and of zeolite and smectite formation is sufficiently high to overprint the influence of diffusion from seawater.
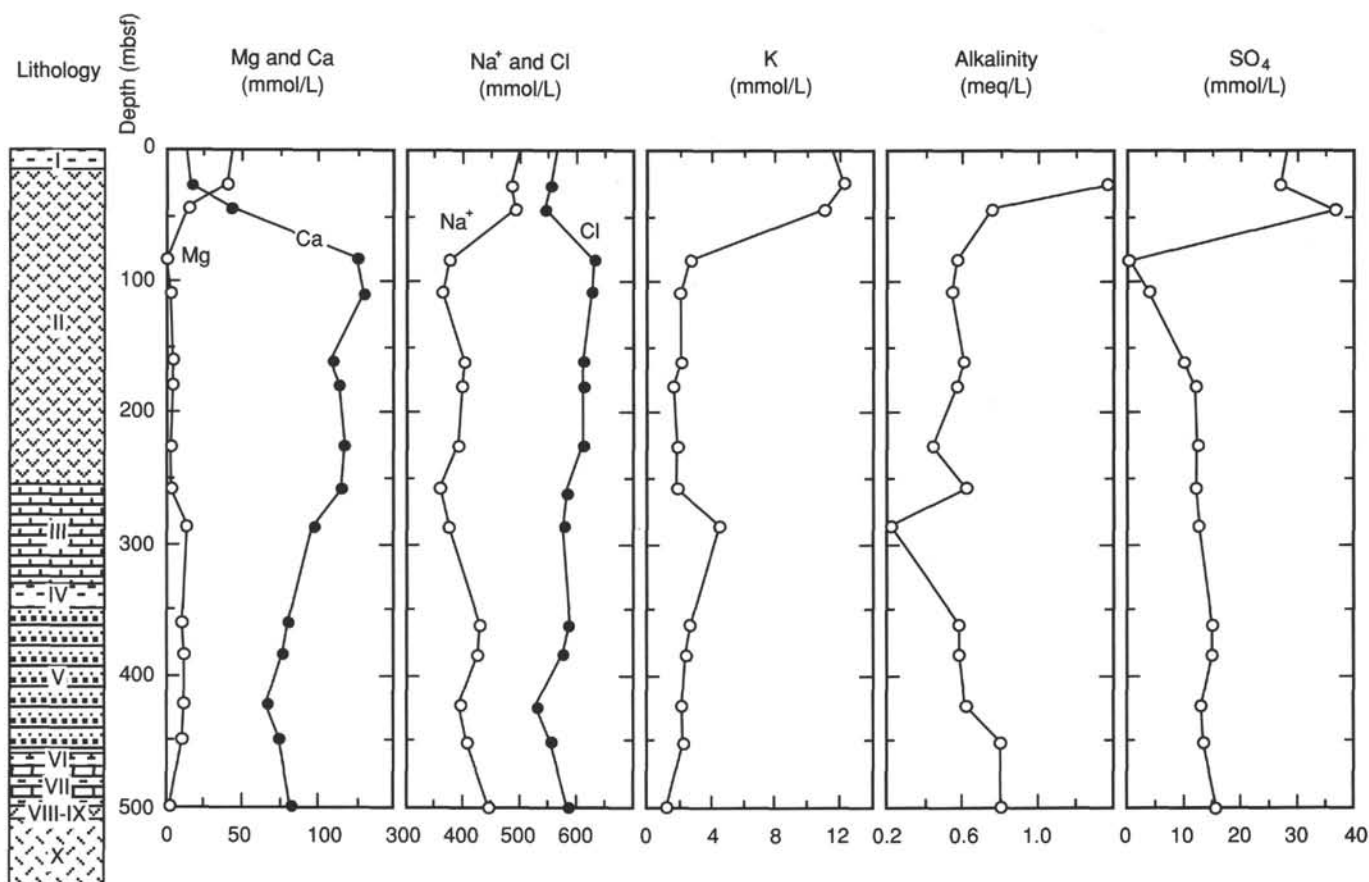
Figure 36. Concentration vs. depth profiles for Mg, Ca, Na*, Cl, K, alkalinity, and SO₄ in interstitial water extracted from sediments in Hole 802A. The lithostratigraphic column refers to the lithologic units defined in the "Lithostratigraphy and Sedimentology" section (this chapter). Unit I, brown pelagic clay; Unit II, tuff; Unit III, nannofossil chalk; Unit IV, claystone; Unit V, volcaniclastic turbidites; Unit VI, claystone and radiolarite; Unit VII, calcareous claystone and radiolarian limestone; Units VIII and IX, claystone and volcaniclastic turbidites; and Unit X, basalt.

PHYSICAL PROPERTIES

Determination of physical properties of sediments and rocks recovered at Site 802 was based only on measurements using discrete samples. Continuous measurements provided by the GRAPE and P-wave logger were not obtained because sediments and rocks did not completely fill core liners. Physical properties measured on discrete samples are listed in Table 6 and include index properties (wet-bulk density, porosity, water content, and grain density), compressional-wave velocity, and thermal conductivity. All techniques and equipment used in making the measurements are described in the "Explanatory Notes" chapter (this volume). Physical properties were determined for samples from lithologic Units II through X. Sediment recovery from Unit I (1 cm) was insufficient for physical properties measurements.

Index Properties

Variations in index properties among the lithologic units identified at Site 802 are described in the following section in terms of porosity, wet-bulk density, and grain density. Water content varies directly with porosity, and values for water content are listed in Table 6 and plotted in Figure 38. Wet-bulk density was determined by gravimetric and 2-min GRAPE techniques. Values cited for bulk density are those of gravi-

metric analyses, unless otherwise specified. Grain density was determined using "solid" chunks for all samples and powdered specimens for four samples (Table 6). The use of pycnometer-chamber inserts designed and fabricated for cube samples reduced previous volume measurement errors and yielded grain density measurements comparable to those obtained using powdered samples.

Index properties of lithologic Unit II (14.6–237.4 mbsf) reflect the division of this unit into two subunits. Subunit IIA (14.6–160.6 mbsf) consists predominantly of sand-sized tuffs (volcaniclastic turbidites), which typically contain 60% to 80% angular, fresh glass shards and tachylite (see "Lithostratigraphy and Sedimentology" section, this chapter). Index properties of the tuffs are moderately variable and display no downsection trends in variation (Fig. 38). Porosity of these rocks ranges from 31.3% to 60.4% and averages 49.3% (Table 6). Wet-bulk density of the tuffs ranges from 1.62 to 2.14 g/cm³ and averages 1.85 g/cm³. Pelagic brown clays, sampled at 15.70 and 108.77 mbsf, are a minor component of Subunit IIA and possess index properties distinctly different than those of the tuffs. At 15.70 and 108.77 mbsf the pelagic clays display porosities of 86% and 78% and wet-bulk densities of 1.25 and 1.35 g/cm³, respectively. Grain density in lithologic Subunit IIA ranges from 2.52 to 2.78 g/cm³ and averages 2.65 g/cm³.

Subunit IIB (160.6–237.4 mbsf) is distinguished from Subunit IIA by an increase in the proportion of redeposited
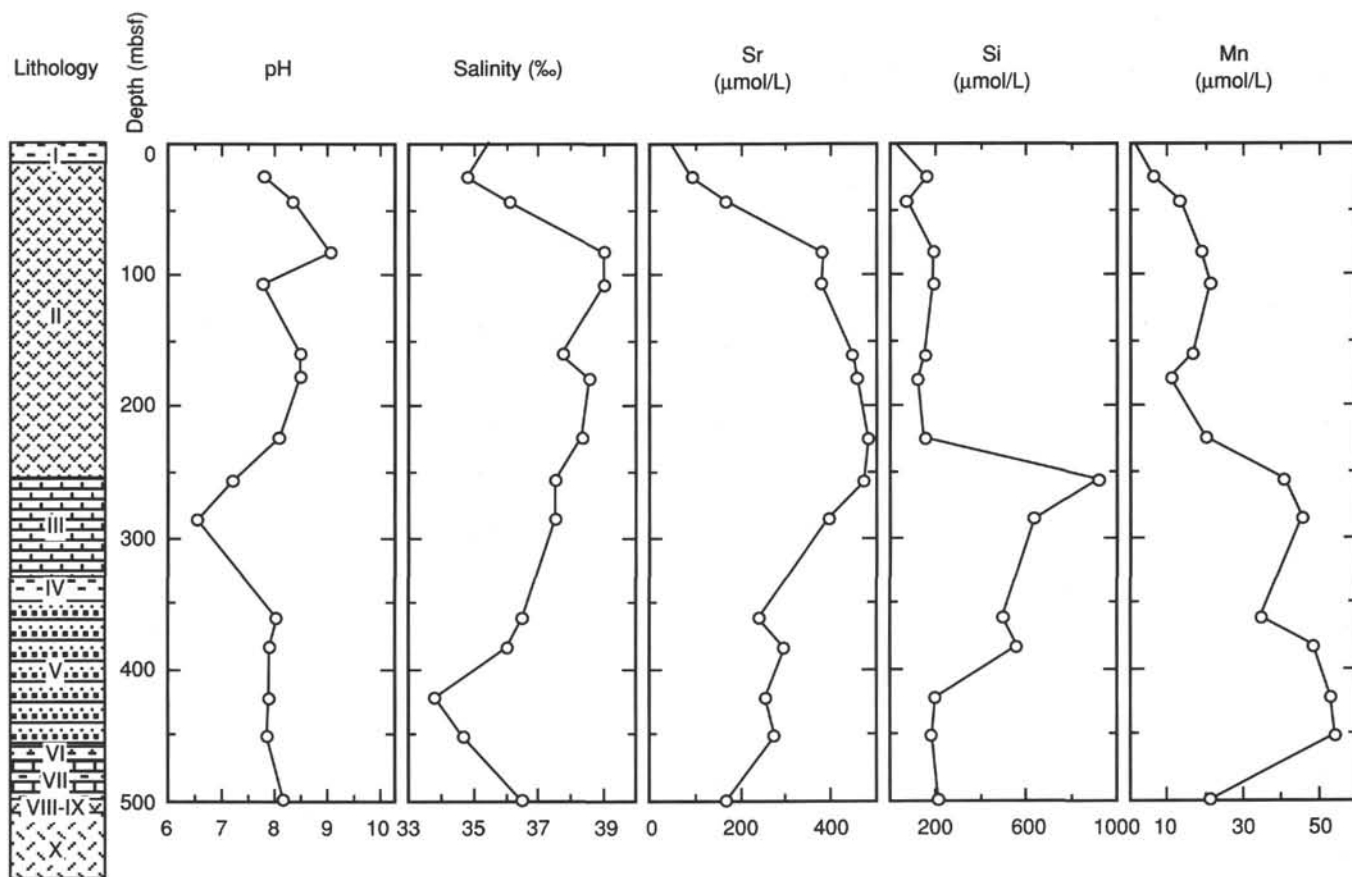
Figure 37. Profiles of depth vs. pH, salinity, and Sr, Si, and Mn concentrations in interstitial water extracted from sediments in Hole 802A. See Figure 36 for legend.

calcareous claystone and chalk and a change in composition of volcaniclastic sandstones, represented by decreased abundance of volcanic glass and increased abundance of igneous rock fragments, secondary calcite, and in some instances, microfossils. The increased abundance of fine-grained sedimentary rocks and the change in composition of volcaniclastic sandstones are reflected in the variation of index properties (Fig. 38). Properties of the sandstones, claystones, and siltstones in Subunit IIB are distinct. The volcaniclastic sandstones are characterized by porosities that range from 44.6% to 54.9% and average 51.1%. The wet-bulk density of these rocks ranges from 1.79 to 2.02 g/cm³ and averages 1.87 g/cm³. The ranges of porosity and wet-bulk density for fine-grained rocks in Subunit IIB are 58.7% to 72.3% and 1.48 to 1.73 g/cm³, respectively. From the top of Subunit IIB to 215.82 mbsf, porosity of the fine-grained rocks increases and their wet-bulk density decreases with depth. At 215.82 mbsf a porosity of 72.3% and wet-bulk density of 1.48 g/cm³ coincide with a local calcium carbonate concentration minimum of 5.2% (see "Lithostratigraphy and Sedimentology" section, this chapter). Below 215.82 mbsf, porosity decreases steadily and wet-bulk density increases in association with increasing carbonate concentration in the claystones. These trends culminate in Unit III at 254.65 mbsf where porosity is 30.9%, wet-bulk density is 2.18 g/cm³, and calcium carbonate content is 78.8%. Grain density in Subunit IIB is slightly higher than that in Subunit IIA, reflecting the decreased abundance of glass and increased concentrations of igneous rock fragments and calcareous constituents. Grain density ranges from 2.63 to 2.86 g/cm³ and averages 2.73 g/cm³ in Subunit IIB.

The chalks and calcareous claystones of lithologic Unit III (237.4–329.9 mbsf) are characterized by highly variable porosity and wet-bulk density (Fig. 38). Grain density, however, is extremely uniform in Unit III with most sediments displaying values between 2.65 and 2.72 g/cm³ (Fig. 38). Sediments sampled at 285.96, 311.56, and 312.42 mbsf exhibit grain densities between 2.49 and 2.59 g/cm³ (Table 6) and occur in an interval marked by a significant increase in silica concentration on wireline geochemical logs (see "Downhole Measurements" section, this chapter) and an increase in the degree of silicification in the cores. As a consequence of the uniformity in grain density, there is a strong inverse relationship between porosity and wet-bulk density. The inverse relationship between porosity and calcium carbonate concentration, which is present in the transition between Subunit IIB and Unit III, is also well developed in the chalks and claystones of Unit III. In these sedimentary rocks porosity ranges from 18.5% to 53.8%, and wet-bulk density ranges from 1.76 to 2.39 g/cm³. One chert nodule was sampled at 312.42 mbsf, and it displays a porosity of 1.5% and wet-bulk density of 2.53 g/cm³.

Only two samples were obtained in the zeolitic pelagic claystones of lithologic Unit IV (329.9–349.2 mbsf). Averages for porosity, wet-bulk density, and grain density for this interval are 49.8%, 1.84 g/cm³, and 2.64 g/cm³, respectively.

The volcaniclastic turbidites of lithologic Unit V (349.2–460.0 mbsf) are similar to those of Unit II in that the properties of sand-sized and fine-grained sediments are distinct and display little evidence of downsection change. The silty claystones of Unit V differ from those of Unit II in that they display a slightly greater degree of compaction. Volcaniclastic

sandstones of Unit V are characterized by porosity and wet-bulk density ranges of 43.2% to 51.7% and 1.86 to 2.04 g/cm³ and averages of 48.5% and 1.94 g/cm³, respectively. Excluding a sample with anomalously low porosity (38.4%) at 457.48 mbsf, porosity of the silty claystones ranges from 49.7% to 61.8% and averages 56.7%. Wet-bulk density of these rocks ranges from 1.60 to 1.89 g/cm³ and averages 1.74 g/cm³. Grain density is moderately variable in Unit V, with sandstones exhibiting slightly higher grain densities than those of the finer-grained sediments. Grain density ranges from 2.76 to 2.85 g/cm³ for the volcaniclastic sandstones and from 2.44 to 2.82 g/cm³ for the silty claystones. Low grain density at 438.27 mbsf (2.44 g/cm³) is associated with increases in radiolarian abundance and degree of silicification of the sediments (see "Lithostratigraphy and Sedimentology" section, this chapter).

The lowermost 45 m of the sedimentary section at Site 802, which encompass lithologic Units VI (460.0–469.9 mbsf), VII (469.9–497.1 mbsf), VIII (497.1–499.6 mbsf), and IX (499.6–509.2 mbsf), contain a variety of rock types, including claystone, radiolarite, nannofossil chalk, siliceous limestone, and volcaniclastic sandstone (Table 6). From Unit VI through Unit VIII, claystones are characterized by decreasing porosity and increasing wet-bulk density, trends initiated in the basal part of Unit V. In this interval porosity decreases from 45.7% to 42.9%, and wet-bulk density increases from 1.90 to 1.93 g/cm³. The volcaniclastic claystone of Unit IX differs from claystones in Units VI through VIII, and at 507.32 mbsf displays a porosity of 48.1%, a wet-bulk density of 1.87 g/cm³, and grain density of 2.77 g/cm³. Radiolarite was sampled at 463.14 mbsf and is characterized by a porosity of 42.0% and wet-bulk density of 1.90 g/cm³. The relatively low grain density (2.53 g/cm³) at this depth reflects the greater abundance of biogenic silica in this sediment. Chalks and limestones of Unit VII are characterized by lower porosities and higher wet-bulk densities than other rock types in Units VI through IX. Porosity of the carbonate rocks decreases downsection, from 43.8% at 470.15 mbsf to 26.1% at 489.04 mbsf, the latter value representing the porosity of a siliceous limestone. Coinciding with the porosity reduction is an increase in wet-bulk density from 1.95 to 2.22 g/cm³. One volcaniclastic sandstone interval was sampled in Unit IX, at 500.43 mbsf, and its index properties are similar to those of sandstones in Unit V. The sandstone in Unit IX is characterized by a porosity of 48.1%, wet-bulk density of 1.93 g/cm³, and grain density of 2.75 g/cm³. With the exception of the low grain density of the radiolarite and the slightly higher density of the volcaniclastic sandstone and claystone, the grain density of rocks from the lowermost 45 m of the sedimentary section at Site 802 is relatively uniform and closely grouped about a mean of 2.66 g/cm³.

Index properties of the basalts of lithologic Unit X (509.2–559.8 mbsf) are representative of fine-grained extrusive basalts. Porosity of five of the seven basalt samples analyzed ranges from 1.2% to 2.6% (Table 6). Rocks from 519.86 and 535.60 mbsf display porosities of 6.3% and 8.2%, respectively. Grain density of the basalts varies in a narrow range between 2.92 and 2.97 g/cm³. The low porosity and narrow range in grain density reflect the relative lack of alteration of basalts recovered at Site 802. At Sites 800 and 801 significant basalt alteration is accompanied by high porosity, between 10% and 20%, and grain densities as low as 2.70 g/cm³. Wet-bulk density of the basalt ranges from 2.77 to 2.94 g/cm³.

Compressional-Wave Velocity

At Site 802 compressional-wave velocities were measured in both vertical and horizontal propagation directions. Velocity anisotropy was calculated as the ratio of the velocity difference and the mean velocity, expressed as a percentage (see "Explanatory Notes" chapter, this volume). Variations in the velocity data generally conform with changes in lithology and physical properties. Unless otherwise noted, the velocity values cited are for measurements made in the vertical propagation direction.

The coarse-grained volcaniclastic turbidites of Subunit IIA are characterized by high and highly variable sonic velocity. Velocity of the sand-sized tuffs ranges from 2221 to 4080 m/s with no apparent downsection trend (Fig. 39). The average velocity for these rocks is 3024 m/s. The tuffs of Subunit IIA are nearly elastically isotropic, with values of velocity anisotropy ranging from 3.6% to 2.6% and averaging 0.4%. The uniformity of composition of the tuffs and abundance of volcanic glass in the rocks is most likely responsible for the low velocity anisotropy. In Subunit IIB, ranges for compressional-wave velocity of the tuffs and silty claystones are distinct (Table 6). The velocity of the tuffs varies narrowly between 2230 and 2562 m/s. The average velocity of these rocks, 2351 m/s, is substantially lower than that of tuffs in Subunit IIA. Higher velocity anisotropy of tuffs of Subunit IIB also distinguishes them from the rocks of Subunit IIA. Velocity anisotropy of the tuffs of the lower subunit range from 1.1% to 2.6% and average 2.2%. Claystones and siltstones of Subunit IIB exhibit sonic velocities that range from 1632 to 1962 m/s and average 1719 m/s. The velocity anisotropy of the fine-grained rocks varies from 0.5% to 3.5% and displays a general downsection increase.

The rocks of Unit III are characterized by highly variable sonic velocity (Fig. 39). Chert sampled at 312.42 mbsf displays the highest velocity measured for sedimentary rocks at Site 802 (5301 m/s). The compressional-wave velocity of the chalks and calcareous claystones that comprise the bulk of Unit III ranges from 1669 to 3181 m/s. The velocity of the chalks varies directly with the calcium carbonate concentration and increases slightly downsection, from approximately 1900 m/s at the top of Unit III to 2500 m/s at the base of the unit (Fig. 39). The most striking feature of sonic velocity variation in Unit III is high anisotropy displayed by chalks and claystones between 254 mbsf and the base of Unit III. Excluding a calcareous claystone sample at 256.68 mbsf, which is approximately isotropic, the range in velocity anisotropy is 5.9% to 13.2%. Anisotropy in this interval averages 8.7%. The range of velocity anisotropy for carbonate rocks of Unit III is comparable to that reported for similar rocks from the Rio Grande Rise (Carlson et al., 1983). Carlson et al. (1983) determined that a negative correlation ($r = 0.74$) exists between velocity anisotropy and carbonate content for the rocks of the Rio Grande Rise and concluded that the anisotropy was primarily controlled by bedding. A positive correlation ($r = 0.70$) between calcium carbonate concentration and velocity anisotropy characterizes the chalks and calcareous claystones of Unit III and may be the result of preferred orientation of calcite, as suggested by Carlson et al. (1983).

The lithologic change from nannofossil chalk in Unit III to pelagic claystone in Unit IV is marked by a sharp decrease in compressional-wave velocity from approximately 3100 m/s in the chalk to 1700 m/s in the claystone. Velocity variation in the volcaniclastic turbidites of Unit V, which underlie the pelagic claystones, is similar to the pattern of velocity variation in Subunit IIB. Sonic velocity of the sandstones in Unit V ranges from 2190 to 2613 m/s and averages 2377 m/s. Velocity anisotropy of these rocks is slightly higher than that of volcaniclastic sandstones and tuffs in overlying units, ranging from 1.2% to 3.9% and averaging 2.9%. Sonic velocity of the claystones in Unit V varies between 1713 and 2234 m/s;

Table 6. Summary of physical properties for Hole 802A.

Core, section, interval (cm)	Depth (mbsf)	Wet-bulk density Gravimetric (g/cm³)	GRAPE (g/cm³)	Grain density[a] (g/cm³)	Porosity (%)	Water content (%)	Vertical velocity (m/s)	Horizontal velocity (m/s)	Velocity anisotropy (%)	Thermal conductivity (W/m · K)	Remarks
129-802A											
3R-1, 21–23	14.81	1.88	1.94	2.58	45.0	24.4	3325	3379	1.6	1.07	Tuff (sand-size)
3R-1, 110–113	15.70	1.25		2.62	86.0	70.1					Pelagic clay
4R-2, 6–8	25.86	2.05	2.05	2.78	41.3	20.5	2881	2779	−3.6	1.31	Volcaniclastic breccia
4R-2, 86–88	26.66	1.71	1.74	2.65	57.6	34.2	2393	2426	1.4	0.99	Volcaniclastic sandy siltstone
5R-1, 126–128	34.96	1.94	1.99	2.64	43.3	22.7	3259	3214	−1.4	1.10	Tuff (sand-size)
6R-2, 70–72	45.10	1.62	1.67	2.54	60.4	37.9	2223	2212	−0.5	1.06	Tuff (sand-size)
7R-1, 101–103	53.41	1.79	1.77	2.68	54.0	30.8	2507	2548	1.6	1.05	Tuff (sand-size)
8R-2, 41–43	63.81	1.93	2.00	2.60	42.5	22.4	3377	3352	−0.7	1.17	Tuffaceous silty sandstone
10R-1, 69–71	81.09	1.71	1.74	2.67	58.3	34.7	2428	2472	1.8	1.09	Tuff (sand-size)
11R-1, 10–12	91.20	1.75	1.77	2.72	57.4	33.4	2654	2674	0.8	1.12	Tuff (sand-size)
12R-1, 7–9	98.97	1.83	1.88	2.62	49.4	27.5	3309	3396	2.6	1.12	Tuff (sand-size)
13R-1, 47–49	108.77	1.35		2.56	78.4	58.9				0.86	Pelagic clay
13R-2, 61–61	109.50									0.95	Pelagic clay
14R-2, 73–75	116.63	2.14	2.22	2.65	31.3	14.9	4082	4163	2.0	1.48	Tuff (sand-size)
15R-2, 37–39	123.97	1.71	1.74	2.68	58.5	34.8	2393	2376	−0.7	1.11	Tuff (sand-size)
16R-1, 108–110	132.18	2.01	2.06	2.52	34.4	17.4	3841	3856	0.4	1.17	Tuff (sand-size)
17R-1, 36–38	140.76	1.74	1.77	2.66	56.0	32.7	2393	2376	−0.7	1.08	Tuff (sand-size)
18R-1, 3–5	149.73	1.88	1.91	2.72	49.5	26.8	2896	2958	2.1		Tuff (sand-size)
19R-1, 112–114	160.22	1.71	1.70	2.75	60.5	36.0	1632	1652	1.2		Silty claystone
19R-2, 79–81	161.39	1.73	1.76	2.74	58.7	34.4	1962	1992	1.5	1.15	Siltstone
20R-1, 10–12	168.40	2.02	2.04	2.82	44.6	22.4	2562	2627	2.5		Tuff (sand-size)
21R-2, 9–11	178.79	1.54	1.56	2.63	68.1	45.1	1773	1782	0.5		Volcaniclastic silty claystone
21R-2, 50–52	179.20	1.80	1.84	2.72	53.9	30.4	2294	2319	1.1	1.12	Tuff (sand-size)
22R-1, 10–12	187.10	1.79	1.79	2.72	54.9	31.2	2254	2310	2.5	1.14	Tuff (sand-size)
23R-1, 10–12	196.50	1.63	1.61	2.86	67.2	42.0	1632	1677	2.7		Calcareous nannofossil clay
23R-1, 66–68	197.06	1.93	1.98	2.76	47.7	25.1	2413	2472	2.4	1.21	Tuff (sand-size)
24R-1, 3–5	206.13	1.57		2.68	66.7	43.0	1662	1722	3.5	1.13	Calcareous mudstone
25R-1, 12–14	215.82	1.48	1.40	2.68	72.3	49.5	1635	1649	0.9		Claystone with nannofossils
26R-1, 42–44	225.82	1.64	1.64	2.73	63.6	39.3	1652	1690	2.3	1.11	Calcareous claystone
27R-1, 103–105	236.13	1.79	1.78	2.70	54.4	30.9	2230	2289	2.6	1.27	Tuff (sand-size)
27R-3, 112–114	239.22	1.89	1.89	2.72	48.9	26.3	1880	1953	3.8	1.54	Nannofossil chalk
27R-5, 26–28	241.36	1.89	1.89	2.65	46.5	25.0	1889	1901	0.6	1.48	Nannofossil chalk
28R-1, 36–38	245.06	1.93	1.90	2.68	45.3	23.9	1983	2039	2.8	1.78	Nannofossil chalk
28R-3, 54–56	248.24	2.08	2.06	2.70	37.2	18.2	2496	2411	−3.5	1.57	Tuffaceous nannofossil foraminiferal packstone
29R-1, 15–17	254.65	2.18	2.18	2.70	30.9	14.4	2205	2517	13.2	2.13	Calcareous claystone
29R-2, 68–70	256.68	1.79	1.91	2.68	53.7	30.5	1669	1673	0.2	1.44	Calcareous claystone
30R-1, 71–73	264.91	1.78	1.78	2.65	53.8	30.8	1808	1960	8.1	1.46	Nannofossil chalk
31R-1, 20–22	274.00	2.00	2.02	2.65	40.2	20.4	1911	2027	5.9	1.59	Nannofossil chalk
32R-1, 13–15	283.63	2.38	2.21	2.70	19.2	8.2	2394	2652	10.2	2.03	Nannofossil chalk
32R-2, 96–98	285.96	1.77	1.84	2.49	48.9	28.0	2243	2417	7.5	1.59	Nannofossil chalk
33R-1, 54–56	293.34	2.12	2.08	2.71	34.8	16.7	2023	2164	6.7	1.95	Nannofossil chalk
34R-1, 60–62	302.90	2.39	2.36	2.70	18.5	7.8	3181	3476	8.9	2.48	Nannofossil chalk
35R-1, 6–8	311.56	1.76	1.75	2.49	49.7	28.7	1975	2114	6.8	1.33	Nannofossil chalk
35R-CC, 5–7	312.42	2.53	2.50	2.55(2.59)	1.5	0.6	5301	4993	−6.0		Chert
36R-1, 31–33	321.01	2.33	2.29	2.70	22.0	9.6	3093	3439	10.6	2.36	Nannofossil chalk
38R-2, 63–65	341.33	1.78	1.82	2.62	52.7	30.1	1699	1729	1.8	1.24	Pelagic claystone
38R-4, 91–93	344.61	1.90	1.93	2.67	46.9	25.1	1728	1774	2.6	1.15	Pelagic claystone
39R-1, 58–60	349.28	1.86	1.84	2.76	51.7	28.2	2304	2396	3.9	1.22	Tuff (sand-size)
40R-2, 103–105	360.63	1.94	1.96	2.82	48.8	25.6	2399	2474	3.1	1.27	Volcaniclastic sandstone
40R-3, 11–13	361.21	1.80	1.83	2.77	55.2	31.1	1713	1770	3.3	1.23	Volcaniclastic claystone
41R-1, 10–12	365.60	1.76	1.78	2.69	55.7	32.2	1728	1809	4.6	1.21	Volcaniclastic claystone
41R-4, 121–123	371.21	1.78	1.80	2.82	57.9	33.0	2034	2081	2.3	1.25	Volcaniclastic sandy, silty claystone
42R-1, 96–98	373.76	1.74	1.73	2.77	59.3	34.7	1809	1856	2.6	1.19	Volcaniclastic sandy siltstone
42R-2, 111–113	375.29	1.78	1.81	2.67	54.1	30.9	1755	1811	3.1	1.30	Volcaniclastic claystone
43R-1, 114–116	383.24	1.83	1.85	2.78	54.2	30.1	1771	1879	5.9	1.33	Volcaniclastic claystone
43R-2, 15–17	383.75	2.06	2.05	2.85	43.2	21.3	2613	2697	3.2	1.43	Volcaniclastic sandstone
44R-1, 50–52	391.80	1.67	1.68	2.50	56.2	34.2	1892	2004	5.7	1.29	Silty claystone
45R-2, 41–43	402.41	1.76	1.76	2.78	58.4	33.8	1957	2023	3.3	1.17	Silty claystone
46R-1, 60–62	410.60	1.69	1.71	2.76	61.8	37.2	1759	1850	5.0	1.24	Silty claystone
47R-1, 45–47	419.65	1.74	1.74	2.73	58.0	33.9	1781	1885	5.7	1.25	Silty claystone
47R-3, 74–76	422.94	1.71	1.73	2.72	59.6	35.4	1760	1887	7.0	1.22	Silty claystone
47R-4, 30–32	424.00	1.91	1.89	2.80	50.3	26.8	2190	2216	1.2	1.26	Volcaniclastic sandstone
48R-1, 66–68	429.36	1.84	1.83	2.78	53.6	29.7	2125	2149	1.1	1.20	Silty claystone
49R-1, 17–19	438.27	1.60	1.60	2.44	59.3	37.7	1753	1775	1.2	1.27	Silty claystone
49R-3, 128–130	442.38	1.71	1.74	2.72	59.3	35.2	1761	1857	5.3	1.24	Silty claystone

Table 6. Summary of physical properties for Hole 802A.

Core, section, interval (cm)	Depth (mbsf)	Wet-bulk density Gravimetric (g/cm³)	GRAPE (g/cm³)	Grain density[a] (g/cm³)	Porosity (%)	Water content (%)	Vertical velocity (m/s)	Horizontal velocity (m/s)	Velocity anisotropy (%)	Thermal conductivity (W/m · K)	Remarks
50R-1, 92–94	448.32	1.89	1.90	2.74	49.7	26.8	1761	1895	7.3	1.40	Volcaniclastic silty claystone
50R-2, 66–68	449.56	1.79	1.82	2.62	52.2	29.7	1867	1973	5.5	1.27	Claystone breccia
51R-1, 66–68	454.16	1.71	1.73	2.75	60.1	35.7	1761	1904	7.8	1.24	Claystone breccia
51R-3, 98–100	457.48	2.03	2.04	2.66	38.4	19.2	2234	2514	11.8	1.55	Claystone
52R-2, 114–116	462.44	1.90	1.92	2.63	45.7	24.5	1889	1984	4.9	1.40	Claystone
52R-3, 34–36	463.14	1.90	1.90	2.53	42.0	22.5	2132	2451	13.9	1.45	Radiolarite
53R-1, 75–77	470.15	1.95	1.88	2.67	43.8	22.8	1872	1968	5.0	1.46	Clayey nannofossil chalk
53R-2, 23–25	470.93	2.10	2.12	2.64	33.7	16.3	2274	2372	4.2	1.56	Nannofossil chalk
54R-1, 15–17	478.75	2.14	2.15	2.71	33.5	15.9	2111	2302	8.7	1.98	Clayey limestone
54R-3, 15–17	481.75	1.98	1.98	2.70	42.8	22.0	2034	2145	5.3	1.71	Clayey siltstone
54R-3, 50–52	482.10	2.00	2.00	2.68	41.3	21.1	2089	2260	7.9	1.64	Claystone
55R-1, 114–116	489.04	2.22	2.18	2.64	26.1	12.0	3070	3344	8.5	1.78	Siliceous limestone
56R-1, 101–103	498.11	1.95	1.99	2.64	42.9	22.4	2088	2244	7.2	1.44	Claystone
56R-3, 33–35	500.43	1.87	1.87	2.75	50.8	27.6	2124	2108	−0.8	1.39	Volcaniclastic sandstone
57R-1, 72–74	507.32	1.93	1.97	2.77	48.1	25.3	1925	2114	9.4	1.51	Claystone
58R-1, 38–40	516.38	2.93	2.89	2.97(2.99)	1.9	0.5	6217	6167	−0.8	2.01	Aphyric basalt
58R-2, 53–55	518.03	2.88	2.87	2.92	2.5	0.7	5966	5992	0.4	2.00	Aphyric basalt
58R-2, 105–107	518.55	2.92	2.92	2.97	2.6	0.8	5944	5939	−0.1	1.86	Moderately olivine-plagioclase microphyric basalt
58R-3, 86–88	519.86	2.82	2.83	2.94	6.3	2.1	5344	5274	−1.3	1.85	Sparsely olivine microphyric basalt
59R-1, 83–85	526.23	2.92	2.91	2.96(3.04)	2.3	0.7	6182	6311	2.1	1.94	Sparsely olivine-plagioclase microphyric basalt
60R-1, 90–92	535.60	2.77	2.78	2.92	8.2	2.8	5072	5074	0.0	1.82	Sparsely plagioclase microphyric to aphyric basalt
62R-1, 129–131	551.89	2.94	2.97	2.97(3.03)	1.2	0.40	6200	6197	0.0	2.09	Moderately olivine-plagioclase microphyric basalt

[a] Values in parentheses were determined using powdered samples.

however, most of the values lie in a relatively narrow range between 1700 and 1900 m/s. A consistent downsection trend in velocity variation is lacking for the claystones, and the rocks are characterized by an average velocity of 1846 m/s. The fine-grained rocks of Unit V, combined with the pelagic claystones of Unit IV, exhibit a general increase in velocity anisotropy with depth, from approximately 2% at 341 mbsf to 8% at 454 mbsf. Over this interval anisotropy of the claystones ranges from 1.1% to 11.8%.

Velocity variation in lithologic Units VI through IX reflects the mixture of lithologies present in this interval. Compressional-wave velocity of the claystones increases from 1889 m/s at 462.44 mbsf to 2088 m/s at 498.11 mbsf (Table 6). Velocity decreases to 1925 m/s in the claystone at 507.32 mbsf in Unit IX. The carbonate sediments of Unit VII display a range in velocities from 1872 m/s in chalk at 470.15 mbsf to 3070 m/s in siliceous limestone at 489.04 mbsf. Other values for compressional-wave velocity measured for rocks in the lowermost 45 m of the sedimentary section include 2132 m/s for radiolarite at 463.14 mbsf and 2124 m/s for volcaniclastic sandstone at 500.43 mbsf. The downsection increase in velocity anisotropy displayed by fine-grained rocks of Units IV and V continues for fine-grained rocks of Units VI through IX, culminating with at a value of 9.4% in the claystone of Unit IX. The radiolarite, which was sampled at 463.14 mbsf, is characterized by thin, parallel laminae and possesses the highest anisotropy (13.9%) in the lower part of the sedimentary section. Velocity anisotropy of the volcaniclastic sandstone of Unit IX is 0.8%.

A sharp increase in compressional-wave velocity marks the boundary between the sedimentary section at Site 802 and the underlying basalt. Sonic velocity in the basalt is high, varying between 5072 and 6217 m/s and averaging 5846 m/s, which attests to the high density and minimal alteration of these rocks. The basalts are essentially elastically isotropic, with velocity anisotropy ranging from 0.13% to 2.1% and averaging zero.

Variation of compressional-wave velocity at Site 802 displays consistent relationships with wet-bulk density that vary with lithology (Fig. 40). The lithologic grouping that includes clays, claystones, and siltstones displays the lowest velocities and the lowest velocity/density gradient (Fig. 40). The field represented by the variety of chalks and limestones sampled at Site 802 overlaps the field for fine-grained sediments and rocks and extends to higher wet-bulk density and velocity values. The velocity/density gradient for the chalks and limestones is greater than that of the claystones and siltstones; however, the carbonate rocks are also characterized by the greatest scatter on the density-velocity crossplot. Variations in composition and degree of silicification possibly influence the variability in the behavior of the carbonate rocks. Based on differences in the relationship between wet-bulk density and compressional-wave velocity, the coarse-grained volcaniclastic rocks at Site 802 can be divided into two groups: (1) tuffs of Subunit IIA and (2) tuffs and volcaniclastic sandstones of the other lithologic units. At equivalent wet-bulk densities, the tuffs and volcaniclastic sandstones of Subunit IIB and underlying lithologic units are characterized by higher velocities than are the chalks, limestones, fine-grained sediments, and rocks. The velocity/density gradient of these sandstones is intermediate between that of the claystone/siltstone group and that of the carbonate rocks. Tuffs of Subunit IIA are characterized by velocities distinctly higher than those of other volcaniclastic rocks at Site 802. These rocks are also
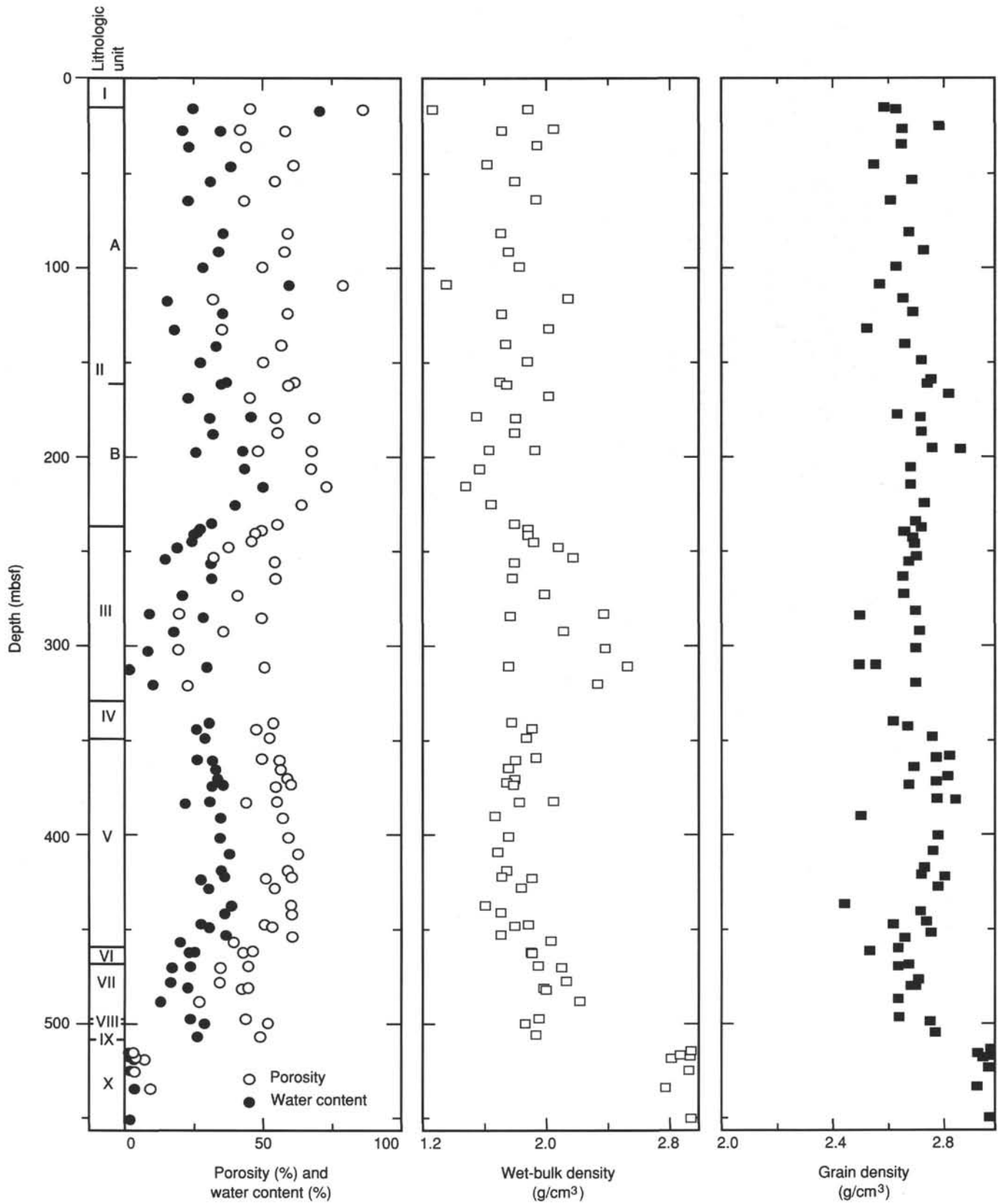
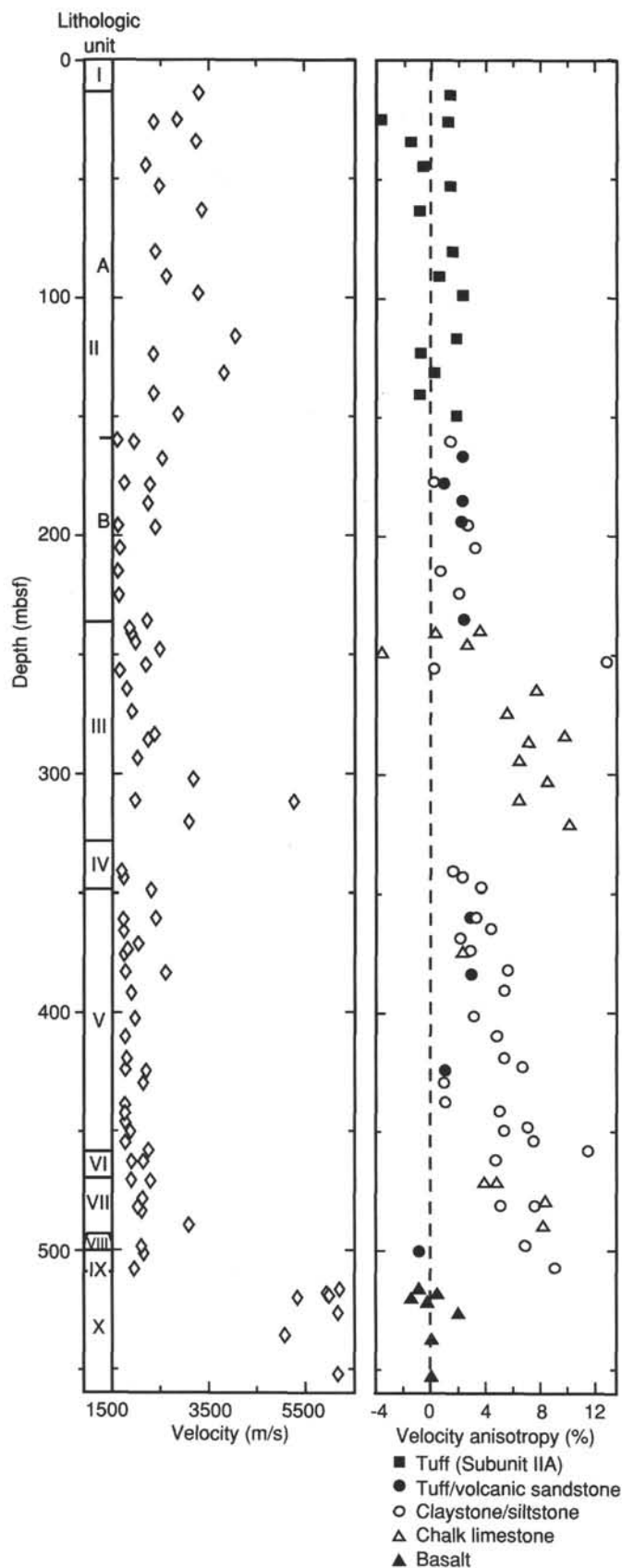Figure 38. Index properties (porosity, water content, wet-bulk density, and grain density) for Hole 802A.

Figure 39. Compressional-wave velocity measured perpendicular to bedding and velocity anisotropy vs. depth for Hole 802A. Velocity anisotropy profile is coded according to sediment and rock type.
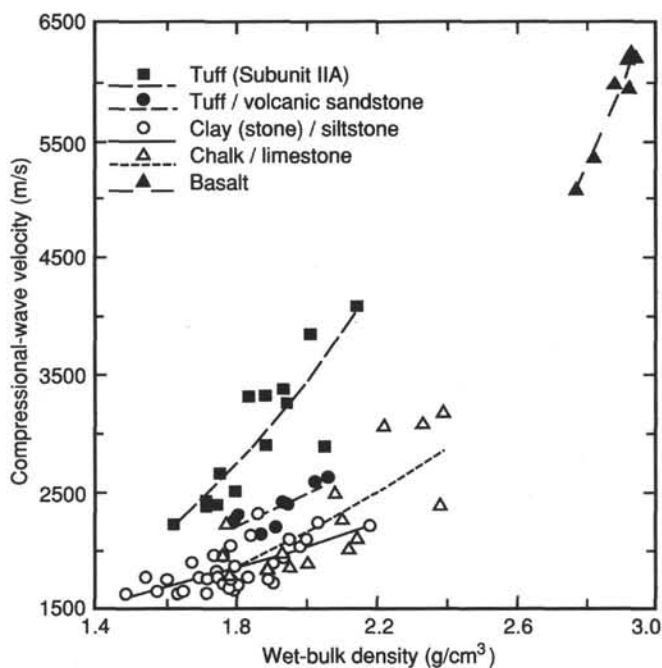

Figure 40. Wet-bulk density vs. compressional-wave velocity (measured perpendicular to bedding) for Hole 802A, coded according to sediment and rock type. Lines are best-fit exponential lines for the data.

characterized by the steepest velocity/density gradient for sedimentary rocks at Site 802.

The basalts sampled at Site 802 are characterized by a very steep velocity/density gradient (Fig. 39), 7700 ms^1/g cm^3. This gradient is twice the gradient of 3850 ms^1/g cm^3 that Christensen and Salisbury (1975) determined in their summary of DSDP basalt velocity data. However, the gradient for the basalts at Site 802 is comparable to that of basalts of the Gulf of California, which display a velocity/density gradient of approximately 7600 ms^1/g cm^3 (Christensen and Lewis, 1983). The basalts sampled in the Gulf of California are similar to those at Site 802 in that they are characterized by a low degree of alteration.

Thermal Conductivity

At Site 802 thermal conductivity measurements were primarily made on sedimentary and igneous rocks. Only two samples of unlithified sediments were analyzed. The conductivity of soft sediments was measured by a heated needle probe inserted in the sediment. Conductivity of lithified sediments and basement rocks was measured by a heated needle probe sandwiched between the sample and a slab of low conducting material. Details for both procedures for measuring thermal conductivity are described in the "Explanatory Notes" chapter (this volume).

Variation of thermal conductivity at Site 802 is characterized by relatively uniform, consistent trends (Fig. 41). In Subunit IIA thermal conductivity of the tuffs and volcaniclastic sandstones ranges from 0.99 to 1.48 W/m · K; however, excluding the two measurements greater than 1.3 W/m · K (from 25.86 and 116.63 mbsf), the conductivities of the coarse-grained volcaniclastic sediments are centered about a mean of 1.09 W/m · K. The thermal conductivity of the coarse- and fine-grained volcaniclastic rocks of Subunit IIB is slightly higher than that of rocks in Subunit IIA. The conductivity of rocks of Subunit IIB ranges from 1.11 to 1.27 W/m · K and averages 1.16 W/m · K. In contrast to patterns of index prop-
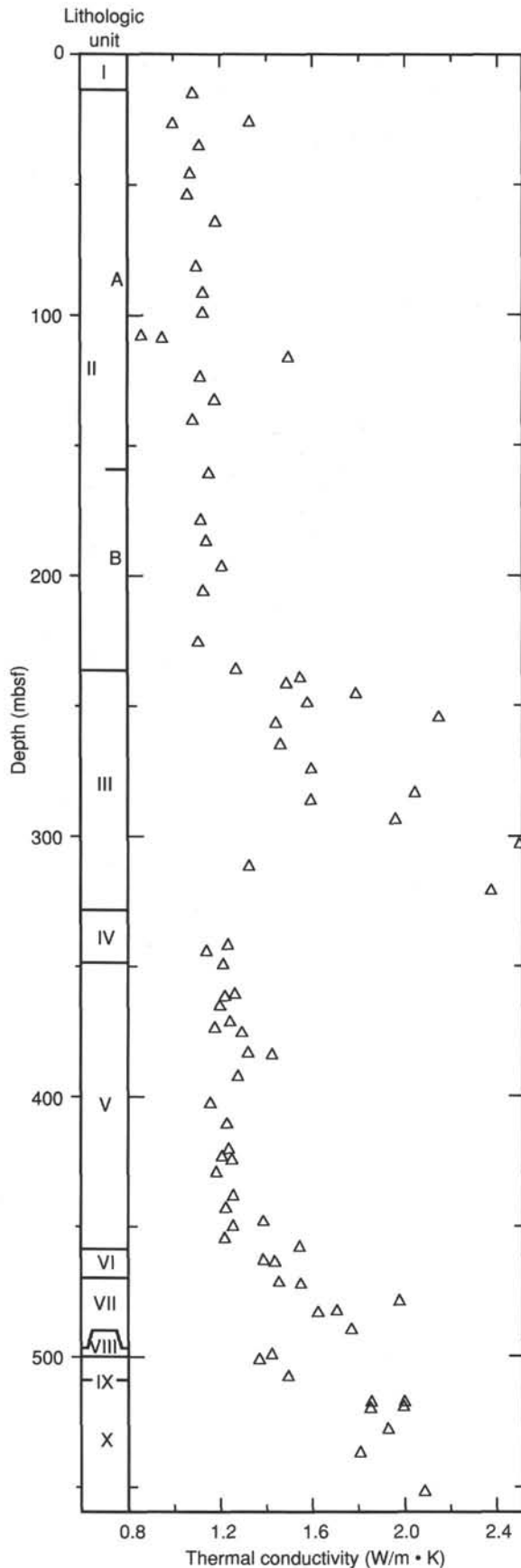
Figure 41. Thermal conductivity vs. depth for Hole 802A.

erty and compressional-wave velocity variation in Subunit IIB, there is not a distinction in thermal conductivity values between volcaniclastic sandstones and volcaniclastic claystones/siltstones. A distinct increase in conductivity is present at the base of Subunit IIB (Fig. 41) and corresponds with an increase in carbonate content.

The chalks and limestones of lithologic Unit III are characterized by high and highly variable thermal conductivity (Fig. 41). Conductivity ranges from 1.33 to 2.48 W/m · K (Table 6). The carbonate rocks of Unit III display a strong inverse relationship between thermal conductivity and porosity, which itself varies inversely with calcium carbonate concentration.

Thermal conductivity is relatively uniform in the pelagic claystones of Unit IV and the volcaniclastic claystones and sandstones of Unit V. In these two units conductivity ranges from 1.15 to 1.43 W/m · K and averages 1.27 W/m · K. As in Subunit IIB, ranges for the conductivities of the claystones and siltstones and sandstones overlap. In Units IV and V there is little change in conductivity with increasing burial depth. In contrast to this pattern a distinct downsection increase in thermal conductivity is present in Units VI and VII (Fig. 41). In these two units conductivity increases from 1.40 W/m · K at 462.44 mbsf to 1.78 W/m · K at 489.04 mbsf. The increase in conductivity in this part of the sedimentary section coincides with an increase in calcium carbonate concentration. A sharp decrease in thermal conductivity marks the boundary between Units VII and VIII. In Units VIII and IX thermal conductivity ranges from 1.39 to 1.51 W/m · K and averages 1.45 W/m · K.

Thermal conductivity of the aphyric to microphyric basalts of Unit X ranges from 1.82 to 2.09 W/m · K. Conductivity variation in the basalts displays a moderately strong inverse relationship with porosity. Average thermal conductivity of the basalts is 1.94 W/m · K.

The combined sediment, sedimentary rock, and igneous rock data sets display a strong inverse relationship between porosity and thermal conductivity that in part varies with lithology (Fig. 42). The grouping of rock types, including tuffs and volcaniclastic sandstones (excluding those of Subunit IIA), claystone and siltstone, and chalk and limestone, exhibits a well-defined trend of increasing conductivity with decreasing porosity. In this grouping the fields that encompass the different lithologies overlap extensively, suggesting that porosity exerts a greater control over thermal conductivity than does variation in grain size or sediment composition. The tuffs and volcaniclastic sandstones of Subunit IIA are represented in a field on the crossplot of porosity vs. thermal conductivity that is, for the most part, separate from the field encompassing the rest of the sedimentary rocks. Lower conductivity of the rocks of Subunit IIA is consistent with the abundant volcanic glass in these rocks and the lower thermal conductivity of silica glass relative to the mineral constituents of the other sedimentary rocks (Clark, 1966). The field represented by basalt in the porosity vs. conductivity crossplot is separate from the trend of the sedimentary rocks. The inverse relationship between porosity and thermal conductivity for these rocks is relatively strong ($r = 0.80$). Glass is abundant in the basalts at Site 802 (see "Igneous Petrology" section, this chapter), which may be responsible for the extent to which the trend of the basalts on the porosity vs. conductivity crossplot falls off the trend of the sedimentary rocks. The compositional similarity of the glass-rich tuffs of Subunit IIA and the basalts is suggested by the appearance of the basalt data falling along the trend defined by the Subunit IIA tuffs on the porosity-conductivity crossplot (Fig. 42).

IGNEOUS PETROLOGY

One of the objectives of Hole 802A in the East Mariana Basin was to recover, on the basis of magnetic lineation data, Jurassic oceanic basement situated beyond magnetic anomaly M37 (~165 Ma). To minimize the input of middle Cretaceous volcanic material (either as volcaniclastics or intrusives), Hole 802A was drilled in an area apparently well removed from mapped seamounts and where "basement" was indicated by seismic stratigraphy at about 500 mbsf. However, a thick sequence of reworked, distal, Cretaceous volcaniclastics was recovered from Hole 802A, as well as a series of extrusive basalt lavas below Cenomanian-late Aptian volcanogenic sediments at about the predicted depth. The sediment data implies an age at least as old as middle Cretaceous for the extrusive rocks directly below. A widespread edifice-building event occurred during the Aptian-Albian in the western Pacific (e.g., Winterer, Riedel, et al., 1971; Larson, Schlanger, et al., 1981) and, hence, the presence of middle Cretaceous volcanics was perhaps not entirely unexpected. Also, extrusive lavas (together with an upper sequence of sills) are a feature of the Nauru Basin igneous complex (Hole 462A), again of a similar or possibly slightly older age (Moberly, Schlanger, et al., 1986). Based on the nature of the extrusive rocks recovered from Hole 802A, however, another possibility is that they could represent local basement, as suggested by the seismic stratigraphy. Unfortunately, shipboard X-ray-fluorescence analytical data were not available during Leg 129, so a chemical signature for the basalts could not be used to constrain their composition and possible eruptive environment.

Lithology

A total of about 16.6 m of basalts were sampled from Cores 129-802A-57R to -62R (32.8% recovery) and divided into 17 volcanic cooling units. The actual recovered portion of each unit and its top and bottom position are shown in Table 7 and Figure 43. The criteria for subdivision are similar to those use in previous holes, although in this case the preservation of

glassy margins, as well as macroscopic textural and grain-size variations, were particularly useful.

One characteristic feature of this hole is the relatively large number of small cooling units recognized, especially where the recovery was good (e.g., Cores 129-802A-58R and -59R; Fig. 43). The curved, glassy selvages that terminate Units 3 and 4 indicate that these are sections of small basaltic pillow lavas, probably no more than about 40–50 cm in diameter (Fig. 44). The glassy rims show all the features that indicate rapid quenching of lavas by seawater, with the preservation of different textural zones (grading inward from glass with coalesced spherulites to quenched crystal morphologies) typical of pillow lavas (Bryan, 1972; Natland, 1980). Many of the other units show similar features and are often quenched throughout, with either preserved subhorizontal margins or very fine-grained contact zones. Hence, these units are also considered to be part of a pillowed sequence. Moreover, the slow rate of drilling coupled with the nature of the recovery (as numerous small, short core lengths) suggest that a number of very thin flow units are present. All these features differ considerably from the thin flows sampled at Hole 801B and from the thick sills at Hole 800A. Only Unit 17 is different from the rest and is interpreted as a thin (<5 m) lava flow, as it is an almost continuously cored segment with a relatively coarser grain size, although it still exhibits a quench texture throughout.

The following discussion illustrates some of the important features displayed by various units. Dark brown and black featureless claystones are separated from the glassy top of Unit 1 by drilling rubble (Fig. 45) composed of similar claystones containing small green glassy fragments and brown smectite. The green clasts match the altered glass in the basalt just below and probably represent spalled pillow rinds subsequently incorporated in the sediment. The reddish brown sediment fragment at the top of Unit 2 (Fig. 43) does not look like interpillow material and probably represents the cave-in of material higher in the hole. As previously noted, the best-preserved pillow sections are exhibited by Units 3 and 4, although other units (e.g., Units 7, 8, and 9) invariably have margins that exhibit coalesced spherulites or fan and plume variolites together with interstitial glass (now altered to smectite). This outer zone is rapidly replaced by larger crystals, although often with quench-texture morphologies that coarsen toward the center of the unit. The top of Unit 11 (Section 129-802A-59R-2, 122 cm) is one of the few rim zones that retains unaltered black glass within a
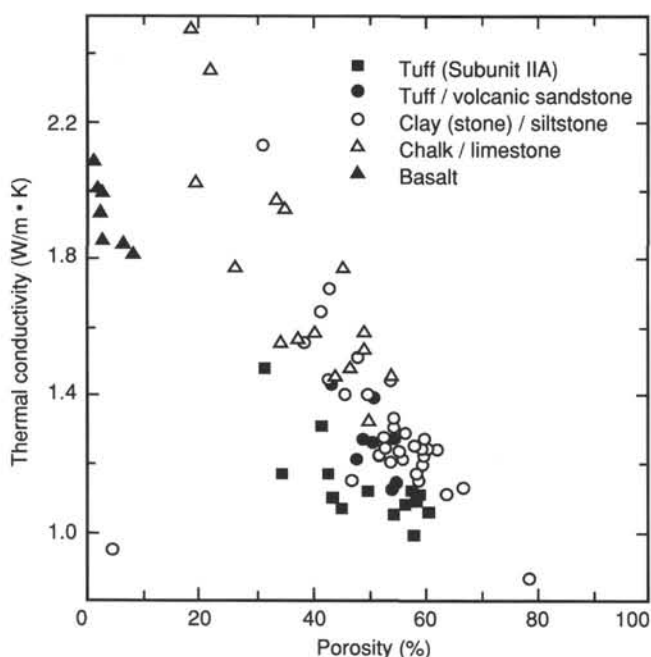

Figure 42. Porosity vs. thermal conductivity for Hole 802A, coded according to sediment and rock type.

Table 7. Extent of igneous units actually observed in Hole 802A.

| Unit	Top	Bottom	Thickness (cm)
	129-802A-	129-802A-	
1	57R-2, 110 cm	57R-3, 43 cm	79
2	58R-1, 2 cm	58R-2, 98 cm	243
3	58R-2, 98 cm	58R-2, 117 cm	19
4	58R-2, 117 cm	58R-2, 149 cm	32
5	58R-3, 0 cm	58R-4, 101 cm	249
6	59R-1, 0 cm	59R-1, 7 cm	7
7	59R-1, 7 cm	59R-1, 51 cm	44
8	59R-1, 51 cm	59R-1, 129 cm	78
9	59R-1, 129 cm	59R-2, 57 cm	78
10	59R-2, 57 cm	59R-2, 122 cm	65
11	59R-2, 122 cm	59R-3, 9 cm	30
12	59R-3, 9 cm	59R-3, 40 cm	31
13	59R-3, 0 cm	59R-3, 142 cm	102
14	60R-1, 0 cm	61R-1, 31 cm	136
15	61R-1, 31 cm	61R-1, 110 cm	79
16	61R-1, 110 cm	61R-2, 22 cm	62
17	62R-1, 0 cm	62R-3, 40 cm	328
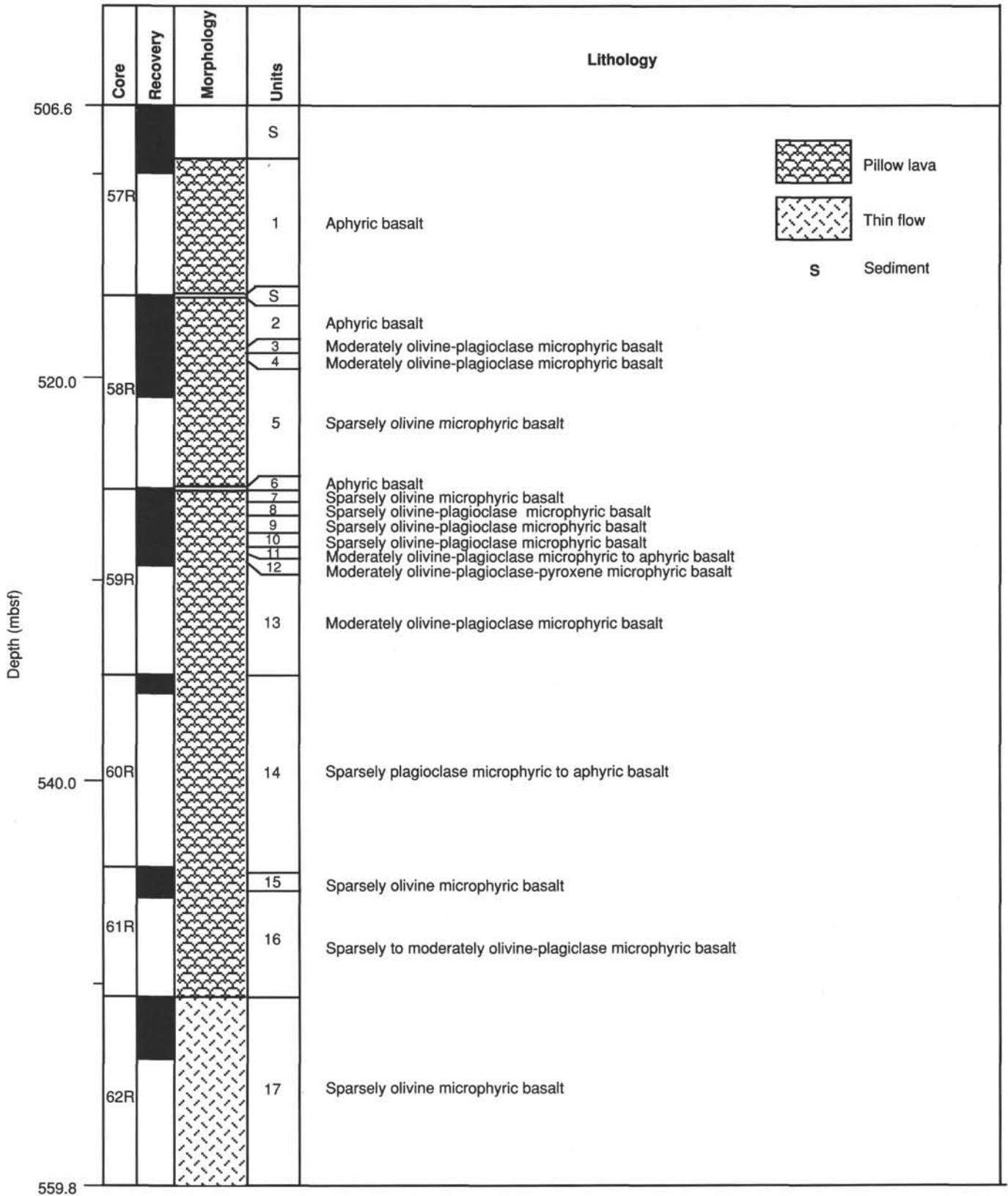
Figure 43. Log of basaltic extrusives at Hole 802A showing distribution of different volcanic units.
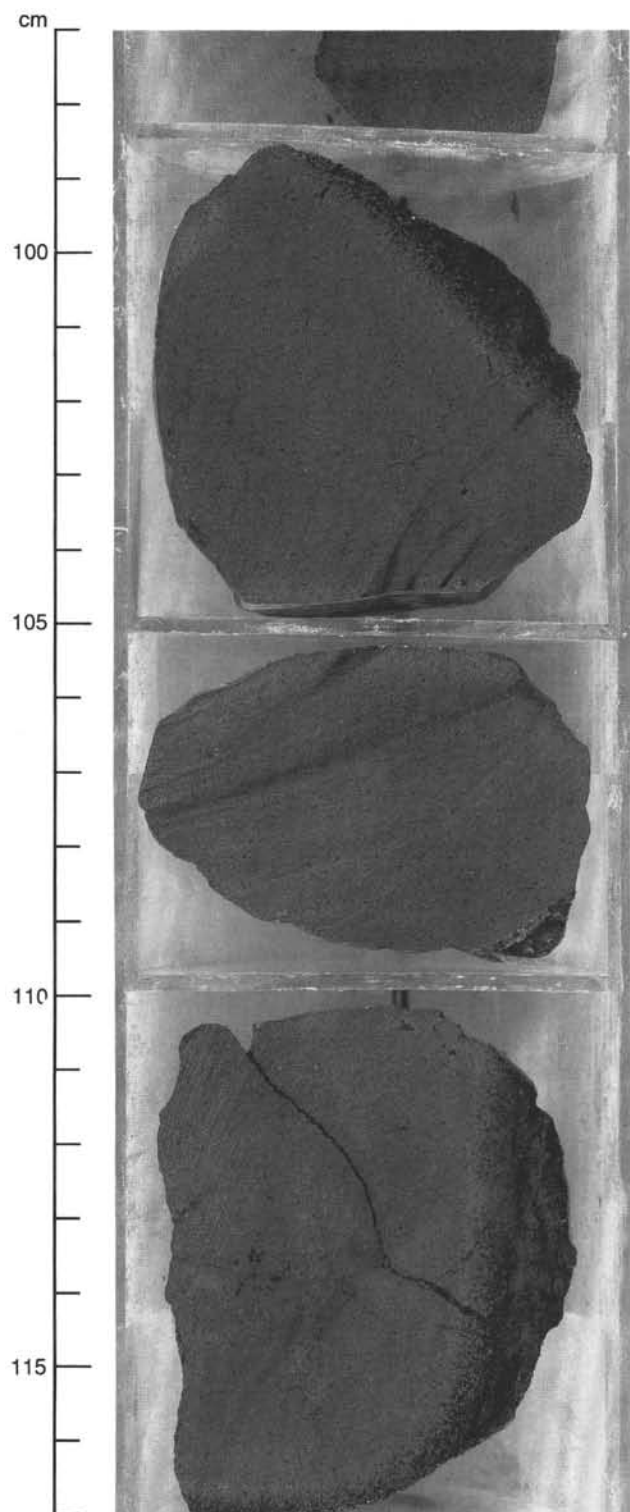
Figure 44. Unit 3 pillow lava (interval 129-802A-58R-2, 98–117 cm). Photograph shows curved glassy rims and speckled spherulitic zone of a small pillow segment.

2-mm-thick spherulitic zone. Unit 17 is a fine-grained hypocrystalline basalt and is distinct from the units above it in being more massive and displaying little internal variation in grain size over its full length. However, Unit 17 has a quench texture throughout and is considered to represent a thin lava flow.
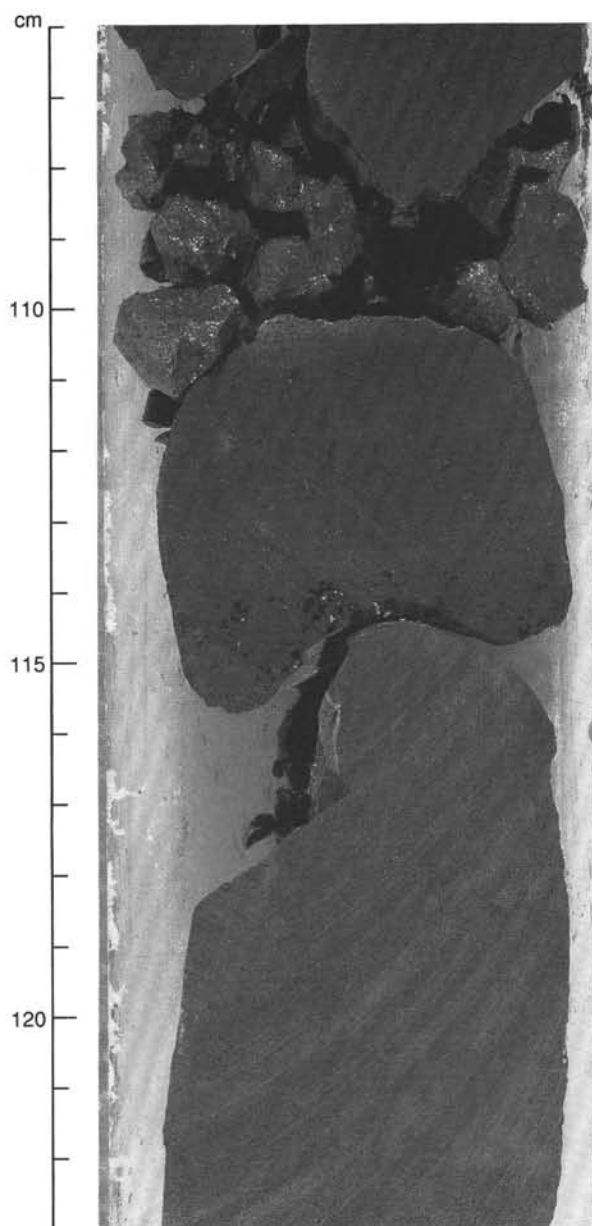
Figure 45. Contact zone between Cenomanian claystones (above) and basalt extrusives at Hole 802A (Section 129-802A-57R-2, 110 cm). The basalt has a thin curved glassy rim largely replaced by smectite.

Petrography

The extrusive sequence is dominated by fine-grained, pale gray, largely nonvesicular, aphyric olivine basalts and sparsely plagioclase-clinopyroxene-olivine microphyric hypocrystalline basalts. Predominantly glassy and spherulitic-textured porphyritic basalts are confined to the rapidly chilled zones at the margins of cooling units. Green smectite-replaced glassy mesostasis is a common feature in all units, although its distribution is variable.

In hand specimen and under the binocular microscope, the proportions of phenocrysts estimated within any cooling unit were generally very low (rarely exceeding about 3%–4%). Their apparent concentration in the glassy and spherulitic contact zones is a consequence of their small size (0.2–0.5 mm), which is more readily recognized within a crypocrystalline matrix

Table 8. Proportions of primary and secondary minerals visually estimated from thin-section studies.

Core, section	129-802A-57R-2	58R-2	58R-4	59R-1	61R-1	62R-2
Sample interval (cm)	126–128	145–149	55–57	126–128	50–52	50–51
Piece number	1B	15	7	11	8	3
Primary minerals						
(1) Phenocrysts						
Olivine	0	0	0	0	0	–
Plagioclase	1	3	2	6	1	–
Clinopyroxene	<1	1	1	3	tr	–
(2) Matrix						
Olivine	0	0	0	–	0	0
Plagioclase	50	5	5	tr	53	40
Clinopyroxene	37	5	3	–	40	50
Opaques	2	3	3	5	4	4
Glass	–	3	–	–	–	–
Crystallites	–	76	82	85	–	–
Mesostatis	tr	–	0	–	0	0
Secondary minerals						
Clays[a]	9	4	4	1	2	6
Carbonate	tr	–	–	–	–	–

Notes: 0 = present but totally replaced; dash = not observed; tr = trace.
[a]Mostly smectite but include some "iddingsite."

relative to the fine-grained matrix of the central portion of the unit. Porphyritic basalts are characterized by plagioclase and, more commonly, by plagioclase-clinopyroxene-olivine microphenocryst assemblages. Plagioclase and clinopyroxene may form small glomerophyric groups (0.5–1.25 mm in diameter) or more dispersed clumps of crystals. Single microphenocrysts or glomerocrysts often provide nucleation sites for spherulites within the chilled rims of some pillows.

The estimated proportions of primary and secondary minerals, together with crystallite material (in spherulites), are shown in Table 8.

The following brief descriptions, based on thin-section studies, illustrate and contrast the typical textures and features of basalts from the spherulitic rim zone (e.g., Sample 129-802A-59R-1, 126-128 cm) and the central hypocrystalline segment (e.g., Sample 129-802A-62R-2, 50-51 cm) of a cooling unit. The outer completely holohyaline rinds of some pillows are missing, although a thin sliver of yellowish sideromelane with small, individual, reddish brown, poorly birefringent spherulites may be preserved. Away from this outer glassy zone, the spherulites are much larger and begin to coalesce, trapping dark brown glass between their round and ovoid-shaped cross sections. Microphenocrysts and glomerocrysts of plagioclase, clinopyroxene, and, to a lesser extent, olivine may form up to 10% of the matrix and provide nucleation sites for the larger spherulites. Plagioclase microlites, sometimes with tuning-fork terminations, are also common in this zone. The red-brown spherulites continue to increase in size, although they begin to lose their round cross section and become more plumose, with several plumes growing from a central nucleation point. No glass remains and opaque ore forms larger granules that are concentrated around the margins of the spherulitic plumes. At about 20–25 mm from the preserved glassy rim the grain size continues to increase, and separate groups of plume-shaped variolites composed of clinopyroxene and/or plagioclase are clearly visible. In contrast, the central portion of large pillows (or thin flows, as in Unit 17) are fine-grained and hypidiomorphic-granular, although many crystals exhibit quench-textured morphologies. Clinopyroxene forms large fan- and plume-shaped variolites, sometimes coaxial with skeletal plagioclase laths. Commonly, plagioclase is present as elongate crystals with serrated edges that may form "bow-tie" pairs that grow out of a central anhedral clinopyroxene crystal. Apart from

these morphologies, olivine, plagioclase, and clinopyroxene are also present as small clumps of subhedral to anhedral grains, which appear to have grown earlier than the quenched crystals. They sometimes act as nucleation sites for the variolites and may range up to the size of any microphenocrysts. These crystals (and the microphenocrysts) are probably pre-eruptive in origin and crystallized during transportation of the lava to the seafloor. After initial quenching and variolite growth, any remaining melt produced a glassy mesostasis often crowded with dendritic and skeletal opaque ore.

Alteration and Geochemistry

In general terms, all the basalts show only slight or occasionally moderate alteration (up to about 15%). Apart from the low degree of post-consolidation alteration, secondary processes are dominated by the development of smectitic clays, carbonate, and pyrite; no zeolites were observed. The preservation of pyrite, both within veins and the matrix of the basalts, indicates a reducing environment. Late oxidative alteration, often typical of the oceanic crust with the development of iron oxyhydroxide-reddened zones (e.g., Robinson et al., 1977; Humphris et al, 1979), is not evident here. This may be a consequence of the mass flow deposition of the featureless volcanogenic claystones that rapidly covered the young extrusive rocks and provided a blanket to downward-seeping oxygenated seawater. The high organic content of the claystones may also have deoxygenated the seawater prior to penetration of the extrusive pile.

Glassy rims and mesostasis are commonly replaced by dark brown and sometimes green smectite and, more rarely, by late carbonate. Rare, irregularly shaped miaroles (<0.5 mm) may be partly lined with smectite or open and showing protruding crystal terminations. Carbonate occurs in random patches throughout the matrix, lining and partly replacing plagioclase laths and sometimes olivine grains. Olivine microphenocrysts are always replaced by brown or green smectite and sometimes by "iddingsite," but generally retain their euhedral or subhedral form.

Much of the macroscopic alteration is related to fractures, although their proportion of the bulk rock is generally only 1%–2%. Veins are normally thin (<0.1–0.2 mm), irregular, branching, and sometimes cross-cutting. No regular pattern or orientation was discerned, with the majority of veins being infilled with light or dark green smectites, with or without

carbonate and pyrite. A few larger veins (1–3 mm) may exhibit a zonation of infilling materials (e.g., Section 129-802A-57R-3, piece 3) with the walls lined with botryoidal masses of radiate smectite fibers and a carbonate center. Associated with some veins was the development of dark gray or greenish alteration halos (e.g., Sections 129-802A-58R-1, piece 12, and 129-802A-60R-1, piece 6) that represented zones of more extensive clay development (Fig. 46). Carbonate analyses for the basalts are presented in Table 9.

Summary and Conclusions

1. The basaltic extrusive rocks from Hole 802A are a series of pillow lavas with a thin lava flow at the base. They are mainly aphyric and sparsely plagioclase-clinopyroxene-olivine microphyric basalts that exhibit glassy spherulitic rims and quench-textured flow interiors.

2. Alteration is generally slight and dominated by smectitic clays, carbonate, and pyrite. The secondary assemblages are typical of the early stages of low-grade submarine weathering, formed under mildly alkaline, reducing conditions. A later, extensive oxidative phase was not developed, possibly because of subsequent rapid sedimentation and burial by impervious, reducing claystones.

3. The development of middle Cretaceous basalts at Site 802 either (1) may be tentatively correlated with or have a lithological analog within the Nauru Basin igneous complex that exhibits a series of pillow lavas in the upper extrusive sequence, or (2) may represent local basement of middle Cretaceous age.

DOWNHOLE MEASUREMENTS

Operations

On 1 January 1990, after reaching a total depth (TD) of 559.8 mbsf, the hole was swept with freshwater bentonite mud, which was subsequently displaced by seawater circulation during bit-release operations at 2230 hr UTC. The bit was dropped at the bottom of the hole and the drill pipe was raised to 50.1 mbsf in preparation for logging. The pipe was eventually placed at 127 mbsf for the beginning of each logging run and raised to approximately 108 mbsf while logging uphole. The three standard logging runs began at Site 802 at 0205 hr on 2 January 1990 and were completed at 0630 hr on 3 January, corresponding to a total logging time of 28 hr (Table 10). An additional 30 hr were spent during an attempted vertical seismic profiling (VSP) experiment and subsequent retrieval of the well seismic tool (WST) that had been stuck. The WST and wireline were successfully recovered and brought on deck at 1209 hr on 4 January. However, no VSP data were recorded.

The quad combination tool string included, from top to bottom, telemetry, long-spaced sonic, lithodensity, natural gamma-ray spectrometry, and dual induction resistivity tools in addition to the Lamont temperature tool (TLT). These tools were rigged at 0205 hr on 2 January, creating a tool string 30.72 m long. At 0400 hr the quad combination tools were run down to the level of the mud line and held stationary for 3 min to obtain a bottom-water calibration point for the TLT. The depth to the end of pipe as recorded on this logging run was within 3 m of that calculated by the driller. As logging continued downhole it was reported that the wireline heave compensator (WHC) was not operating. The tool string continued downhole until a bridge was encountered at 104 mbsf (0410 hr). The tool string was unable to penetrate below this depth and at 0433 hr it was decided to trip the tool out of the hole without recording any data, and to run the pipe through this bridge. The quad combination tool string was returned to
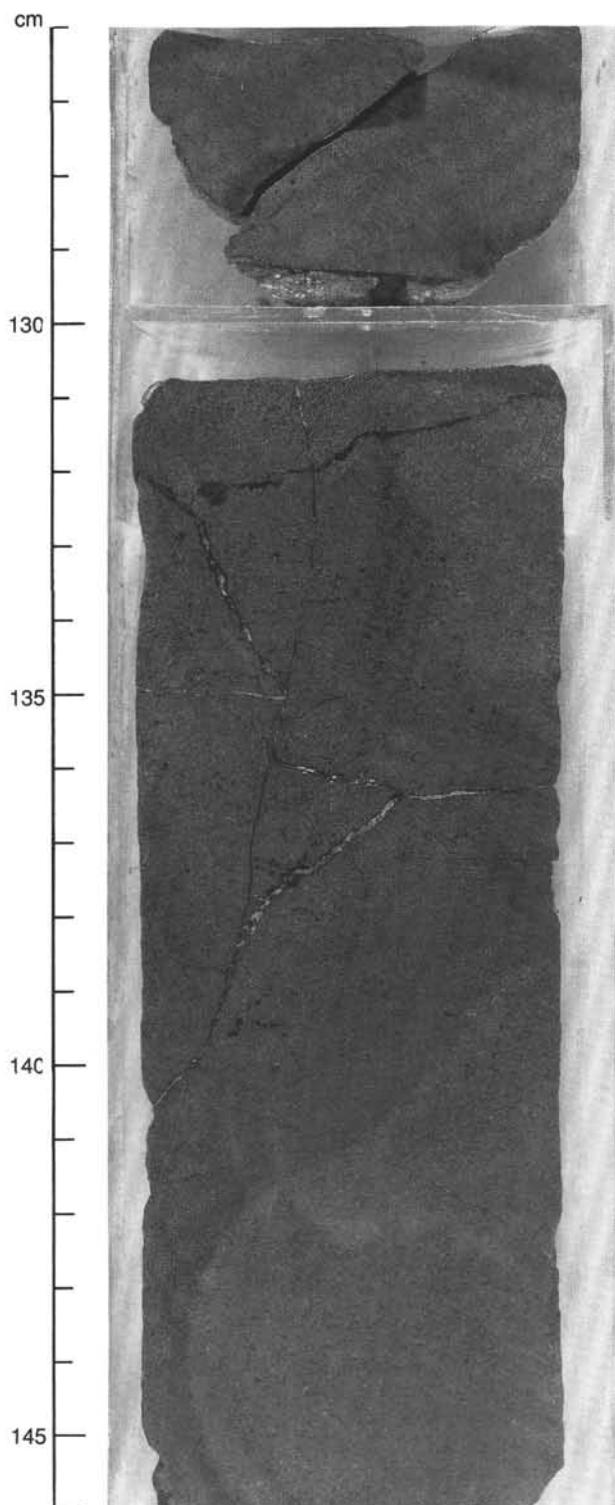

Figure 46. Dark alteration halos associated with smectite-carbonate veins in Hole 802A (interval 129-802A-58R-1, 126–146 cm).

the rig floor at 0615 hr. At 1027 hr the pipe was able to break the bridge with 5000–8000 lb of bit weight. The quad combination tool string was rigged again at 1050 hr and the tool was lowered down the pipe and held stationary for 3 min at the mud line at 1310 hr. Again it was reported that the WHC was not operating. Downgoing logging data were acquired to 325 mbsf, where the tool string hit another bridge. The tool string

Table 9. Carbonate analyses of basalts from Hole 802A.

Core, section, interval (cm)	Depth (mbsf)	CaCO₃ (wt%)
129-802A-		
58R-1, 38–40	516.38	0.8
58R-2, 53–55	518.03	0.3
58R-2, 105–107	518.55	0.3
58R-3, 86–88	519.86	0.2
59R-1, 83–85	526.23	0.4
60R-1, 90–92	535.60	0.4
62R-1, 129–131	551.89	0.4

was unable to go through this bridge and at 1354 hr it was decided to record what was left of the hole. Logging data were recorded successfully as the tool string moved uphole at 300 m/hr from 323 to 108 mbsf (Figs. 47, 48, and 49), with a repeat section taken from 207 to 108 mbsf. The bottom of pipe was encountered at 127 mbsf and another bottom-water temperature calibration point for the TLT was obtained at the mud line. The quad combination tool string was returned to the rig floor at 1735 hr on 2 January. The TLT was then taken to the downhole measurements lab, opened, and hard-wired to the Masscomp computer to download the recorded temperature/time measurements.

The geochemical combination tool string, which included telemetry, natural gamma-ray spectrometry, aluminum clay, and induced gamma-ray spectrometry tools and the TLT, was rigged at 1830 hr on 2 January, creating a tool string 18.13 m long. The string was lowered down the pipe and held stationary for 3 min at the mud line to obtain a bottom-water calibration point for the TLT. Logging data were recorded from 323 mbsf up into the pipe as the tool string moved uphole at 200 m/hr (Figs. 48 and 49), with a repeat section taken from 207 to 108 mbsf. During this run the WHC was operating. The geochemical logging run was completed at 0100 hr on 3 January.

The next tool combination run at Site 802 was the formation microscanner (FMS), which included telemetry, natural gamma-ray spectrometry, and FMS tools and the TLT. This tool string was rigged and in the hole at 0115 hr on 3 January. FMS data were recorded uphole at 260 m/hr from 323 to 108 mbsf without problems. The FMS tool string was returned to the drill floor at 0620 hr on 3 January.

The final tool run at Site 802 was the WST, which was rigged and in the hole at 0711 hr on 3 January. The 400-in.³ water gun was operating at 2000 psi, but no signal was apparent on the real-time WST display. Test shots were taken in pipe down to the TD of the previous logging runs, during which time it appeared as if the caliper arms of the WST were not locking the instrument securely against the borehole wall, resulting in an extremely poor signal-to-noise ratio. At 1244 hr on 3 January we finally received a good signal at 248 and 253 mbsf and we lowered the tool back to the TD. The WST apparently broke through the bridge at 325 mbsf and reached a depth of 370 mbsf, where test shots were again poorly received, and at 1327 hr it was decided to trip out of the hole in order to replace the WST. At 1345 hr the tool became stuck at 245 mbsf by a bridge not previously encountered, and from this time to 1500 hr we attempted to pull free with up to 9500 lb of tension on the wireline (hanging weight was 5500 lb). At this time it was decided to crimp and cut the wireline at the base of pipe (500 m above the WST), reel in the remaining cable, and pull up pipe, with little hope of recovering anything but the majority of the wireline. This would at least assure us of enough wireline to log Hole 801C. The severing tool cut the cable, but on retrieval, we discovered that the cut had been

made 3164 m above the WST. The remaining wireline (including 100 m of knots) was recovered along with an apparently undamaged WST at 1209 hr on 4 January.

The quad combination logging run was tied into the depth given from the drill string (i.e., log depth tied to core depth). All logging runs were then shifted by the Schlumberger engineer relative to the quad combination logging run using the natural gamma-ray log response. The geochemical combination run was shifted to shallower depths by 1.78 m and the FMS was shifted to greater depths by 1.14 m.

Summary log figures appear at the end of this chapter. The FMS images are presented on microfiche in the back of this volume.

Log Quality

These are the highest quality logs recorded during Leg 129 (Figs. 47, 48, and 49). The raw sonic data required only minor shipboard processing and editing to create a useful sonic log (Figs. 47 and 50). The data recorded from the induced gamma-ray spectrometry tool will require post-cruise processing; references made to silicon, calcium, and iron are therefore only broadly qualitative. In contrast, the natural gamma-ray spectrometry tool produces reliable values for the concentration of potassium, thorium, and uranium, and the aluminum clay log is generally little improved through post-cruise processing. The quad combination was not obviously affected by the ship's heave; the small degree of elasticity within the wireline summed over its extreme length (6000 m) may have acted to slightly decouple these logging tools from the heave of the ship. The WHC was operational during the geochemical and FMS logging runs and effectively decoupled these tool strings from the heave of the ship. No adverse effects from ship's motion are apparent on the raw FMS records; however, the FMS data will still require significant shore-based image processing to achieve an interpretable record. The FMS images are presented on microfiche in the back of this volume.

Logging Units

Four logging units were identified in Hole 802A (Fig. 51) based on log response and analyses of recovered cores. These logging units should not be confused with the lithologic units defined earlier (see "Lithostratigraphy and Sedimentology" section, this chapter). The boundaries between adjacent logging units were placed at significant inflection points resulting from simultaneous variations on at least several of the logs illustrated in Figures 47 through 51. These units display consistent log responses or distinct overall trends.

Core recovery was much higher throughout the logged interval (average recovery 26%) than at either Sites 800 or 801, as both well-indurated and softer interbedded portions of Hole 802A were actually recovered. The lithologies for unrecovered intervals have been inferred from the logs based on the broad assumption that the logging tools respond to varying proportions of the primary constituents in samples actually recovered (e.g., biogenic silica, carbonate, pelagic clay, volcanogenic clay) and to their relative porosity.

Logging Unit 1 (108–167 mbsf)

Logging Unit 1 is distinguished by extreme variability in covarying velocity (1.7–4.1 km/s), resistivity (1–11 ohm-m), density (1.5–2.4 g/cm³), aluminum (1.2–6 wt%), and silica (0.026–0.156) contents. The topmost (108–118 mbsf) portion of Unit 1 contains local maxima in potassium and thorium and an absolute minimum in uranium concentration along with minima in resistivity, density, and aluminum values. The abrupt change from highly variable logging responses to uniformly low values for velocity, resistivity, and density at 167 mbsf was chosen as the lower boundary of logging Unit 1.

Table 10. Actual time schedule (UTC) for logging operations at Hole 802A and tools used during each logging run.

Tool String	Time	Procedure
Quad combination (TCCB-LSS-HLDT-NGT-DIL-TLT)	RIH 0205 hr 2 January 1990 POOH 1735 hr	Log down to 104 mbsf. Hit a bridge. Run pipe through bridge. Log down to 325 mbsf. Log up to 108 mbsf with repeat section from 207 to 108 mbsf.
Geochemical combination (TCCB-NGT-ACT-GST-TLT)	RIH 1830 hr POOH 0100 hr 3 January 1990	Run down to 323 mbsf, log up to 108 mbsf. Run down to 207 mbsf, log up to 108 mbsf.
Formation microscanner (FMS-TCCB-NGT)	RIH 0115 hr POOH 0620 hr	Run down to 323 mbsf, log up to 108 mbsf.
Vertical seismic profile (WST)	RIH 0711 hr POOH 1209 hr 4 January 1990	Run down to 323 mbsf, log up with poor results. Run down and break through bridge. Test at 370 mbsf. Run up. Tool stuck at 245 mbsf; decide to crimp and cut wireline.

Notes: Total logging time is 58 hr, including initial rig-up and final rig-down of tool strings. Abbreviations used above are as follows: TCCB = telemetry tool, LSS = long-spaced sonic tool, HLDT = lithodensity tool, NGT = natural gamma-ray spectrometry tool, DIL = dual induction tool, TLT = Lamont temperature tool, FMS = formation microscanner, ACT = aluminum clay tool, GST = induced gamma-ray spectrometry tool, WST = well seismic tool, RIH = run in to hole, and POOH = pull out of hole.

The extreme logging responses appear to correlate to changes in grain size and an inferred variation in the amount of silica cementation. The highest values of velocity, resistivity, density, aluminum, and silica correlate to relatively coarse-grained intervals (volcaniclastic sandstone), inferred to be relatively well cemented by recrystallized silica (e.g., Cores 129-802A-14R and -15R). The coarse-grained interval is juxtaposed against a less-indurated, finer-grained (silty sandstone) interval that is also apparent on the logs. The distinct logging response observed from 108 to 117 mbsf is indicative of a poorly cemented, nonvolcaniclastic, clay-rich interval and suggests that the 1.67 m of pelagic clay recovered in Core 129-802A-13R is representative of the entire cored interval. The uniformly low total gamma-ray values which do not covary with velocity, resistivity, and density indicate that volcaniclastic clay-rich intervals observed within volcaniclastic deposits at Sites 800 and 801 are not abundant within logging Unit 1 in Hole 802A.

Logging Unit 2A (167–210 mbsf)

Logging Unit 2A is characterized by uniformly low velocities (1.75–1.9 km/s), resistivities (1 ohm-m), densities (1.55–1.9 g/cm^3), and relatively low total gamma-ray (10–21 API) and silicon values. Aluminum concentration remains elevated. These general logging responses also characterize the upper portion of logging Unit 2B (210–233 mbsf). However, a logging boundary was chosen at 210 mbsf based on a distinct shift toward higher potassium concentration along with restricted local maxima in thorium and uranium and local minima in density, aluminum, calcium, and iron values. The logging responses defining this unit appear to be an extended version of those responses observed in logging Unit 1 that characterized the poorly cemented, finer-grained portion of lithologic Unit IIA. The lack of interbedded, well-cemented volcaniclastic sandstone results in the more uniform and lower log values.

The logging responses that define the boundary between logging Units 2A and 2B at 210 mbsf provide evidence of an unidentified unconformity (a contact between two turbidite events) within the lower Miocene sediments. This boundary is inferred to result from juxtaposition of a clay-rich layer below 210 mbsf with a relatively coarser-grained (siltstone), clay-poor interval above. This boundary also roughly correlates to a reported increase in nannofossil clay and chalk lithologies below Core 129-802A-23R, although there is no corresponding increase in relative calcium concentration at this depth (see "Lithostratigraphy and Sedimentology" section, this chapter).

Logging Unit 2B (210–260 mbsf)

Logging Unit 2B is characterized by initially high values of potassium, thorium (total gamma ray), and aluminum, which steadily decline to relative minima at approximately 232 mbsf. Restricted local minima in silicon, calcium, and iron also occur at this depth.

The logging responses at the top of Unit 2B (210–232 mbsf) provide evidence of a volcanic clay-rich interval that gradually becomes more carbonate-rich with depth. The logging responses at 232 mbsf may indicate an unconformity corresponding to a contact between coarse-grained debris flow deposits below 232 mbsf (e.g., base of lithologic Unit IIB) to more uniformly fine-grained deposits above this level.

From 232 to 250 mbsf, logging Unit 2B displays gradually increasing density and calcium values, along with covarying maxima/minima in velocity, resistivity, density, aluminum, and, to a lesser extent, calcium. This type of logging response appears to correspond to interbedded, coarse-grained, well-cemented debris flows with less-indurated, fine-grained, nannofossil clay- or chalk-dominated intervals where calcium carbonate is the primary cementing agent rather than silica (as in logging Unit 1).

A distinct sinusoidal variation on nearly all the logs was observed at 250 mbsf. This boundary is characterized by relative minima in potassium, total gamma-ray, aluminum, silicon, iron, and sulfur values along with maxima in velocity, resistivity, density, uranium, and calcium. These variations
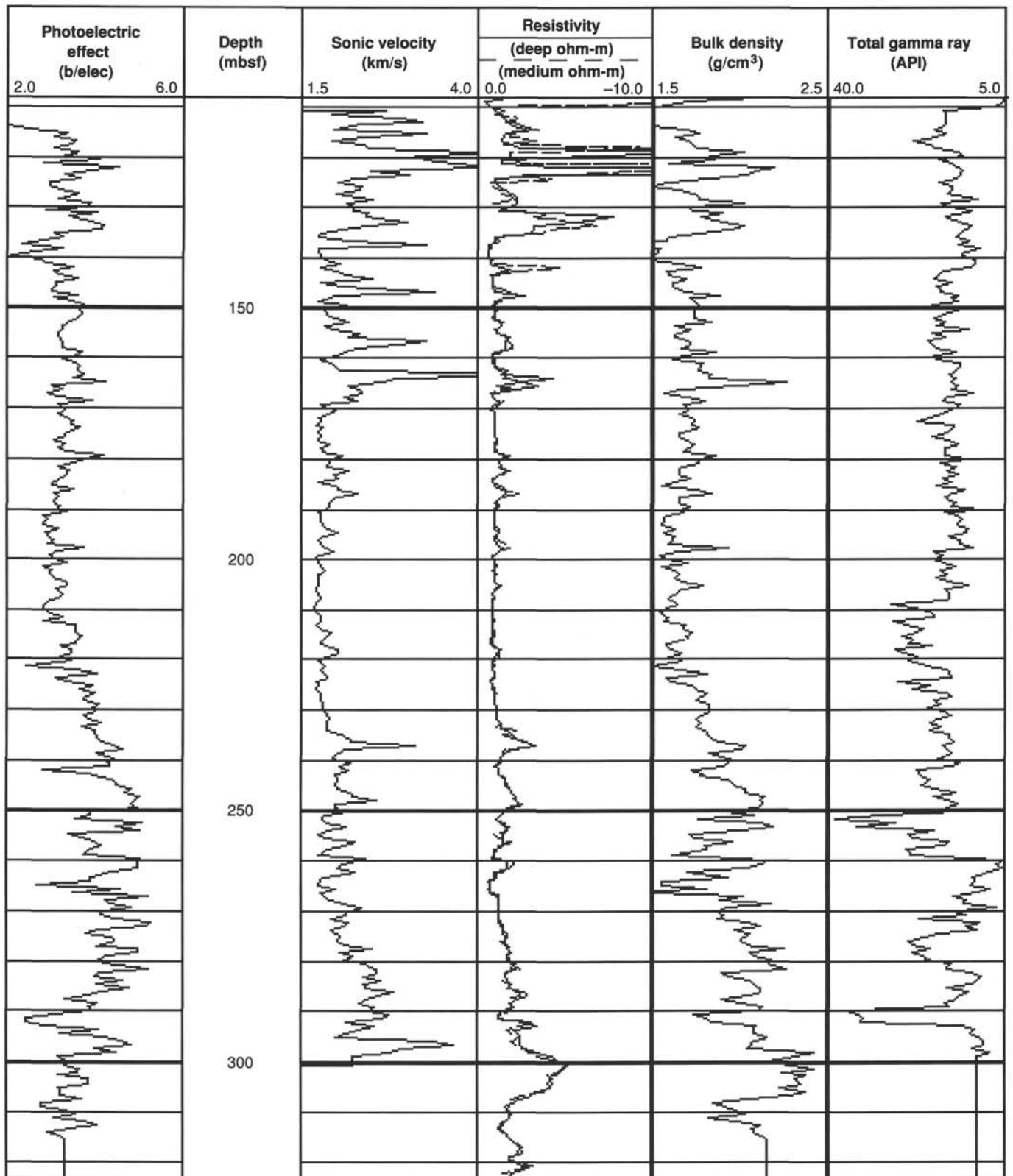
Figure 47. Selected downhole logs from the quad combination tool string for the interval from 108 to 323 mbsf in Hole 802A: Photoelectric effect, sonic velocity, resistivity, bulk density, and total gamma ray. Stratigraphic units defined by logging data (logging units) are shown in Figure 51. Sonic velocity, resistivity, and density reflect the porosity of the formation and thus the degree of lithification or cementation.
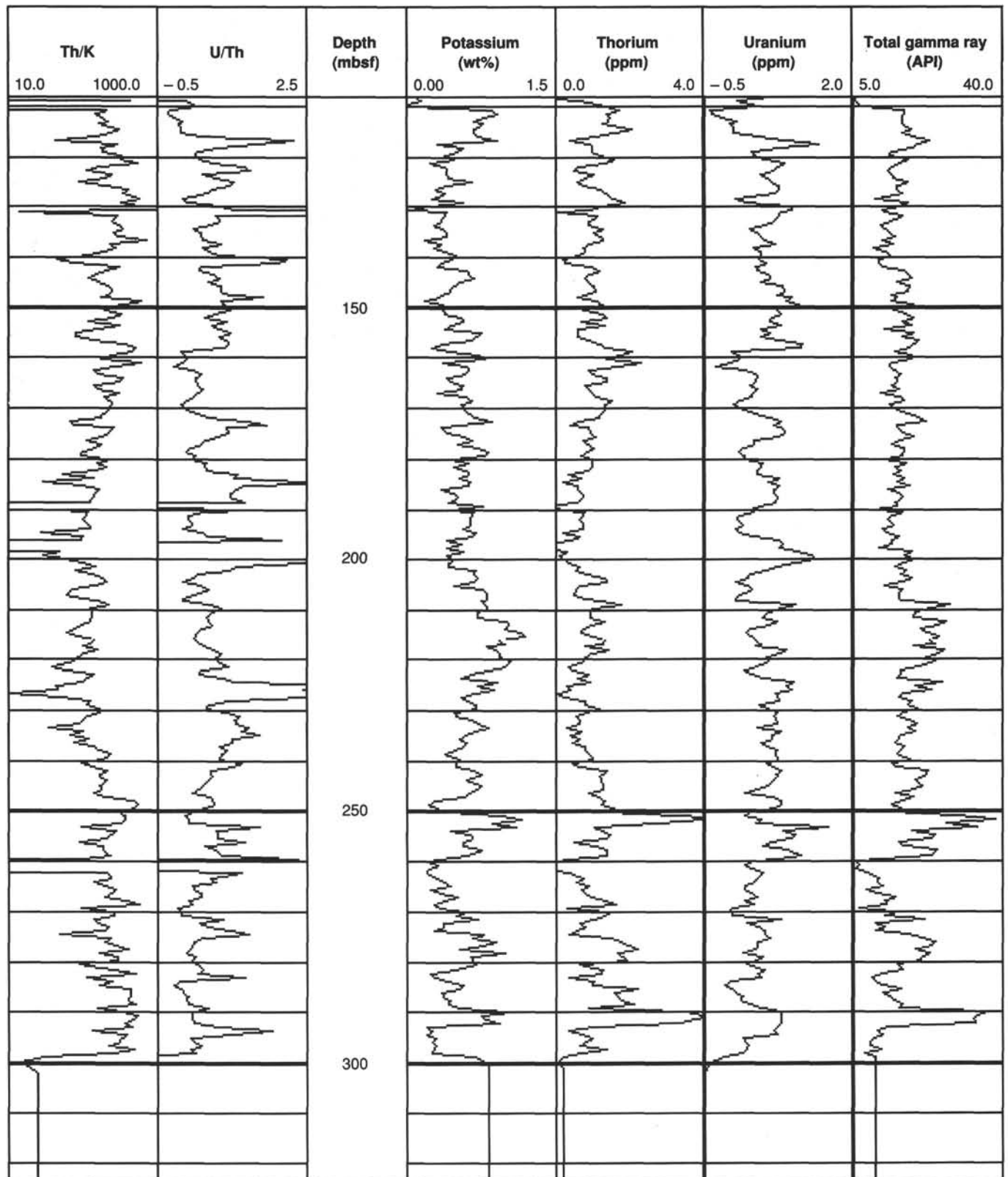
Figure 48. Selected downhole logs from the geochemical combination tool string for the interval from 108 to 323 mbsf in Hole 802A: Total gamma ray, sulfur, aluminum, silicon, calcium, and iron. Stratigraphic units defined by logging data (logging units) are shown in Figure 51. The relative abundances of these elements serve to identify the primary constituents that distinguish the major lithologies recovered from Hole 802A (e.g., biogenic silica and carbonate, pelagic clay, and volcanogenic material, including clay).

Figure 49. Downhole logs from the natural gamma-ray spectrometry tool on the quad combination tool string for the interval from 108 to 323 mbsf in Hole 802A: thorium/potassium ratio, uranium/thorium ratio, potassium, thorium, uranium, and total gamma ray. Stratigraphic units defined by logging data (logging units) are shown in Figure 51.
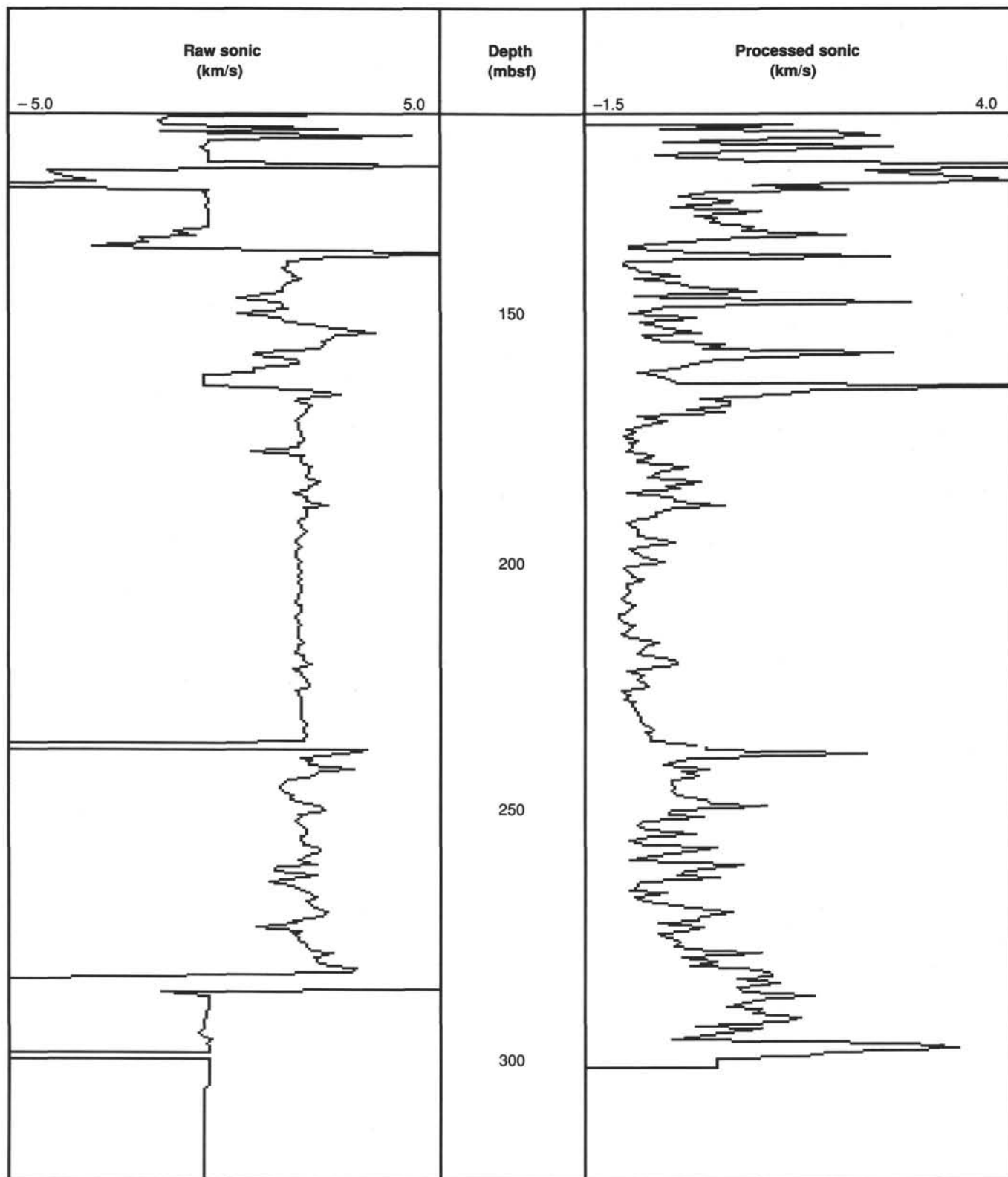
Figure 50. Comparison of observed "raw" (left column) and processed (right column) velocity logs for Hole 802A. Covariation of the processed sonic log with resistivity, gamma ray, and bulk density logs (Figs. 47 and 51) indicates that a useful velocity log was produced. One notable exception occurs at about 108 mbsf, where high velocities are matched by low resistivities and densities.
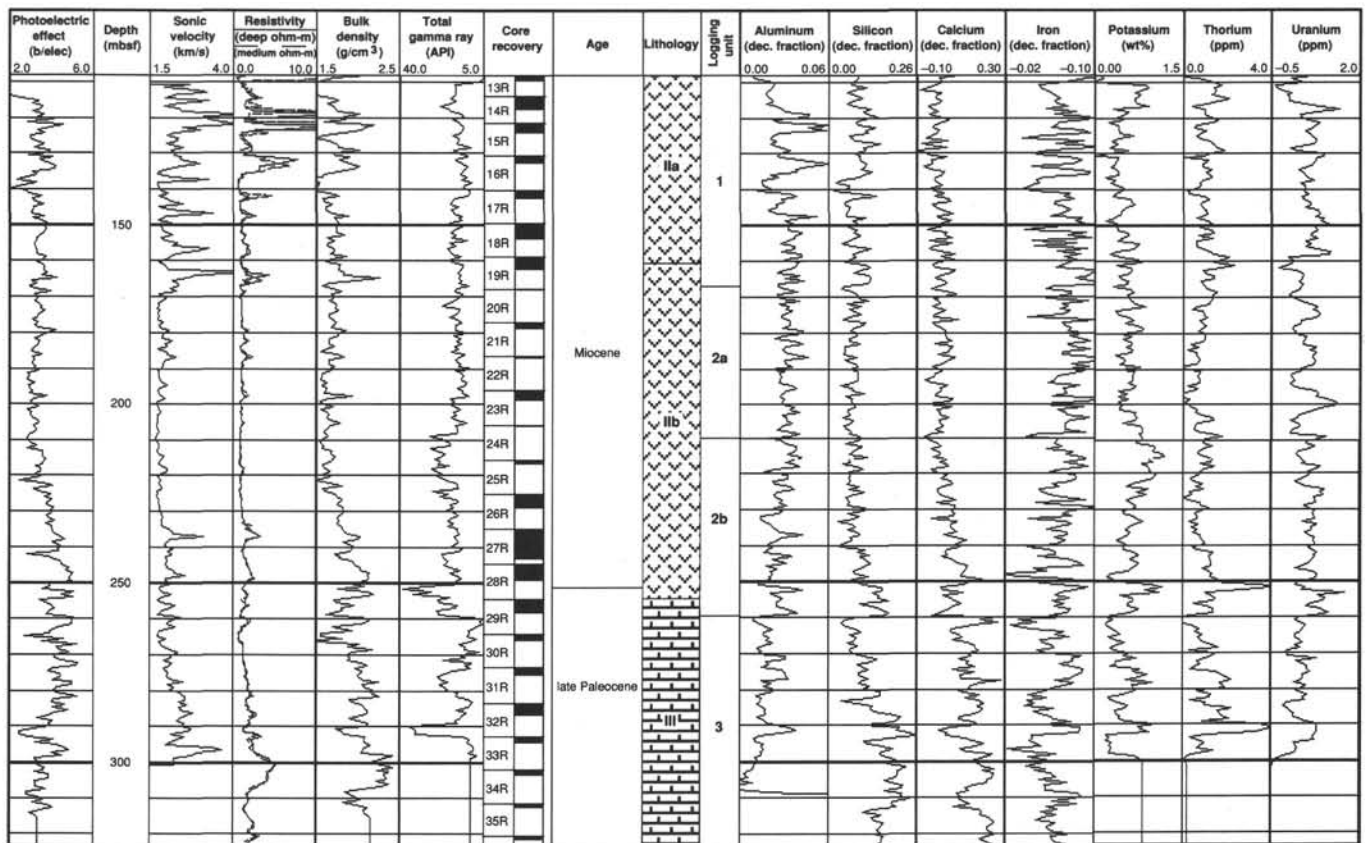
Figure 51. Summary compilation of downhole logs, intervals of core recovery, lithology, and downhole logging units at Hole 802A. Lithologic units are based on coring results (see "Lithostratigraphy and Sedimentology" section, this chapter).

are juxtaposed against underlying local minima/maxima in the opposite sense for all the above-mentioned logs, including an absolute maximum in thorium concentration (>4.0 ppm). This logging response indicates a well-cemented, clay-poor interval overlying poorly cemented volcanic clay and silica-rich sediments with carbonate cement. This boundary corresponds to a sharp contact between coarse-grained volcanic debris flows (Core 129-802A-28R) and the underlying fine-grained claystone/siltstone, which is poorly cemented despite evidence for high silicon content. This interval from 250 to 260 mbsf corresponds to Core 129-802A-28R and -29R, which are reported to contain abundant, redeposited radiolarians, perhaps accounting for the high silicon concentration (see "Biostratigraphy" section, this chapter).

The base of logging Unit 2B at 260–262 mbsf is marked by a dramatic minima in potassium, thorium, uranium, aluminum, silicon, and iron concentrations coinciding with an abrupt unidirectional shift to high calcium concentrations coupled with small maxima in velocity, resistivity, and density values. The logging response at this boundary marks a sharp contact between a clay-rich, poorly cemented interval overlying a clay-poor, well-cemented (calcareous cement) unit. This boundary correlates to a major lithologic change from claystone to nannofossil chalk at 260 mbsf (see "Lithostratigraphy and Sedimentology" section, this chapter).

Logging Unit 3 (260–323 mbsf)

Logging Unit 3 extends from 260 mbsf to the TD for logging operations at Site 802. This unit is defined by generally high calcium values along with consistently increasing potassium,

thorium, velocity, resistivity, density, and silicon values. This unit also contains the highest sulfur concentrations observed at Site 802. This logging response strongly suggests the declining phase of an interval of high primary productivity which reaches a maximum no shallower than 290 mbsf. This evidence suggests that Site 802 was within a region of high productivity, presumably associated with an equatorial crossing no later than the late Paleocene, which by the early Eocene had moved beyond this high productivity zone (see "Paleomagnetism" and "Biostratigraphy" sections, this chapter). At 270–280 mbsf there is a maximum in iron concentration which possibly reflects the iron-manganese oxides recovered in Core 129-802A-31R (see "Lithostratigraphy and Sedimentology" section, this chapter).

Logging Unit 3 is punctuated at 292 mbsf by local maxima in potassium, thorium, uranium, aluminum, silicon, and iron, coupled with local minima in resistivity, density, and calcium. Calcium, resistivity, and density return to elevated levels below this depth and reach maximum values, including high silicon, at approximately 300 mbsf.

The logging responses observed at 292 mbsf again indicate an unconformity, in this case marked by a clay-rich interval (the base of Core 129-802A-32R) overlying an extended interval high in silica and calcium. This logging response illustrates the abrupt change from nannofossil chalk to nannofossil chalk with chert nodules below 292 mbsf, which can be interpreted to represent hard ground development resulting from a hiatus. This boundary corresponds exactly to a hiatus between upper Oligocene and lower Eocene ages determined from micropaleontology studies (see "Biostratigraphy" section, this chapter).

Synthetic Seismogram

A synthetic seismogram was computed for Hole 802A to accurately tie the drilled sequence in the hole to seismic reflection data over the site (Fig. 52). The seismogram covers the interval from 110 to 300 mbsf, approximately 7.576 to 8.185 seconds two-way traveltime (s twt).

The unprocessed sonic velocity log from Hole 802A (Fig. 50) contains very high and/or low values corresponding to cycle skipping ("Downhole Measurements" section, "Explanatory Notes" chapter, this volume), almost exclusively from 108 to 140 mbsf. The sonic log-processing software aboard the *JOIDES Resolution* allowed us to set a window of possible velocity values and then recalculate a new log using only the traveltime data that result in velocities within the chosen window. A minimum-maximum window of 1.69 to 5.1 km/s was chosen, resulting in the processed sonic log displayed in Figure 50. This processed sonic log was used in combination with the raw bulk density log to calculate reflection coefficients which were convolved with a source wavelet to produce a synthetic seismogram. The synthetic seismogram shown in Figure 52 incorporated the source wavelet from the air-gun array used during FM35-12. The synthetic seismogram was shifted to the proper two-way traveltime on the seismic profile by matching the reflection created by the first chert encountered at this site. This method of matching synthetic to seismic profile works well if both the depth and the two-way traveltime to a given horizon are known (as was the case with first chert at Site 800). In the case of Site 802 we assumed that the relatively high amplitude reflection at 8.185 s twt corresponded to 300 mbsf, just below the first chert horizon. This correlation does not result in the best possible match between synthetic and multichannel seismic (MCS) reflections. It does, however, result in more reasonable interval velocities and velocity trends (i.e., high velocities over low velocities). The synthetic seismogram (Fig. 51) is compared with the MCS line shot during FM35-12 at its closest approach to Site 802 (within 2 km). The major reflectors apparent on the derived synthetic seismogram are correlated with the seismic 10-trace mix and seismic reflection profile. Improved synthetic seismograms will be produced for Site 802 after shore-based processing, which will include incorporation of physical properties data, repicking of sonic traveltimes, and the use of improved source wavelets.

A few general interpretations of the rocks comprising a portion of the sedimentary section at Site 802 have been made by extrapolating the downhole logging results onto the seismic profile. A further description of the correlation between seismic stratigraphy and lithostratigraphy is given in the "Site Geophysics and Seismic Stratigraphy" section (this chapter).

Seismic Intervals

1. 7.88 to 7.985 s twt (average velocity 2.06 km/s). This zone encompasses a thin layer of pelagic clay (lithologic Unit I). The thickness of this unit is most accurately determined with the 3.5-kHz profiler at 30 ms, where the first lithified volcanic tuff was encountered (Fig. 53; see "Site Geophysics and Seismic Stratigraphy" section, this chapter). The velocity (porosity) contrasts between alternating zones of coarse-grained and fine-grained, variably cemented tuff with pelagic clay create these high-amplitude reflections (also observed within logging Unit 1). Measurements made on individual samples show both high and highly variable velocities within lithologic Unit IIA (see "Physical Properties" section, this chapter).

2. 7.985 to 8.041 s twt, logging Unit 1 (average velocity 2.11 km/s). The velocity (porosity) contrasts between alternating

zones of coarse-grained and fine-grained, variably cemented tuff create these high-amplitude, flat-lying reflections (lithologic Subunit IIA).

3. 8.041 to 8.144 s twt, logging Unit 2A and 2B (average velocity 1.81 km/s). This interval contains less-continuous, moderate-to-low-amplitude reflections that are the result of small velocity-density contrasts within an interval of more uniform, generally fine-grained material with fewer interbedded, well-cemented volcaniclastic sandstones. A single low-amplitude reflector observed on the synthetic seismogram and MCS profile at 8.088 s twt corresponds to the inferred unconformity at the base of logging Unit 2A (210 mbsf). A high-amplitude reflection observed on the synthetic seismogram at 8.11 s twt, matched by a lower amplitude event on the MCS profile, is correlated to another apparent unconformity at 232 mbsf.

4. 8.144 to 8.210 s twt, logging Unit 3 (average velocity 1.91 km/s). This interval contains the transition from low-amplitude, discontinuous reflections to slightly higher amplitude and more continuous flat-lying reflections. This transition occurs at 8.185 s twt or approximately 300 mbsf, just below the first occurrence of chert within a chalk-dominated sequence (lithologic Unit III). The high carbonate content inferred for this interval from both logs and cores apparently creates a low-porosity matrix that results in a high-interval velocity.

The synthetic seismogram coupled with the geochemical logs indicate that the moderate-amplitude reflections at approximately 8.2 stwt are created by velocity/density (porosity) contrasts associated with sharp changes in silicon and calcium content.

Summary

A suite of eight downhole logs were successfully recorded at Site 802, resulting in the identification of four distinct logging units. Compositional trends and boundaries were inferred from these logs through intervals of poor recovery by assuming that unrecovered intervals are composed of varying proportions of recovered materials. The logs were most useful in defining boundaries (unconformities) and in characterizing the unrecovered majority of the formation.

A synthetic seismogram correlates moderately well with the observed seismic profile and indicates (along with geochemical logs, physical properties, and lithostratigraphy) that the largest impedance contrasts are associated with significant changes in grain size within the volcaniclastic section, often corresponding to variations in silica concentration. These correlations also indicate that the moderate-amplitude reflections at approximately 8.2 s twt are created by impedance (porosity) contrasts associated with variations in silicon and calcium content.

SITE GEOPHYSICS AND SEISMIC STRATIGRAPHY

Site 802 (proposed site EMB-2A) in the East Mariana Basin is located within the Jurassic magnetic quiet zone (JQZ) near the intersection of MCS line 18 (six 80-in.³ water guns) obtained during the MESOPAC II expedition aboard *Le Suroit* in August-September 1989 and MCS line 7 (2576-in.³ air-gun array) collected during the FM35-12 expedition aboard the *Fred H. Moore* in November-December 1987. Because Leg 129 began only three months after the *Le Suroit* cruise, only single-channel, real-time records of the water-gun data obtained during MESOPAC II were used to locate proposed site EMB-2A. The location of this MESOPAC II MCS profile was dictated by the preceding MCS expedition aboard the
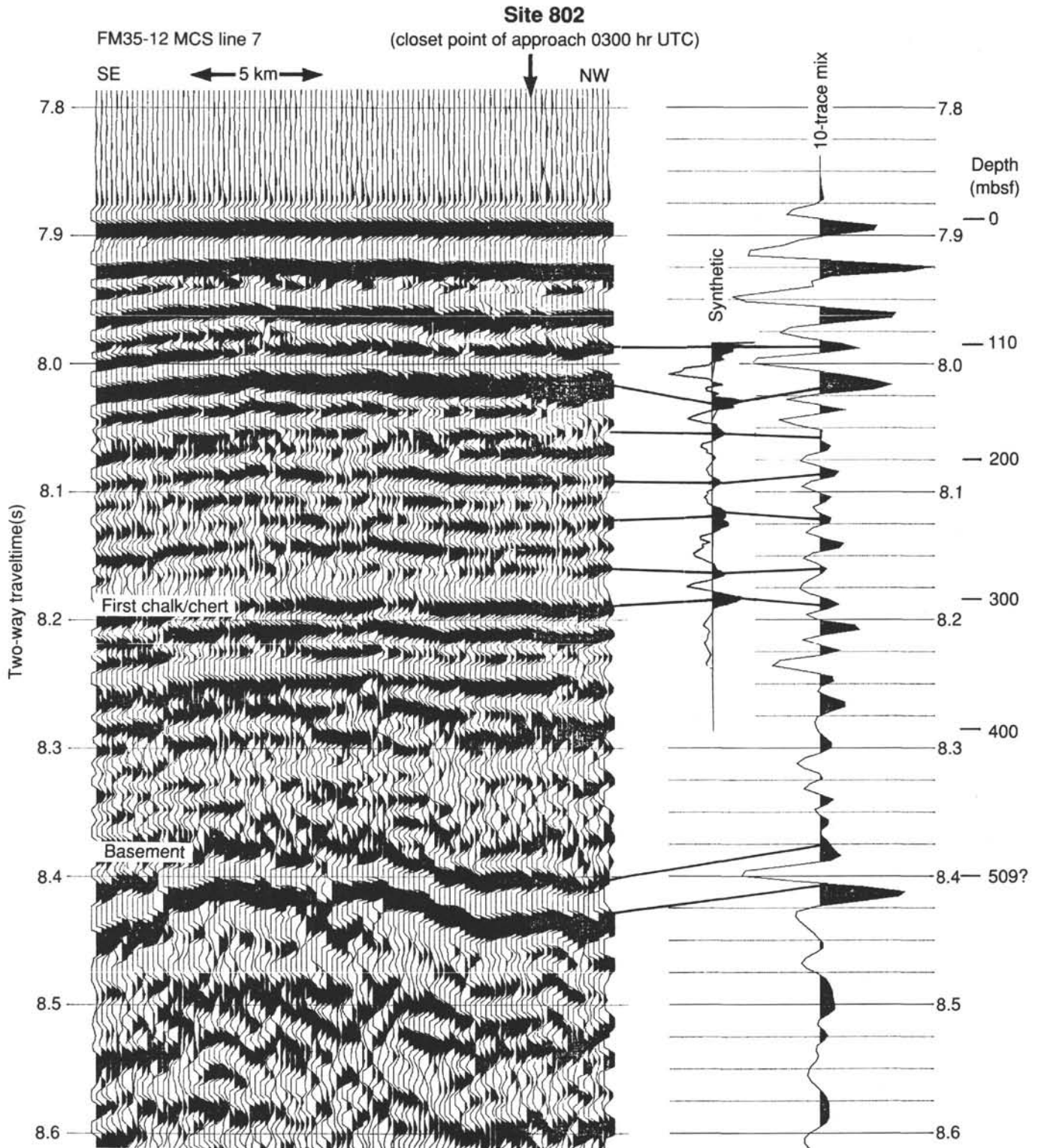
Figure 52. Comparison of vertical incident MCS data recorded during the FM35-12 expedition, with a 10-trace mix of this data and a synthetic seismic reflection trace computed from logged velocity and density measurements and the far-field source signature of the air-gun array used during FM35-12. Basement at this location along FM35-12 line 7 (within 2 km of Site 802) is imaged at 8.4 s twt, whereas at Site 802 basement deepens to 8.425 s twt (see Figs. 54 and 56). The seismic processing and display parameters are as follows: 120-fold stack, post-stack predictive decon, band-pass filter 20–60 Hz, and 500 ms AGC.
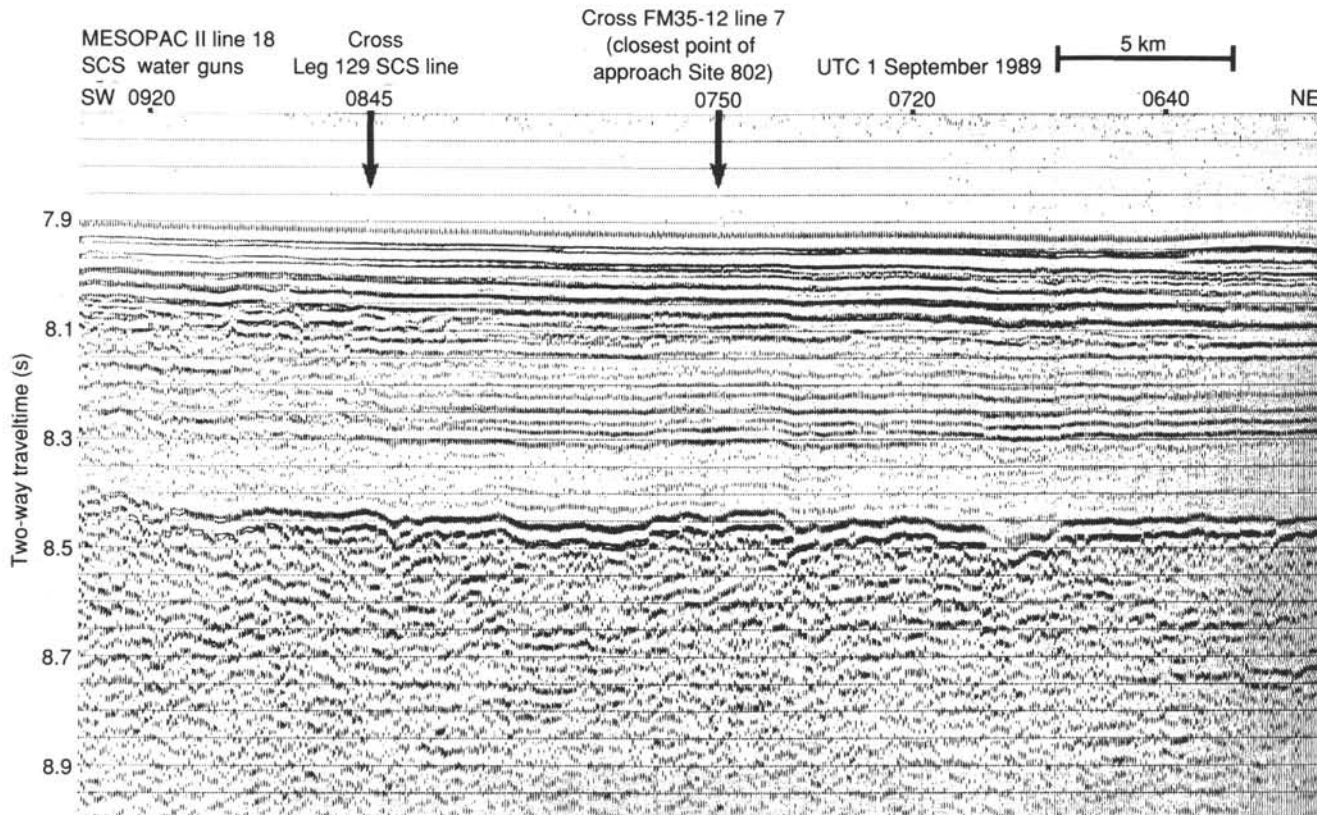
Figure 53. MESOPAC II line 18 SCS record (six 80-in.³ water guns) showing closest approach to Site 802 at its intersection with FM35-12 line 7 (0750 hr UTC, 1 September 1989). High-velocity basement lies at approximately 8.4 s twt, 0.4 s deeper than Jurassic oceanic crust penetrated at Site 801. This near-channel record was processed and displayed with the following parameters: water-velocity F/K migration, mute, 2-trace mix, band-pass filter 25–100 Hz, 500 ms AGC, and vertical exaggeration ~22× at 1.5 km/s.

Fred H. Moore (FM35-12). The proposed site was located approximately 2 km southwest of FM35-12 profile 7 at its closest approach and about 4 km west of the intersection of FM35-12 line 7 and MESOPAC II line 18 (see Figs. 4, 53, and 54). The MCS basement images and velocity structure derived from sonobuoy data (specifically, sonobuoys 7, 8, 18, and 20) obtained during the FM35-12 expedition provided the regional seismic framework for locating Site 802 (Fig. 55). Site EMB-2A was specifically located at 0030 hr UTC on 17 November 1987 along FM35-12 line 7, approximately 5 km northwest of its intersection with MESOPAC II line 18. FM35-12 sonobuoy 7 (167 km northwest of Site 802), sonobuoy 8 (120 km northwest of Site 802), sonobuoy 18 (130 km northeast of Site 802), and sonobuoy 20 (370 km northeast of Site 802) were used to constrain basement depth and velocity structure (Fig. 55). The only other seismic data in the area are single-channel air-gun analog profiles (e.g., V3506) and a digitally recorded, two 80-in.³ water-gun, single-channel survey collected aboard the *Kana Keoki* (KK 810626 Leg 4; Shipley et al., 1983).

Single-channel seismic (SCS) reflection and 3.5-kHz and 12-kHz profiling were conducted during the approach of the *JOIDES Resolution* to Site 802 (see "Operations" section, this chapter, for detailed approach plan). The actual site is located on the approach SCS water-gun profile at 2040 hr on 24 December 1989 (Figs. 4 and 56) within 2 km of the proposed site location on FM35-12 line 7.

The water-gun data collected during Leg 129 (two 80-in.³) and from MESOPAC II (six 80-in.³), and the FM35-12 air-gun data (2576-in.³) are corroborative, and together with 3.5-kHz

and sonobuoy data, provided the following seismic criteria for locating Site 802:

1. The relatively thin (30 ms) transparent layer over acoustic basement imaged with an excellent 3.5-kHz record (Fig. 57) was interpreted as pelagic clay overlying distal turbidites. We believed these turbidites could be penetrated with a minimum thickness of pelagic clay, providing lateral support for the drill string during spud-in.

2. A high-amplitude reflection imaged regionally at 0.30 to 0.55 s below the seafloor (bsf) corresponds to the onset of velocities characteristic of oceanic crust as recorded on FM35-12 sonobuoys 7, 8, and 18, indicating that approximately 300 to 550 m of sediment overlie volcanic basement in this area.

3. In the majority of the East Mariana Basin, this horizon is flat-lying and smooth. However, in restricted areas (e.g., Site 802), this high-amplitude reflection appears relatively rough, undulating, and slightly deeper, resulting in an image interpreted to be the top of oceanic crust, although not as clear as example of buried abyssal hills as found in the vicinity of Site 801.

Seismic Stratigraphy

The acoustic stratigraphy of large portions of the western Pacific consists of four units originally defined by Ewing et al. (1968); (1) an upper transparent layer, (2) an upper opaque layer, (3) a lower transparent layer, and (4) acoustic basement. These seismic facies descriptions were made from observations of SCS analog air-gun profiles. Acoustic basement has been characterized by the presence of a prominent zone of
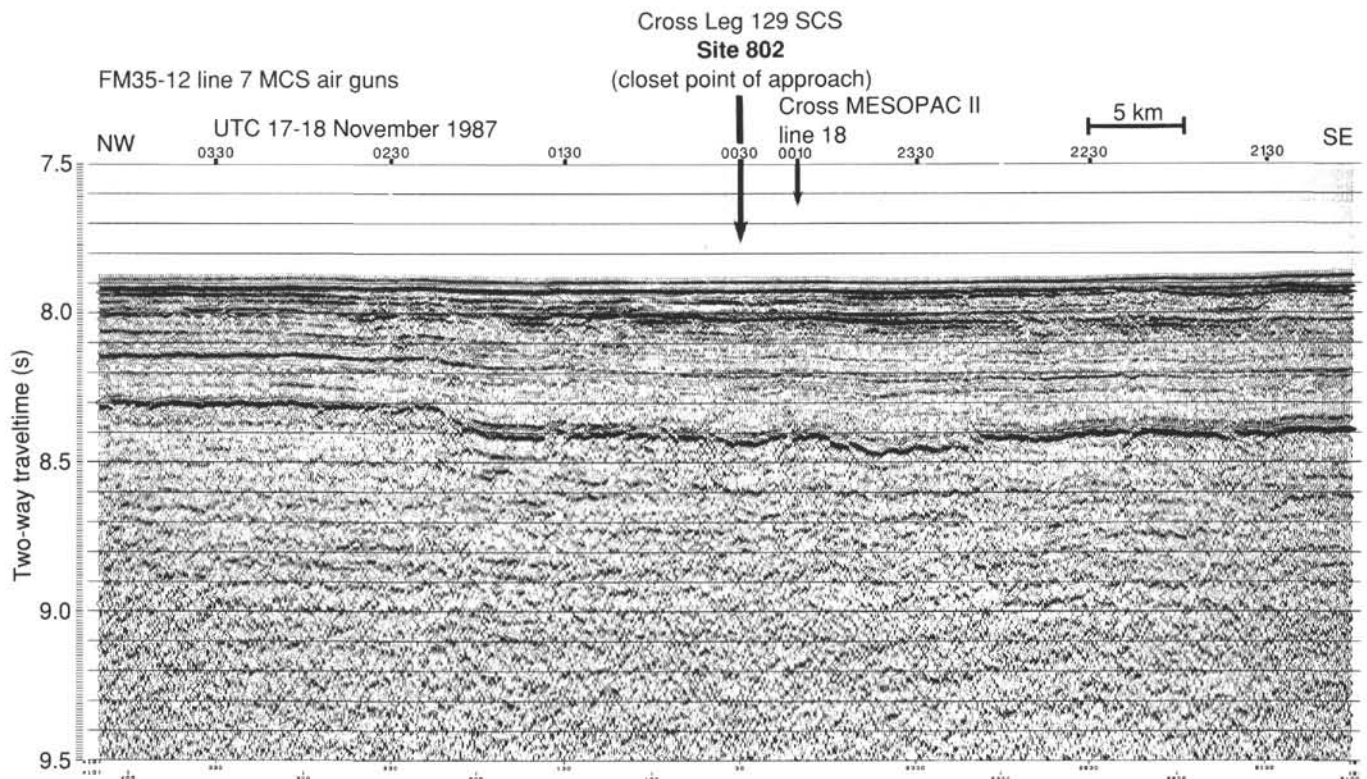
Figure 54. FM35-12 MCS air-gun profile showing the intersection with Leg 129 SCS (Fig. 56) at its closest approach (0030 hr UTC) to Site 802 and the intersection with MESOPAC II line 18 (Fig. 53) approximately 4 km east of Site 802. The depth and character of the basement reflector changes from a flat-lying, smooth reflection at 8.3 s twt to a rolling, higher-relief reflection at 8.4 s twt between 2300 and 0200 hr. These reflection characteristics were interpreted as a change from flat-lying sills to extrusive igneous material. This rough basement surface was correctly interpreted as extrusive basalt. However, it is not as obvious an example of buried abyssal hills as is found in the vicinity of Site 801. The seismic processing and display parameters are as follows: pre-stack spike decon, 120-fold stack, time-varying band-pass filter (20–60 Hz), 500 ms AGC, drop every other trace, and vertical exaggeration ~22× at 1.5 km/s.

flat-lying ("smooth"), high-amplitude, closely spaced reflections referred to as "horizon B" by Ewing et al. (1968), as the "deep opaque layer" by Heezen et al. (1973), and as the "reverberant layer" by Houtz et al. (1970) and Houtz and Ludwig (1979). It is now recognized that the reverberant nature of acoustic basement in such profiles is usually the result of a trailing bubble pulse oscillation reflecting from a single high-impedance boundary (Shipley et al., 1983). This characteristic of the air-gun source is now routinely compensated for through the use of tuned air-gun arrays and deconvolution techniques. The use of water guns in these surveys provides a much more implosive and bubble pulse-free source signature that provides a high-resolution record with little processing effort (Hutchinson and Detrick, 1984).

Although modern acquisition and processing techniques have allowed a more detailed and quantitative assessment of the stratigraphic units originally proposed by Ewing et al. (1968) (especially acoustic basement), these units can still serve to describe the general seismic character of the Pigafetta Basin. It is understood that the following qualitative seismic facies descriptions are largely controlled by the type of seismic source (air gun vs. water gun), processing, and display parameters. The final seismic facies identification and interpretation will be made after the MESOPAC II MCS data have been stacked and properly displayed and a final synthetic seismogram has been generated.

The East Mariana Basin is bounded to the south by the Caroline Ridge and is separated from the Pigafetta Basin

tectonically and physically by the northwest-trending Ogasawara fracture zone and Magellan seamounts (Tamaki et al., 1987; Handschumacher et al., 1988). These features isolated the Pigafetta Basin from the sources that supplied extensive Tertiary volcaniclastic turbidites to the East Mariana Basin. These Tertiary deposits represented the greatest anticipated difference in the stratigraphy between the East Mariana and Pigafetta basins.

The stratigraphy of the East Mariana Basin can be divided into three sequences (Fig. 58) that are comparable to the lowest three units of Ewing et al. (1968) and essentially to those described by Shipley et al. (1983). The lowermost sequence known as "horizon B" or the "reverberant layer" can be better characterized as a single, very high-amplitude, smooth reflector at approximately .30 to .55 s twt bsf. This most prominent horizon is continuous and flat-lying in the majority of the East Mariana Basin and identical in appearance to the reverberant layer in the southeastern Pigafetta Basin (see "Site Geophysics and Seismic Stratigraphy" section, "Site 801" chapter). There is no clear relationship between this horizon and the seamounts surrounding the East Mariana Basin. In restricted areas of this basin the reverberant layer deepens and becomes noticeably more rugged and undulating, for example, between 2330 and 0200 hr on FM35-12 line 7 (Fig. 54). The relief displayed by the reverberant layer in the East Mariana Basin, however, is never as great as observed in portions of the central Pigafetta Basin within the JQZ (e.g., Site 801). Site 802 was specifically
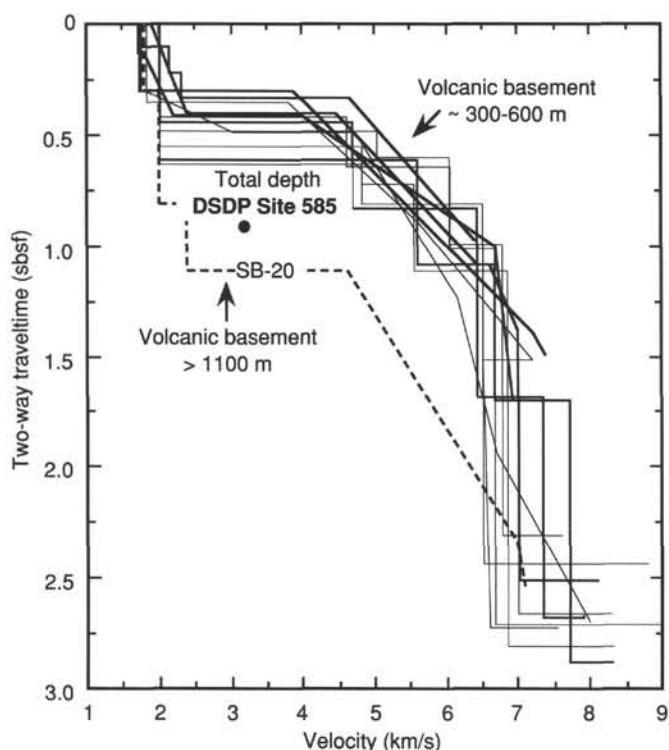
Figure 55. Velocity vs. two-way traveltime below seafloor (bsf) from sonobuoy data collected during FM35-12 and MESOPAC II in the East Mariana and Pigafetta basins. Crustal velocities begin from 300 to 600 ms bsf (approximately 300 to 600 mbsf), with the exception of sonobuoy 20. Sonobuoy 20 (dashed line) was shot over DSDP Site 585 and indicates that approximately 1150 m of sediment overlie the anomalously deep basement of the Ogasawara Fracture Zone trough (see total depth of DSDP Site 585). The onset of velocities and velocity gradients characteristic of oceanic crust corresponds to the reflection imaged at approximately 8.4 s twt in Figures 53, 54, and 56. (Note total depth of Hole 802A at about 560 ms bsf.)

located where the reverberant layer is deepest and relatively rough (8.4 to 8.425 s twt or 520 to 545 ms bsf).

There is a third, somewhat questionable type of basement reflection event observed in the East Mariana Basin. The suppression of any bubble pulse multiples from the flat-lying reverberant horizon on the processed FM35-12 MCS data has revealed much weaker discontinuous reflections approximately 100 ms below the reverberant horizon. The identification of these weak reflections, which are often identical in shape to the overlying dominant reflection (multiples?), as "real" primary reflection interfaces rather than bubble pulse or interbedded multiples is strengthened by the appearance of a similar sequence imaged with a water-gun source (Shipley et al., 1983). There are isolated instances where these weak reflections display significant relief independent of the flat, overlying reverberant layer, further indicating that they may be real events, possibly representing extrusive basement beneath basaltic sills and/or flows.

Sonobuoy velocity solutions indicate that velocities and velocity gradients characteristic of oceanic crust begin at or just below the dominant flat-lying reverberant horizon imaged regionally at 300 to 550 ms bsf (Fig. 55). Sonobuoy 7, for instance, displays crustal arrivals that begin .491 s bsf, just below the deepest high-amplitude reverberant-layer reflection, and may correlate to a weaker, high-relief basement reflector (Abrams et al., 1988). Sonobuoy 20, located on the

eastern border of the East Mariana Basin over DSDP Site 585, is the one exception to this trend and indicates that approximately 1150 m of sediment overlie the anomalously deep basement of the Ogasawara fracture zone trough. The reverberant layer at this location lies at approximately 9.0 s twt and is apparently created by well-cemented volcaniclastic debris flows that lie about 260 m above basement.

Immediately overlying the reverberant layer (Fig. 58) is the "lower transparent" layer (8.041–8.425 s twt), which is characterized by low-amplitude, more widely separated, discontinuous reflectors, making this sequence distinctly transparent on both air-gun and water-gun seismic records (Figs. 53, 54, and 56). This sequence is flat-lying, mirroring the dominant reverberant horizon and does not appear to pond (onlap) against any of the large guyots traversed during FM35-12. However, it does thin in areas where the underlying reverberant horizon rises (300 ms), suggesting that this sequence is not pelagic drape. At Site 802 the lower transparent layer is bounded on top by another sequence of high-amplitude, flat-lying, continuous reflectors that are visible at 161 ms twt bsf (8.041 s twt). The transparent layer is divided in two by a sequence of distinct, moderate-amplitude, continuous reflections from approximately 8.185 to 8.275 s twt. The top of this sequence can be traced for hundreds of kilometers across the majority of the East Mariana Basin, including the area surrounding DSDP Sites 199 and 585.

The sequence from the seafloor down to approximately 8.04 s twt (Fig. 58) is comparable to that described by Ewing et al. (1968) as the "upper opaque layer." This interval contains closely spaced, moderate- to high-amplitude reflections that are traceable for 30 to 50 km. This uppermost sequence is distinct in that reflections onlap basement highs including a large, unnamed Magellan seamount to the north and Ita Mai Tai guyot to the south, and tends to thicken in minor lows and thin over minor highs.

The upper transparent zone as envisioned by Ewing et al. (1968) is very much attenuated in the East Mariana Basin and extends from 0 to approximately 30 ms bsf (7.88–7.91 s twt) at Site 802. This interval is best displayed on the 3.5-kHz records obtained during Leg 129 (Fig. 52) and MESOPAC II, and is not apparent on SCS records. These four seismic facies are essentially identical on the SCS monitor records of both Leg 129 and MESOPAC II, and are comparable to the processed FM35-12 air-gun data.

Correlation between Seismic Stratigraphy and Lithology at Site 802

During DSDP Legs 6, 17, 61, and 89, there were instances when a flat-lying, high-amplitude "acoustic basement" or "reverberant layer" was correlated to middle Cretaceous volcanic material (sills, flows, and volcanogenic turbidites) which, according to magnetic lineations, significantly postdate the formation of oceanic crust. However, the physical nature of a similar seismic facies observed throughout the majority of the East Mariana Basin and all of the Pigafetta Basin had not been determined before Leg 129.

The reverberant layer at Site 800, located on a correlatable magnetic anomaly (M33) in the northern Pigafetta Basin, is created by a massive chert overlying a series of dolerite sills and appears as a flat-lying sequence of reflections approximately 100 ms thick (see "Site Geophysics and Seismic Stratigraphy" section, "Site 800" chapter, this volume). This type of smooth, flat-lying, high-velocity horizon is characteristic of much of the Pigafetta Basin and the majority of the East Mariana Basin (Abrams et al., 1988). In contrast, the reverberant layer at Site 801, located well within the JQZ, appears as a rough, undulating horizon that is created by

A

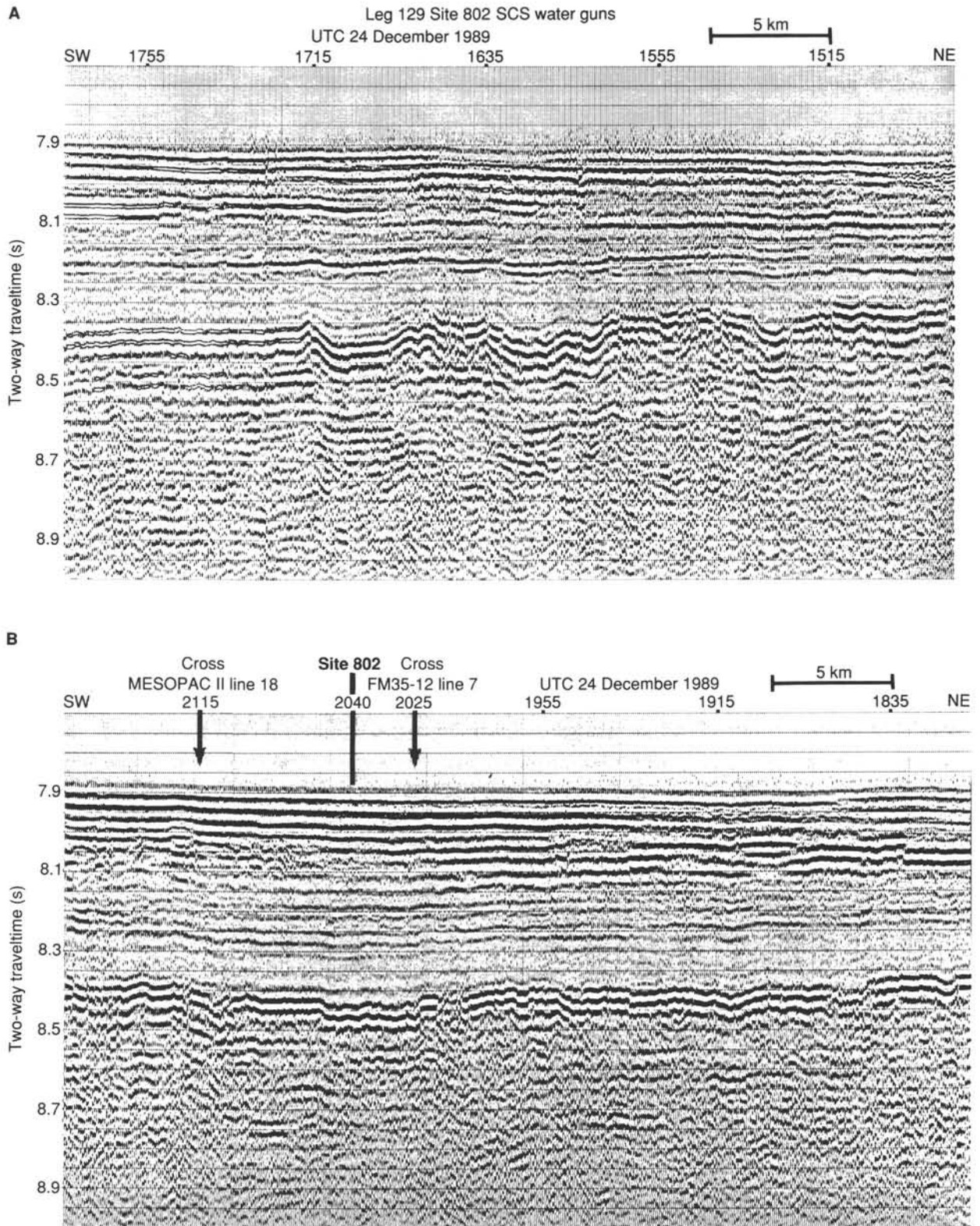Leg 129 Site 802 SCS water guns
UTC 24 December 1989

B

Figure 56. The entire SCS profile (two 80-in.³ water guns) obtained on approach to Site 802 (2040 hr UTC, 24 December 1989) during Leg 129. This profile crosses FM35-12 MCS line 7 (Fig. 54) 2 km northeast of Site 802 at 2025 hr, where proposed site EMB-2A was originally located. The basement reflection and total depth at Site 802 lie at 8.425 and 8.446 s twt, respectively, which is 0.4 s twt deeper than Jurassic oceanic crust penetrated at Site 801. The SCS data were processed and displayed with the following parameters: water-velocity F/K migration, mute, 2-trace mix, band-pass filter 30–100 Hz, 500 ms AGC, and vertical exaggeration ~22× at 1.5 km/s.

ODP Leg 129–3.5 kHz
Site 802
JD358/2302 UTC
(Beacon dropped)
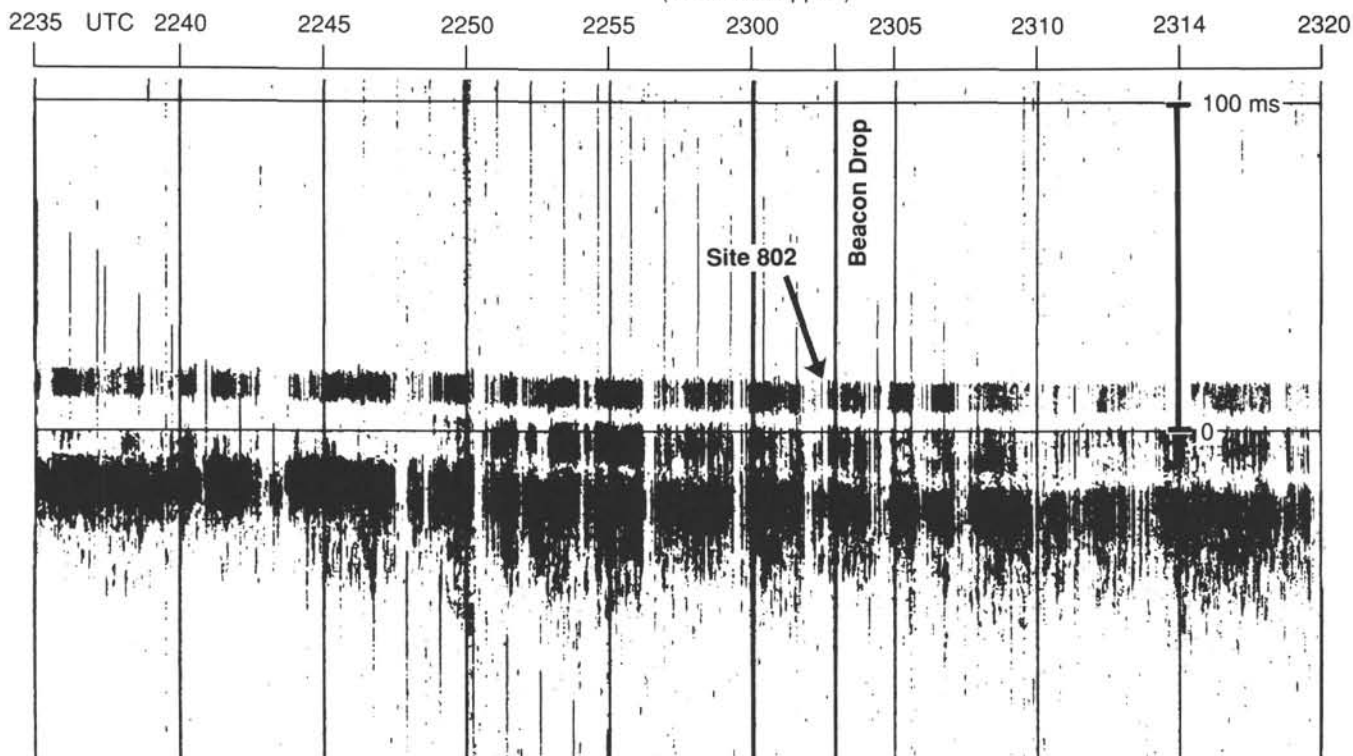
Figure 57. The 3.5-kHz record collected on approach from Site 802 during Leg 129. Horizontal lines represent 100-ms intervals. Acoustic basement on this record marks the top of the first volcaniclastics and indicates 30 ms of pelagic clay. A weak, intermittent reflection is also visible at 13 ms bsf.

interbedded basalt and chert overlying a series of contiguous basalt flow units (see "Igneous Petrology" section, "Site 801" chapter, this volume). The reverberant layer at Site 802, located within the JQZ of the East Mariana Basin appears as a restricted (30-km-wide) window of relatively rough, high-amplitude reflections lying slightly deeper than the surrounding, more typical, flat-lying reverberant horizon. This seismic facies is interpreted to result primarily from a single impedance contrast between the claystone/radiolarite and the top of extrusive basalt at 509 mbsf.

Sonobuoy solutions show velocities and velocity gradients characteristic of "normal" oceanic crust beginning from 300 to 490 ms bsf, which correlates to the reverberant layer imaged at 520 to 540 ms over Site 802. The relatively high relief horizon penetrated by Hole 802A appears to be the top of oceanic crust. This interpretation is questionable, however, because the basement age is at least 50 m.y. less than predicted (see "Summary and Conclusions" section, this chapter), while lying at a depth of nearly 6500 mbsf. In the areas where the reverberant horizon becomes flat-lying and shallow and the overlying transparent layer thins, intrusive volcanics are expected to overly extrusive basement (oceanic crust?).

In the East Mariana Basin there is no comparable distinctive change in the seismic character of the reverberant layer from smooth to rough that can also be correlated to a change in magnetic anomaly amplitudes and field strength as observed in the JQZ of the Pigafetta Basin (Handschumacher et al.,

1988) (see "Site Geophysics and Seismic Stratigraphy" section, "Site 801" chapter, this volume).

The lower transparent layer at Site 802 (Fig. 58) correlates with the sequence of calcareous claystone and radiolarite between 460 and 509 mbsf (lithologic Units VI through IX), as well as the lower portion of the volcaniclastic turbidites (388 to 460 mbsf within lithologic Unit V). The moderate-amplitude reflections dividing the transparent layer in half at 305 to 395 ms bsf (8.185–8.275 s twt) are believed to correspond to the occurrence of chert within a chalk-dominated sequence overlying a transition zone containing volcaniclastic turbidites, calcareous claystone, and porcellanite (lithologic Units III, IV, and V). Downhole logging results indicate that these moderate-amplitude reflections are created by velocity-density contrasts associated with variations in the extent and concentration of recrystallized silica and/or calcium carbonate (see "Downhole Measurements" section, this chapter). The reflector at approximately 305 ms bsf that marks the top of this unit has been assigned an age of late Paleocene to early Eocene (see "Biostratigraphy" section, this chapter). This distinctive horizon can be traced eastward for over 360 km along the FM35-12 MCS track past a point 40 km south of DSDP Site 199 and directly over DSDP Site 585. This horizon can be correlated to the first cherts of similar age encountered at 285 mbsf at DSDP Site 199 and at 256 mbsf at DSDP Site 585 and is believed to mark the passage of the Pacific plate beneath the equatorial zone of high productivity (Lancelot and Larson, 1975; see "Paleomagnetism" section, this chapter).
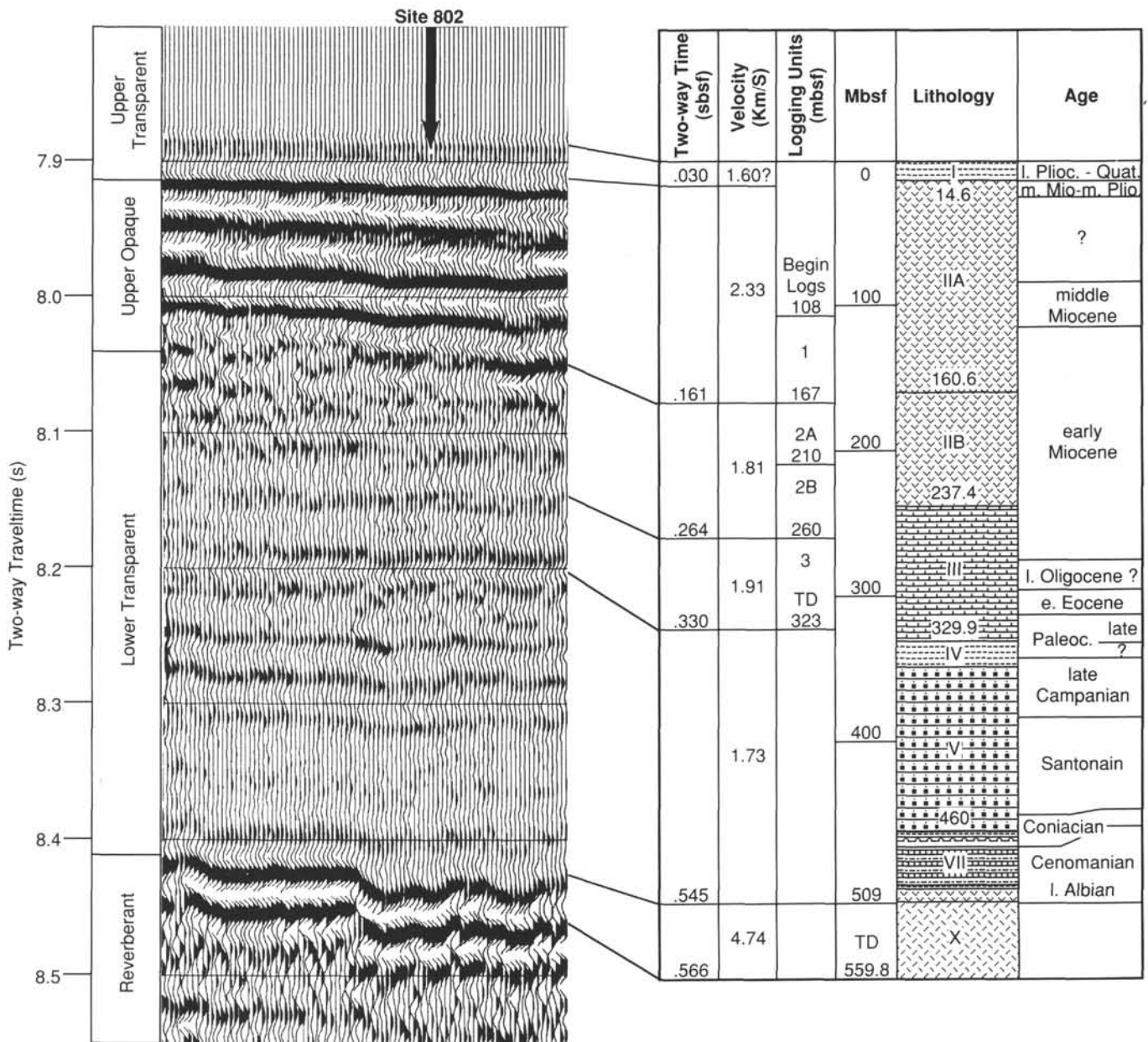
Figure 58. Summary of seismic stratigraphy at Site 802 showing correlations with logging units, lithologic units, ages, and depths. These correlations should be considered only as best estimates until further constraints are provided by improved synthetic seismograms. The velocity of volcanic basement (Unit X) is based on traveltime modeling of sonobuoy data. The 1.6-km/s(?) velocity given for the pelagic clay interval assumes 24 m thickness over .03 s twt, which is 10 m more than indicated from the drill-string mud line (see text and Fig. 56 in "Site Geophysics and Seismic Stratigraphy" section, "Site 801" chapter, this volume). The 2.33-km/s velocity corresponds to the interval from 14.6 to 167 mbsf. This SCS water-gun record is displayed with a vertical exaggeration of 33× at 1.5 km/s and with the same parameters given for Figure 56.

The relatively transparent interval above the first chert at 8.185 s twt and below the onset of high-amplitude reflections at 8.041 s twt corresponds to lithologic Unit IIB and the upper portion of Unit III between approximately 167 to 300 mbsf. This interval is characterized by lower and less variable compressional-wave velocities relative to Unit IIA (see "Physical Properties" and "Downhole Measurements" sections, this chapter). In this interval, moderate- to low-amplitude reflections are the result of small velocity-density contrasts within relatively uniform, fine-grained claystone/siltstone, with few interbedded, well-cemented, coarser-grained volcaniclastic sandstone intervals (see "Lithostratigraphy and Sedimentology" and "Downhole Measurements" sections, this chapter).

The upper opaque zone corresponds to lithologic Unit IIA and extends essentially from 30 to approximately 161 ms bsf. This interval is characterized by high and highly variable compressional-wave velocities relative to the transparent layer below (see "Physical Properties" and "Downhole Measurements" sections, this chapter). The high-amplitude, continuous reflections that characterize this interval are interpreted to arise from impedance contrasts between alternating zones of variably cemented, coarse-grained volcanic sandstone, fine-grained volcanic siltstone/claystone, and pelagic clay. The topmost 30 ms correspond to the pelagic brown clay of lithologic Unit 1. The thickness of this interval derived from the drill string length is 14.6 m. We believe that, as at Site 801,

this layer is actually 5 to 10 m thicker (see Fig. 56, "Site 801" chapter, this volume). These correlations are based on preliminary, log-generated synthetic seismograms (108–323 mbsf), and are consistent with the trends in velocities given by physical properties measurements. The two-way traveltime and depth to the seafloor reflector, the reflections at approximately 0.330 s bsf that can be correlated to DSDP Site 199, and the volcanic basement reflector also provided a framework for correlations. The seismic stratigraphic correlations, summarized in Figure 58, should be considered only as best estimates until further constraints are provided by a improved synthetic seismogram.

SUMMARY AND CONCLUSIONS

Introduction (Nauru Basin Revisited?)

Although Site 801 provided the most immediately spectacular result of Leg 129 in the form of Jurassic sediments and oceanic crust, Site 802 provided the greatest justification for future exploration work in the deep western Pacific, as it poses more basic questions than it answers. Because this site was chosen as a typical deep-water site in the East Mariana Basin, these questions apply to the geology and geophysics of an area that encompasses at least this deep basin and, as we shall see, extends considerably beyond its margins for adequate explanations of certain problems.

Site 802 was positioned at the southeastern edge of a set of low-amplitude magnetic lineations that are not positively identified at Site 802. However, M22 to M31 have been identified to the northwest as part of this same lineation sequence, and the simplest explanation is that the lineations near Site 802 are an older continuation of this sequence, probably extending to about M35. The site is located in the middle of the East Mariana Basin, more than 300 km from any known seamounts, guyots, island chains, or plateaus, and beneath nearly 6000 m of water. This was done in order to minimize the possibility that the site would be "contaminated" with volcaniclastic or carbonate turbidites in the sedimentary section, and/or with off-ridge volcanism in the igneous section. These precautions failed on both counts, and yielded instead what will eventually prove to be the most intriguing results recovered on Leg 129.

Acoustic Basement: "The Real Thing" or a "Pepsi Generation" Volcanic Event?

Igneous volcanic rocks were recovered from Hole 802A below 509 mbsf to the bottom of the hole at 560 mbsf. These equate to total depths of 6478 to 6529 mbsl. Multiple cooling units were identified that consist mainly of thin sequences of pillow basalts. They are olivine basalts with aphyric to microphyric textures that are remarkably fresh. They have about 10% matrix alteration, which is consistent with low-grade alteration under mildly alkaline, *reducing* conditions. Based on their crystal textures and pillow basalt structures, there is almost no doubt that they cooled under extrusive, submarine conditions.

This conclusion is consistent with the interpretation of the seismic reflection data that show a "rough" acoustic basement surface interpreted as extrusive basement, in contrast to adjacent areas that have a "smooth" or "flat" surface interpreted as intrusive sills. The rough basement at Site 802 is not as obviously a case of buried abyssal hills, as were found at Site 801. It is better described as "rolling" than "hyperbolic echoing" and its lineation, parallel to the magnetic anomaly lineations, is suppressed. Nevertheless, our prediction that it is an extrusive, igneous, volcanic surface proved to be correct.

The only problem with equating these extrusive basalts with original basement formed by seafloor spreading at a Mesozoic ridge crest is the age of the oldest sediments. They are dated by both nannofossils and dinoflagellates to range from Albian to late Aptian in age, whereas the magnetic anomalies, supported by the depth to basement, predict an Oxfordian/Callovian age. Thus, the oldest sediments are *at least* 50 m.y. younger than the age suggested by the magnetic anomalies/basement depth. Either the magnetic anomaly identifications are incorrect, and the basement is anomalously deep, or the basalts represent an off-ridge volcanic event that extruded igneous volcanic rocks over Jurassic-aged crust and possibly sediments that were already 50 m.y. old at the time. Because these rocks are extrusive, and there is no adjacent volcanic edifice to act as a point source, it is more difficult to be convinced that these basalts represent off-ridge volcanism than was the case for the dolerites recovered at Site 800. However, Site 802 is reminiscent of DSDP Site 462 in the Nauru Basin located about 1200 km to the southeast on magnetic anomaly M26 of Oxfordian age (160 m.y.). At DSDP 462, Cenomanian/Upper Albian sediments overlie a sequence of basalts that consist of 200 m of intrusive sills at the top, underlain by at least 450 m of extrusive flows. The upper sills have been radiometrically dated at 110 m.y., and the lower flows at 130 m.y., both ages being intermediate between the overlying sediments and the magnetic anomaly sequence.

Because the magnetic anomalies are well preserved at DSDP Site 462, it is difficult to argue that any of these basalts represent the original basement of the Nauru Basin. Put another way, the results from DSDP Site 462 and ODP Site 802 suggest that Jurassic magnetic anomalies are a necessary but insufficient condition for the recovery of Jurassic basement rocks just below the base of their sediment sections. It is likely that the basalts of Site 802 also resulted from an off-ridge volcanic eruption in the Cretaceous. Radiometric dating of this material and its geochemistry will lend considerable insight on this problem. Of special interest will be their rare earth element chemistry that may demonstrate a clear relationship, or lack thereof, with the basalts of Sites 800 and 462.

Cretaceous and Tertiary Volcanic Events

The majority of the sediment section is dominated by tuffs and volcaniclastic turbidites of Miocene and Late Cretaceous age. In addition, volcaniclastic turbidites occur in the thin, basal sedimentary sequence of late Aptian to Albian age. These latter turbidites are notable because they contain the only dinoflagellates recovered on Leg 129. The dinoflagellates are associated with wood fragments and spores that indicate a warm, humid climate at their source. As with the much thicker, Upper Cretaceous volcaniclastics, this source is unknown.

The lower portion of the sediment section is dominated by 110 m of volcaniclastic turbidites ranging in age from Coniacian to Late Campanian. Much of the sequence is coarse-grained, indicating debris flows from a relatively proximal source. No edifices are known to exist within 300 km of Site 802. The most likely sources of known or probable Late Cretaceous age are the seamounts and guyot platforms that fringe the East Mariana Basin on its north and east sides. However, the mystery is heightened because the Upper Cretaceous volcaniclastics do not thicken to the east at DSDP Sites 199 and 585, which is the most likely source direction. Instead, the dominant volcaniclastics found there are of Albian to Aptian age.

The upper portion of the sediment section is dominated by 146 m of tuff, regarded as volcaniclastic turbidites or redepos-

ited hyaloclastites. They range in age from early to middle Miocene, with a small amount of Pliocene material at the top of the sequence. They are notably well-lithified, coal-black sedimentary rocks. Pelagic clay and calcareous claystone are included in the lower and upper parts, respectively. They are most likely derived from the Caroline Islands and their associated volcanic platform 350 km south of Site 802.

In summary, the majority of the sediment section at Site 802 is dominated by unexpected thicknesses of turbidite deposits. Most of this material appears either to have been derived from proximal sources that are unknown on the most recent bathymetric charts of the area, or to have been transported over several hundred kilometers by exceptionally high-energy turbidity currents.

Paleolatitudes Recorded at Site 802

Paleolatitude information to be gained from Site 802 is more limited than at our two previous sites because the hole terminated in younger (Aptian) material. In addition, most of the "background sedimentation" is limited to brown pelagic clays, whereas the main sedimentary component is turbiditic material of dubious value for biogenic accumulation studies.

Remanent magnetic inclination values for the sedimentary section yield a reasonable story. Low northern paleolatitudes are recorded down to Campanian/upper Paleocene sediments, and appear to coincide with the equator crossing of Site 802. Remanent inclination values then increase, indicating higher southern paleolatitudes, leveling off at about 10°S latitude for Santonian to Cenomanian time. These results are consistent with previous models for Pacific plate motion for the last 100 m.y. Because drilling at this site terminated in middle Cretaceous material, the results do not add a large body of new information to this subject.

REFERENCES

Abrams, L. J., Larson, R. L., Shipley, T., and Lancelot, Y., 1988. Cretaceous volcanic sequences and Jurassic(?) crust in the western Pacific. *Trans. Am. Geophys. Union,* 69:1442.

Bolli, H. M., and Saunders, J. B., 1985. Oligocene to Holocene low latitude planktonic foraminifera. *In* Bolli, H. M., Saunders, J. B., and Perch-Nielsen, K. (Eds.), *Plankton Stratigraphy:* Cambridge (Cambridge Univ. Press), 155–262.

Bryan, W. B., 1972. Morphology of quench crystals in submarine basalts. *J. Geophys. Res.,* 77:5281–5289.

Carlson, R. L., Schaftenaar, C. H., and Moore, R. P., 1979. Causes of compressional-wave anisotropy in calcareous sediments from the Rio Grand Rise. *In* Barker, P. F., Carlson, R. L., et al., *Init. Repts. DSDP,* 72: Washington (U.S. Govt. Printing Office), 565–576.

Caron, M., 1985. Cretaceous planktonic foraminifera. *In* Bolli, H. M., Saunders, J. B., and Perch-Nielsen, K. (Eds.), *Plankton Stratigraphy:* Cambridge (Cambridge Univ. Press), 17–86.

Christensen, N. L., and Lewis, B.T.R., 1983. Physical properties of Leg 65 basalts. *In* Lewis, B.T.R., Robinson, P., et al., *Init. Repts. DSDP,* 65: Washington (U.S. Govt. Printing Office), 693–696.

Christensen, N. L., and Salisbury, M. H., 1975. Structure and constitution of the lower oceanic crust. *Rev. Geophys. Space Phys.,* 13:57–86.

Clark, S. P. (Ed.), 1966. *Handbook of Physical Constants.* Mem. Geol. Soc. Am., 97:1–587.

Ewing, J., Ewing, M., Aitken, T., and Ludwig, W. J., 1968. North Pacific sediment layers measured by seismic profiling. *In* Drake, C. L., and Hart, P. J. (Eds.), *The Crust and Upper Mantle of the Pacific Area.* Am. Geophys. Union. Monogr., 12:147–173.

Gradstein, F. M., and Sheridan, R. E., 1983. On the Jurassic Atlantic Ocean and a synthesis of results of DSDP Leg 76. *In* Sheridan, R. E., Gradstein, F. M., et al., *Init. Repts. DSDP,* 76: Washington (U.S. Govt. Printing Office), 913–943.

Handschumacher, D. W., and Gettrust, J. F., 1985. Mixed polarity model for the Jurassic "Quiet Zones": new oceanic evidence of frequent pre-M25 reversals. *Eos,* 66:867.

Handschumacher, D. W., Sager, W. W., Hilde, T.W.C., and Bracey, D. R., 1988. Pre Cretaceous tectonic evolution of the Pacific Plate and extension of the geomagnetic polarity reversal time scale with implications for the origin of the Jurassic "Quiet Zone." *Tectonophysics,* 155:365–380.

Harland, W. B., Cox, A. V., Llewellyn, P. G., Pickton, C.A.G., Smith, D. G., and Walters, R., 1982. *A Geologic Time Scale:* Cambridge (Cambridge Univ. Press).

Heezen, B. C., MacGregor, I. D., et al., 1973. *Init. Repts. DSDP,* 20: Washington (U.S. Govt. Printing Office).

_____, 1973. Mesozoic chalks beneath the Caroline abyssal plain: DSDP Site 199. *In* Heezen, B. C., MacGregor, I. D., et al., *Init. Repts. DSDP,* 20: Washington (U.S. Govt. Printing Office), 65–85.

Helsley, C. E., and Steiner, M. D., 1969. Evidence for long intervals of normal polarity during the Cretaceous period. *Earth Planet. Sci. Lett.,* 5:325–332.

Houtz, R. E., Ewing, J., and Buhl, P., 1970. Seismic data from sonobuoy stations in the northern and equatorial Pacific, *J. Geophys. Res.,* 75:5093–5111.

Houtz, R. E., and Ludwig, W. J., 1979. Distribution of reverberant subbottom layers in the southwest Pacific Basin. *J. Geophys. Res.,* 84:3497–3504.

Humphris, S. E., Thompson, R. N., and Marriner, G. F., 1979. The mineralogy and geochemistry of basalt weathering, Holes 417A and 418A. *In* Donnelly, T., Francheteau, J., Bryan, W., Robinson, P., Flower, M., Salisbury, M., et al., *Init. Repts. DSDP,* 51, 52, 53: Washington (U.S. Govt. Printing Office), 1201–1217.

Hutchinson, D. R., and Detrick, R. S., 1984. Water gun vs. air gun: a comparison. *Mar. Geophys. Res.,* 6:295–310.

Irving, E., and Pullaiah, G., 1976. Reversal of the geomagnetic field, magnetostratigraphy and relative magnitude of palaeosecular variation in the Phanerozoic. *Earth-Sci. Rev.,* 12:35–64.

Karpoff, A. M., 1989. Les faciès pélagiques condensés cénozoiques des océans Pacifique et Atlantique: témoins des grandes crises géodynamiques [Thèse Doc. ès Sci.]. Univ. Louis Pasteur, Strasbourg.

Keene, J. B., 1975. Cherts and porcellanites from the North Pacific DSDP, Leg 32. *In* Larson, R. L., Moberly, R., et al. *Init. Repts. DSDP,* 32: Washington (U.S. Govt. Printing Office), 429–507.

Kent, D. V., and Gradstein, F. M., 1985. A Cretaceous and Jurassic geochronology. *Geol. Soc. Am. Bull.,* 96:1419–1427.

_____, 1986. A Jurassic to Recent chronology. *In* Tucholke, B. E., and Vogt, P. R. (Eds.), *The Geology of North America: The Western Atlantic Region.* Geol. Soc. Am. DNAG Ser., 1:45–50.

Kono, M., 1980. Statistics of paleomagnetic inclination data. *J. Geophys. Res.,* 85:3878–3882.

Lancelot, Y., 1978. Evolution sedimentaire et tectonique de la plaque Pacifique. *Mem. Soc. Geol. France,* Nelle Ser., 134.

Lancelot, Y., and Larson, R. L., 1975. Sedimentary and tectonic evolution of the northwestern Pacific. *In* Larson, R. L., Moberly, R., et al., *Init. Repts. DSDP,* 32: Washington (U.S. Govt. Printing Office), 945–957.

Larson, R. L., and Hilde, T.W.C., 1975. A revised time scale of magnetic reversals for the Early Cretaceous and Late Jurassic. *J. Geophys. Res.,* 80:2586–2594.

Larson, R. L., and Lowrie, W., 1975. Paleomagnetic evidence for motion of the Pacific plate from Leg 32 basalts and magnetic anomalies. *In* Larson, R. L., and Moberly, R., et al., *Init. Repts. DSDP,* 32: Washington (U.S. Govt. Printing Office), 571–577.

Larson, R. L., Schlanger, S. O., et al., 1981. *Init. Repts. DSDP,* 61: Washington (U.S. Govt. Printing Office).

Martini, E., 1971. Standard Tertiary and Quaternary calcareous nannoplankton zonation. *In* Farinacci, A. (Ed.), *Proc. 2nd Planktonic Conf. Roma:* Rome (Ed. Technosci.), 2:739–785.

Marty, J. C., and Cazenave, A., 1989. Regional variations in subsidence rate of oceanic plates: a global analysis. *Earth Planet. Sci. Lett.,* 94:301–315.

Moberly, R., Schlanger, S. O., et al., 1986. *Init. Repts. DSDP,* 89: Washington (US Govt. Printing Office).

_____, 1986. Site 585. *In* Moberly, R., Schlanger, S. O., et al., *Init. Repts. DSDP,* 89: Washington (U.S. Govt. Printing Office): 29–99.

Natland, J. H., 1980. Crystal morphologies in basalts dredged and drilled from the East Pacific Rise near 9°N and the Sequeiros fracture zone. *In* Rosendahl, B. R., Hekinian, R., et al., *Init. Repts. DSDP,* 54: Washington (U.S. Govt. Printing Office), 605–634.
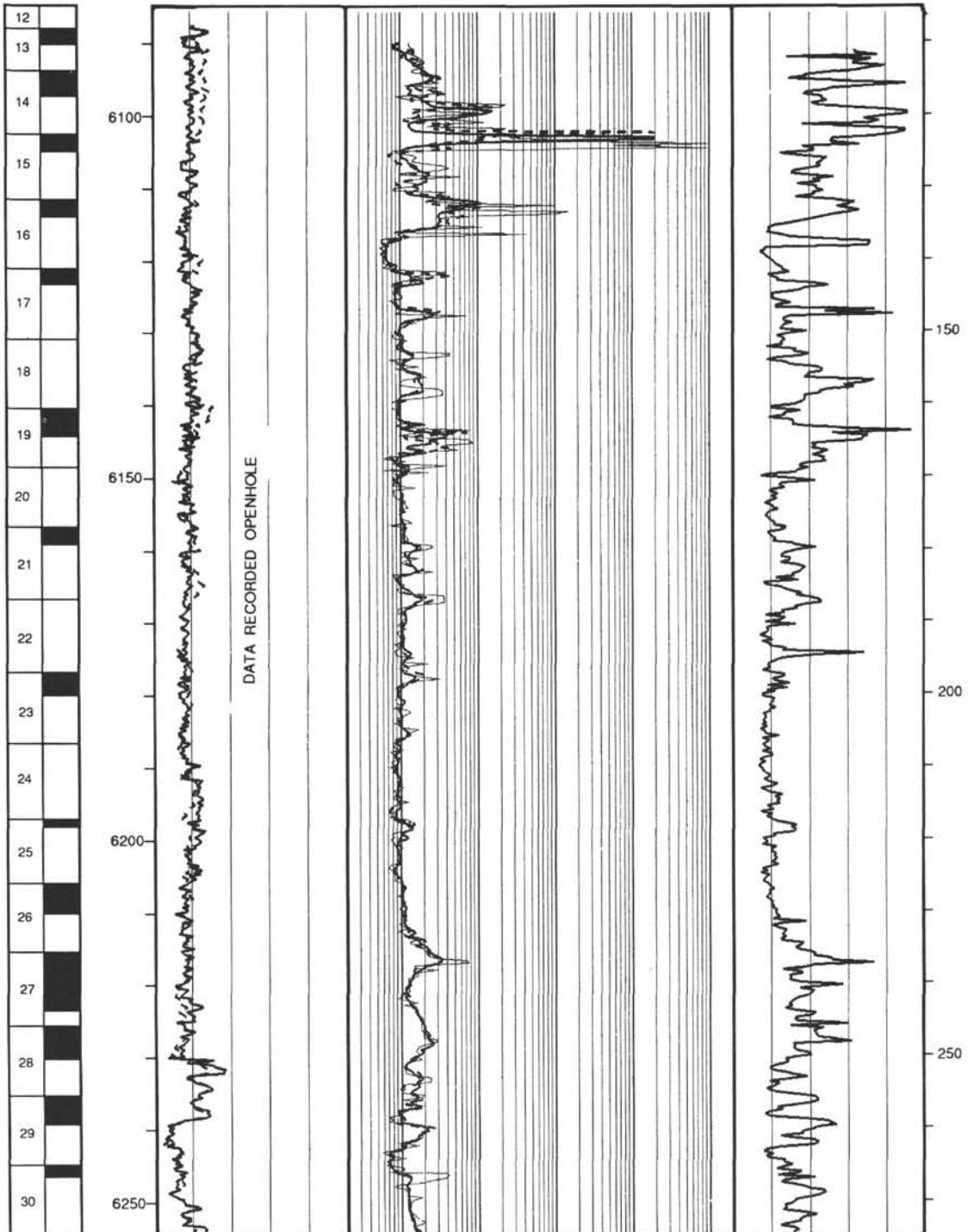
Okada, H., and Bukry, D., 1980. Supplementary modification and introduction of code numbers to the low-latitude coccolith biostratigraphic zonation (Bukry, 1973; 1975). *Mar. Micropaleontol.*, ·5:321–325.

Palmer, A. R., 1983. The decade of North American geology, 1983 geological time scale. *Geology*, 11:503–504.

Parsons, B. and Sclater, J. G., 1977. An analysis of the variation of ocean floor bathymetry and heat flow with age. *J. Geophys. Res.*, 82:803–827.

Perch-Nielsen, K., 1985a. Cenozoic calcareous nannofossils. *In* Bolli, H. M., Saunders, J. B., and Perch-Nielsen, K. (Eds.), *Plankton Stratigraphy:* Cambridge (Cambridge Univ. Press), 427–554.

_____, 1985b. Mesozoic calcareous nannofossils. *In* Bolli, H., Saunders, J. B., and Perch-Nielsen, K. (Eds.), *Plankton Stratigraphy:* Cambridge (Cambridge Univ. Press), 329–426.

Robinson, P. R., Flower, M.F.J., Schmincke, H.-U., and Ohnmacht, W., 1977. Low temperature alteration of oceanic basalts, DSDP Leg 37. *In* Aumento, F., Melson, W. G., et al., *Init. Repts. DSDP*, 37: Washington (U.S. Govt. Printing Office), 775–793.

Sager, W. W., and Pringle, M. S., 1989. Mid-Cretaceous to Early Tertiary apparent polar wander path of the Pacific Plate. *J. Geophys. Res.*, 93:11753–11771.

Shipboard Scientific Party, 1981. Site 462: Nauru Basin, Western Pacific Ocean, DSDP Leg 61. *In* Larson, R. L., Schlanger, S. O., et al., *Init. Repts. DSDP*, 61: Washington (U.S. Govt. Printing Office), 19–395.

Shipboard Scientific Party, 1990. Site 793. *In* Taylor, B., Fujioka, K., et al., *Proc. ODP, Init. Repts.*, 126: College Station, TX (Ocean Drilling Program).

Shipley, T. H., Whitman, J. M., Dunnebier, F. K., and Peterson, L. D., 1983. Seismic stratigraphy and sedimentation history of the East Mariana Basin, Western Pacific. *Earth Planet. Sci. Lett.*, 64:257–275.

Sissingh, W., 1977. Biostratigraphy of Cretaceous calcareous nannoplankton. *Geol. Mijnbouw*, 56:37–65.

Tamaki, K., Nakanishi, M., Sayanagi, K., and Kobayashi, K., 1987. Jurassic magnetic lineations of the western Pacific Ocean and the origin of the Pacific plate. *Eos*, 68:1493.

Toumarkine, M., and Luterbacher, H., 1985. Paleocene and Eocene planktic foraminifera. *In* Bolli, H. M., Saunders, J. B., and Perch-Nielsen, K. (Eds.), *Plankton Stratigraphy:* Cambridge (Cambridge Univ. Press), 87–154.

Tucholke, B. E., and Vogt, P. R., 1979. Western North Atlantic: sedimentation evolution and aspects of tectonic history. *In* Tucholke, B. E., Vogt, P. R., et al., *Init. Repts. DSDP*, 43: Washington (U.S. Govt. Printing Office), 791–825.

Winterer, E. L., Riedel, W. R., et al., 1971. *Init. Repts. DSDP*, 7: Washington (U.S. Govt. Printing Office).

Zotto, M., Drugg, W. S., and Habib, D., 1987. Kimmeridgian dinoflagellate stratigraphy in the Southwestern North Atlantic. *Micropaleontology*, 33:193–213.

Ms 129A-104

NOTE: All core description forms ("barrel sheets") and core photographs have been printed on coated paper and bound as Section 3, near the back of the book, beginning on page 247.
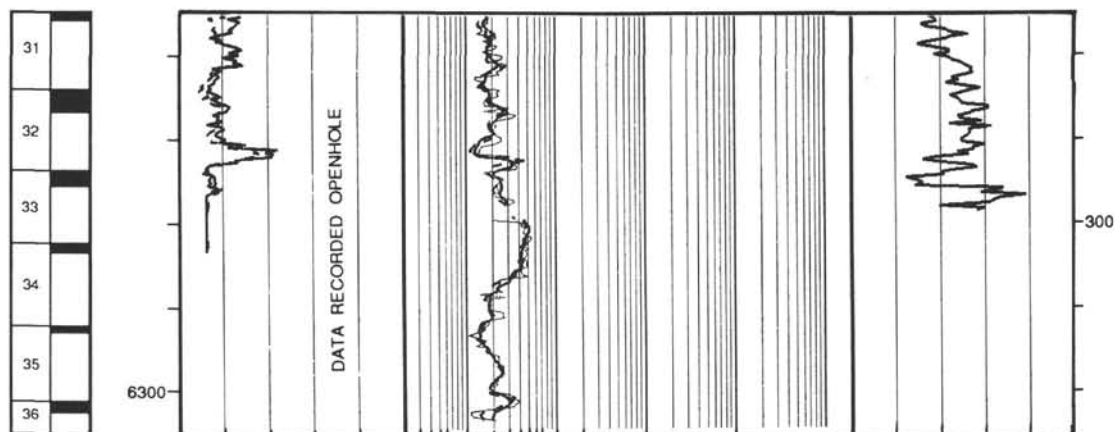
Hole 802A: Resistivity-Sonic-Gamma Ray Log Summary

Hole 802A: Resistivity-Sonic-Gamma Ray Log Summary (continued)

Hole 802A: Density-Caliper-Gamma Ray Log Summary

Hole 802A: Density-Caliper-Gamma Ray Log Summary (continued)

Hole 802A: Geochemical Log Summary

Hole 802A: Geochemical Log Summary (continued)